Interactions of Chitin and Lignin Thin Films with Other Molecules

Guoqiang Yu

Dissertation submitted to the faculty of the Virginia Polytechnic Institute and State University in partial fulfillment of the requirements for the degree of

Doctor of Philosophy
in
Chemistry

Alan R. Esker, Chair
Maren Roman
Louis A. Madsen
Michael Schulz

September 22, 2021
Blacksburg, VA

Keywords: Chitin, Lignin, Thin Films, Enzymatic Degradation, Fenton Reagents, Quartz Crystal Microbalance with Dissipation Monitoring, Atomic Force Microscopy

Copyright 2021, Guoqiang Yu

Interactions of Chitin and Lignin Thin Films with Other Molecules

Guoqiang Yu

ABSTRACT

As two of the most abundant natural polymers, chitin and lignin not only play critical roles in fungal and plant cell walls but are also important functional materials and promising feedstocks for a variety of chemicals. This study investigated the interactions of chitin and lignin thin films with several other molecules via a quartz crystal microbalance with dissipation monitoring (QCM-D) and atomic force microscopy (AFM).

Interactions between chitin and family 18 chitinases are vital for understanding bacterial invasion of fungi and human defense against fungal infection. Regenerated chitin (RChitin) thin films were prepared via chemical conversion and spin-coating. Changes in their mass and viscoelasticity were monitored by a QCM-D in real time during incubation with family 18 chitinases. The optimal temperature for the activity of chitinases on surfaces was lower than bulk solution studies in the literature. Family 18 chitinases showed greater activity on dissolved chitin oligosaccharides while family 19 chitinases showed greater activity on RChitin films, which was attributed to chitin-binding domains in family 19 chitinases.

Catechyl lignin (C-lignin) is a promising substrate for lignin valorization. Films of C-lignin were synthesized via adsorbed horseradish peroxidase-catalyzed dehydrogenative polymerization (DHP) of caffeyl alcohol (C-alcohol), and degraded through Fenton chemistry with all processes observed by a QCM-D and AFM. The synthetic rate and yield for C-DHP films was lower than DHP films made from coniferyl alcohol (G-alcohol) and *p*-coumaryl alcohol (H-alcohol). The C-DHP film underwent complete Fenton mediated degradation in contrast to the G-DHP and H-

DHP films regardless of their thicknesses.

Conventional lignin suffers from recalcitrance to degradation. Copolymer lignin films were synthesized through surface-initiated copolymerization of C and G or C, G and H monolignols. As the concentration of C-alcohol increased, the percentage degradation of the synthesized DHP copolymer films increased. Almost all the CG-DHP or CGH-DHP films were degraded when the percentage of the C-alcohol in the polymerization feed was $\geq$ 75% and $\geq$ 60% for CG-DHP and CGH-DHP, respectively.

Interactions of Chitin and Lignin Thin Films with Other Molecules

Guoqiang Yu

GENERAL AUDIENCE ABSTRACT

Natural polymers are widely considered as an alternative to fossil fuels for the production of biofuels, biochemicals, and biomaterials. The features of their biodegradability, biocompatibility, and sustainability can significantly alleviate concerns about environmental pollution and energy security. The surfaces of natural polymers are critical to their properties and applications. This dissertation focuses on the study of interfacial behaviors occurring at two of the most abundant natural polymers, chitin and lignin, via surface analysis techniques, a quartz crystal microbalance with dissipation monitoring (QCM-D) and atomic force microscopy (AFM).

When an endosymbiont bacteria enter a fungal host, they secrete chitinases to soften and loosen the chitin layer in the fungal cell wall. Small chitin fragments will be released from digestion of the chitin layer of the fungal cell wall by chitinases in humans suffering from fungal infections. In order to fully understand the interactions between the fungal chitin layer and chitinases, a chitin thin film was fabricated to mimic the chitin layer, and the changes of the chitin film in mass, viscoelasticity, and morphology during treatment with family 18 chitinases were studied at various temperatures and pH using a QCM-D and AFM. Family 19 chitinases produced greater degradation of chitin thin films than family 18 chitinases, even though the family 18 chitinases had greater activity in solution. Greater surface activity for family 19 chitinases were attributed to chitin-binding domains in their chemical structure that are absent in family 18 chitinases.

Millions of tons of lignin are produced in the lignocellulosic biorefinery and are discarded

every year due to their recalcitrance to degradation as a result of their heterogeneous and complex structure. A newly discovered lignin, catechyl lignin (C-lignin), has potential for enhancing degradation on account of its simple linear structure. In this dissertation, C-lignin thin films were synthesized on gold-coated QCM-D sensor surfaces via surface-initiated dehydrogenative polymerization of caffeyl alcohol (C-alcohol). Their enzymatic and chemical degradation was investigated. It was found that the C-lignin films underwent complete chelator-mediated Fenton degradation in contrast to conventional lignin films.

Although the C-lignin promises to be an ideal substrate for lignin valorization, its narrow distribution in nature severely limits its wide application. In view of this limitation, some people are trying to incorporate C units into conventional lignin through genetically engineered plants. This dissertation demonstrates the successful copolymerization of C-alcohol with conventional monolignols and the improved degradation of the synthesized C unit-containing copolymer lignin films relative to conventional lignin films. The results are expected to inform the design of lignocellulosic biomass for greater utilization.

Acknowledgements

First and foremost, my deepest thanks are given to my advisor, Prof. Alan R. Esker. There is no way that I am writing this dissertation without his guidance, support, encouragement, and patience in the past four years. I really appreciate all the time he has spent on me. Before I was admitted into his group, I was confused about my future, but now I am ready to pursue another career. He was always the person from whom I could get help whenever and whatever I needed during this long journey.

I would like to thank my committee members, Prof. Maren Roman, Prof. Louis A. Madsen, and Prof. Michael Schulz for their time, insightful suggestions, and constructive feedback on my work. They have assisted me in completing every milestone during my Ph.D. study.

I am grateful to all my colleagues in the Esker group, Candace E. Wall, Jianzhao Liu, Gehui Liu, Tianyi Liu, Austin Holland, and Ethan Fink for their help with my research and my daily life. I am so lucky to have them as my friends, and they make my every day full of joy.

I would like to thank the Department of Chemistry for offering me assistantships and providing me with such a wonderful place to learn and study. I want to give special thanks to Prof. Guoliang (Greg) Liu for being my advisor in the Spring and Summer 2018 semesters, Prof. John R. Morris for being the graduate program director and my committee member in the Spring 2021 semester, Joli Huynh for being the graduate program coordinator, and Victoria Long and Michelle Dalton for being in charge of the general chemistry lab.

Last but not least, I would like to thank my wife, Miao Hong, my father, Tianwen Yu, my mother, Aimei Xu, and my sister, Yanmei Yu, for their love, support, and encouragement over the years. They have always been there for me and driving me forward.

Attributions

Gehui Liu (Ph.D. candidate in the Department of Chemistry at Virginia Tech) aided in the preparation of the manuscript in Chapter 3.

Tianyi Liu (Ph.D. candidate in the Department of Chemistry at Virginia Tech) conducted experiments about H-DHP films in Chapter 4 and aided in the preparation of the manuscript in Chapter 3.

Ethan Fink (undergraduate student in the Department of Chemistry at Virginia Tech) conducted partial QCM-D experiments about synthesis and degradation of CGH-DHP copolymer films in Chapter 5 and aided in the preparation of the manuscripts in Chapters 3, 4, and 5.

Mehdi Ashraf-Khorassani (manager of the Mass Spec and Chromatography Center in the Department of Chemistry at Virginia Tech) did the MS experiments in Chapters 4 and 5.

Prof. Alan R. Esker (professor in the Department of Chemistry at Virginia Tech) supervised all the projects in Chapters 3, 4, and 5, provided numerous valuable instructions, and greatly aided in the preparation of the manuscripts associated with those chapters.

Table of Contents

List of Figures

Chapter 2

List of Tables

Chapter 1: Overview

Natural polymers are receiving greater attention due to their biodegradability, biocompatibility, and sustainability. They are widely considered as a solution to environmental pollution and resource crises resulting from consumption of fossil fuels. A giant number of natural polymers are distributed in plant and fungal cell walls, and a complete understanding of their interactions with other molecules is of great importance for their applications.

Chitin and lignin are the most abundant naturally-occurring polymers after cellulose.[1-3] A chitin layer in the fungal cell wall is located next to the plasma membrane.[4-7] Chemical changes to chitin after attack by family 18 chitinases is essential for understanding the penetration of endosymbiont bacteria into fungal cells and human defense against fungal infections, which promises to greatly promote the areas of agriculture, biotechnology, and medicine. Lignocellulosic biomass provides an alternative to petrochemical fossil resources for the production of biofuels and biochemicals.[8-11] However, the huge amount of lignin generated in the biorefinery suffers from inefficient valorization due to its heterogeneously complex structure and recalcitrance to degradation.[11-13] A recently discovered lignin, catechyl lignin (C-lignin), has potential for overcoming many challenges as a result of its simple structure.[14-15] Given the above information, the interactions between chitin thin films and family 18 chitinases, the synthesis and degradation of C-lignin films, and the effects of catechyl (C) units on conventional lignin films are studied in this dissertation via surface analysis techniques, including the use of a quartz crystal microbalance with dissipation monitoring (QCM-D) and atomic force microscopy (AFM).

Chapter 2 gives an overall introduction to the structure of plant and fungal cell walls and the various biopolymers they contain, including glycoproteins, polysaccharides and lignocellulosic biomass (cellulose, lignin, pectin, chitin, and glucan). The molecular structure, synthesis,

degradation, and applications of C-lignin are discussed. Then, the degradation of polysaccharides and lignocellulosic biomass by enzymes (cellulases, ligninolytic enzymes, pectinases, and chitinases) are presented. In addition, the conformation of adsorbed and grafted polymer chains on a solid substrate surface in liquid is briefly introduced, and a variety of methods to prepare lignin and chitin thin films are summarized. Finally, a brief introduction to the key surface analysis technique, QCM-D, is provided.

Chapter 3 describes the activity of family 18 chitinases from *Trichoderma viride* on regenerated chitin (RChitin) thin films at various temperatures and pH. Changes in the mass, viscoelasticity, and morphology of the RChitin films when treated with the family 18 chitinases are monitored by QCM-D and AFM. A detailed comparison between the performances of family 18 chitinases and family 19 chitinases from *Streptomyces griseus* on the degradation of RChitin films and dissolved chitin oligosaccharides is conducted.

Chapter 4 introduces the synthesis of C-lignin on gold-coated QCM-D sensor surfaces via surface-immobilized horseradish peroxidase-catalyzed dehydrogenative polymerization (DHP) of caffeyl alcohol (C-alcohol). Effects of different solvents on their synthesis are investigated. Enzymatic and chemical degradation of the synthesized C-DHP films by ligninolytic enzymes (lignin peroxidase and manganese peroxidase) and Fenton reagents are explored. Effects of Fe ions (Fe^{2+} and Fe^{3+}) and Fe chelator/reducer (2,3-dihydroxybenzoic acid) in the Fenton reagents on the degradation are further studied. Additionally, the C-DHP films are compared with conventional lignin films prepared from coniferyl alcohol (G-alcohol) and *p*-coumaryl alcohol (H-alcohol) with respect in their synthesis and degradation.

Chapter 5 presents the incorporation of C units into copolymers with G- or G- and H-monolignols to form lignin films through a surface-initiated polymerization. The effects of C

units on the degradation of the synthesized CG- and CGH-DHP copolymer lignin films by a chelator-mediated Fenton system are then investigated. Changes in degradation kinetics with an increase in the ratio of the C units are studied via QCM-D.

Chapter 6 provides the overall conclusions of this dissertation and gives some suggestions for future work related to the studies in this dissertation.

References

1. Rinaudo, M., Chitin and chitosan: properties and applications. *Prog Polym Sci* **2006,** *31*, 603-632.

2. Whetten, R.; Sederoff, R., Lignin biosynthesis. *Plant Cell* **1995,** *7*, 1001-1013.

3. Notley, S. M.; Norgren, M., Adsorption of a strong polyelectrolyte to model lignin surfaces. *Biomacromolecules* **2008,** *9*, 2081-2086.

4. Kang, X.; Kirui, A.; Muszynski, A.; Widanage, M. C. D.; Chen, A.; Azadi, P.; Wang, P.; Mentink-Vigier, F.; Wang, T., Molecular architecture of fungal cell walls revealed by solid-state NMR. *Nat Commun* **2018,** *9*, 2747.

5. Bowman, S. M.; Free, S. J., The structure and synthesis of the fungal cell wall. *Bioessays* **2006,** *28*, 799-808.

6. Gow, N. A. R.; Latge, J. P.; Munro, C. A., The fungal cell wall: structure, biosynthesis, and function. *Microbiol Spectr* **2017,** *5*, FUNK-0035-2016.

7. Free, S. J., Fungal cell wall organization and biosynthesis. *Adv Genet* **2013,** *81*, 33-82.

8. Gillet, S.; Aguedo, M.; Petitjean, L.; Morais, A. R. C.; da Costa Lopes, A. M.; Łukasik, R. M.; Anastas, P. T., Lignin transformations for high value applications: towards targeted

modifications using green chemistry. *Green Chem* **2017,** *19*, 4200-4233.

9. Ragauskas, A. J.; Beckham, G. T.; Biddy, M. J.; Chandra, R.; Chen, F.; Davis, M. F.; Davison, B. H.; Dixon, R. A.; Gilna, P.; Keller, M.; Langan, P.; Naskar, A. K.; Saddler, J. N.; Tschaplinski, T. J.; Tuskan, G. A.; Wyman, C. E., Lignin valorization: improving lignin processing in the biorefinery. *Science* **2014,** *344*, 1246843.

10. Zhang, X. Adsorption of biomacromolecules onto polysaccharide surfaces. Ph.D. Dissertation, Virginia Tech, Blacksburg, VA, 2014.

11. Xu, Z.; Lei, P.; Zhai, R.; Wen, Z.; Jin, M., Recent advances in lignin valorization with bacterial cultures: microorganisms, metabolic pathways, and bio-products. *Biotechnol Biofuels* **2019,** *12*, 32.

12. Wang, H.; Pu, Y.; Ragauskas, A.; Yang, B., From lignin to valuable products-strategies, challenges, and prospects. *Bioresour Technol* **2019,** *271*, 449-461.

13. Bruijnincx, P. C. A.; Rinaldi, R.; Weckhuysen, B. M., Unlocking the potential of a sleeping giant: lignins as sustainable raw materials for renewable fuels, chemicals and materials. *Green Chem* **2015,** *17*, 4860-4861.

14. Berstis, L.; Elder, T.; Crowley, M.; Beckham, G. T., Radical nature of C-lignin. *ACS Sustainable Chem Eng* **2016,** *4*, 5327-5335.

15. Stone, M. L.; Anderson, E. M.; Meek, K. M.; Reed, M.; Katahira, R.; Chen, F.; Dixon, R. A.; Beckham, G. T.; Roman-Leshkov, Y., Reductive catalytic fractionation of C-lignin. *ACS Sustainable Chem Eng* **2018,** *6*, 11211-11218.

Chapter 2: Introduction and Literature Review

2.1 Introduction to Natural Polymers

Natural polymers or biopolymers are naturally occurring polymers, such as cellulose, starch, lignin, chitin, proteins, deoxyribonucleic acids, and ribonucleic acids. They can roughly be classified into polysaccharides, polynucleotides, and polypeptides based on their monomeric units and structures, and according to their sources, they can be divided into three classes: plants, animals, and microbes. Compared to petrochemical (fossil)-based polymers, notable features of natural polymers are their biodegradability, biocompatibility, and sustainability. Natural polymers are receiving greater attention due to environmental concerns and resource crises associated with finite supplies of fossil fuels. They are widely considered as a solution to those challenges. Numerous natural polymers have been isolated, and they are being applied to various areas, such as health care, adhesives, food, cosmetics, personal care, and paints.[1-3]

2.2 Main Polymers in Plant Cell Walls

Plant cell walls are one of the most abundant sources of natural polymers. They have an outer layer surrounding plant cells that is outside of the cell membrane. The major function of plant cell walls is to maintain the shape and form of the cell. It also plays essential roles in structural and mechanical support, resisting turgor pressure, controlling cell growth, regulating diffusion of materials though apoplast, protection against pathogens and water loss, carbohydrate storage, and intercellular communication.[4-5]

2.2.1 Structure of Plant Cell Walls

Plant cell walls are dynamic structures whose composition and architecture change with cell growth and development.[4] They consist of up to three layers — the middle lamella, primary cell

wall, and secondary cell wall, as shown in Figures 2.1 and 2.2.[5-7] The middle lamella is the first layer formed during cell division and is the outermost layer. It is shared by neighboring cells and can glue them together. The middle lamella is rich in pectin. The primary cell wall is formed between the middle lamella and plasma membrane while the cell is growing. It is a flexible and extensible layer at a thickness of 100 to 200 nm, which provides the strength and flexibility for a cell to grow. The primary cell wall is predominantly composed of polysaccharides with lesser amounts of structural glycoproteins, phenolic esters, minerals, and enzymes. The major polysaccharides are cellulose, hemicellulose, and pectin. Cellulose exists in the form of microfibrils, which are physically cross-linked by hemicelluloses to form a cellulose-hemicellulose network that is embedded in a pectin matrix. Many models, including the covalently cross-linked model, tether model, diffuse layer model, and stratified layer model, have been proposed to describe the organization and interactions of the primary cell wall components.[5, 7-9] Once the primary cell wall has ceased to grow, it thickens to form the secondary cell wall in some plants.[10-11] The secondary cell wall is a rigid layer deposited inside the primary cell wall, which can strengthen and support the cell. Compared to the primary cell wall, the secondary cell wall is much thicker, stronger, and accounts for most of the carbohydrate in biomass. Some cells, such as the conducting cells in xylem, tracheids, and sclereids, possess secondary cell walls containing lignin in addition to cellulose and hemicellulose. The lignin considerably strengthens and waterproofs the wall by filling the spaces in the cellulose-hemicellulose network. The secondary cell wall often consists of three layers: S_1, S_2, and S_3, as shown in Figure 2.2.[6] The outermost S1 layer has a thickness of 0.1 to 0.3 μm in which the cellulose microfibrils form a crossed structure. The cellulose microfibrils in the S2 layer that is typically 1 to 5 μm in thickness are oriented almost parallel to the fiber axis, and the innermost

S3 layer at a thickness of ~0.1 μm is characterized by a flat helix of cellulose microfibrils.

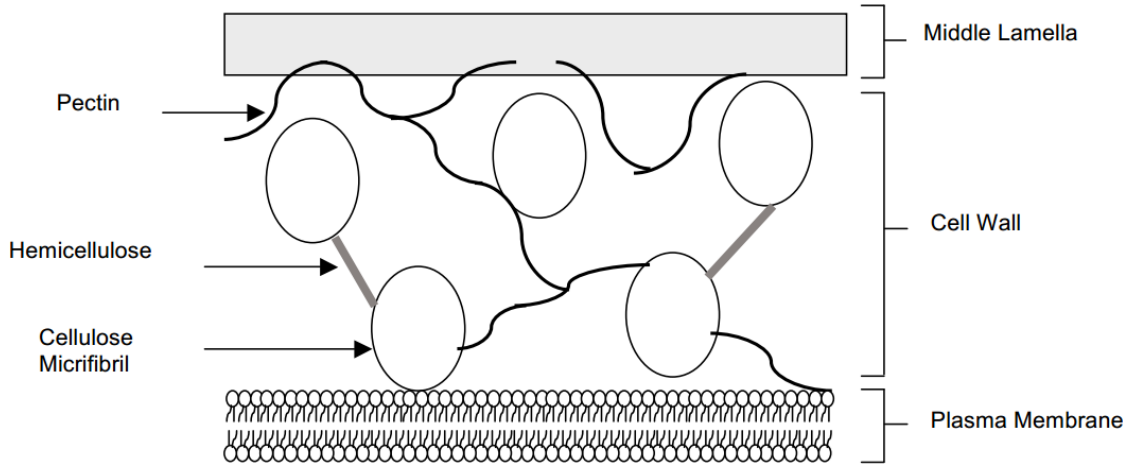

Figure 2.1 Cross-sectional depiction of the structure of a primary plant cell wall. The cellulose microfibrils run into the page. Reproduced from Palin (Copyright 2011 Robert John Palin).[5]

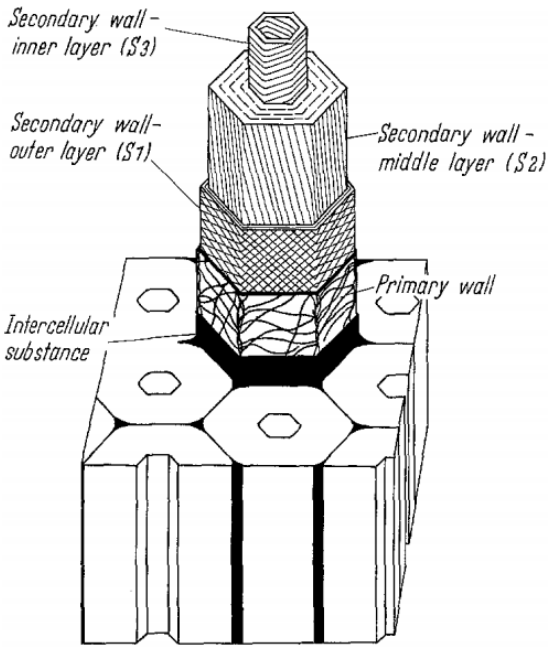

Figure 2.2 Schematic depiction of the structure of the cell wall of a softwood tracheid or a hardwood fiber. Reproduced from Timell et al. (Copyright 1967 Springer Nature).[6]

2.2.2 Cellulose

Cellulose has been characterized by its hydrophilicity, chirality, biodegradability,

polyfunctionality, and polymorphism since it was first discovered and isolated by Anselme Payen in 1838.[12] It is the most abundant biopolymer in nature with a wide distribution in plants, bacteria, fungi, algae, and even some animals.[13-14] Cellulose is a linear polysaccharide with a repeat unit consisting of a pair of D-anhydroglucose units (AGUs) joined by β-(1→4) glycosidic oxygen linkages in which every AGU unit is rotated 180^{o} with respect to the previous one.[12-13] The degree of polymerization (DP) of the cellulose varies with source and method of isolation. For example, the cellulose in wood pulp has typical DP values of 300 to 1,700, while the DP values for the cellulose in cotton range from 800 to 10,000.[12, 14] In nature, cellulose molecules first aggregate into elementary fibrils with lateral dimensions between 1.5 and 3.5 nm and then pack into microfibrils that have cross-sectional dimensions ranging from 10 to 30 nm.[13] The cellulose chains are oriented along the direction of the microfibrils, and exist in both primary and secondary plant cell walls. Compared to secondary cell walls, primary cell walls have cellulose of lower DPs. Numerous physicochemical properties of cellulose are ascribed to the supramolecular structure with highly ordered (crystalline) and less ordered (amorphous) regions within the microfibril.[12, 14] Cellulose cannot be dissolved in water or common organic solvents. However, it is soluble in some aqueous alkali containing solvents, ionic liquids, amine oxides, and organic solvents/salts. Some specific examples of cellulose solvents include sodium hydroxide/poly(ethylene glycol), 3-methyl-N-butyl-pyridinium chloride, N-methylmorpholine-N-oxide monohydrate, and dimethylacetamide (DMA)/lithium chloride (LiCl).[15]

The molecular structure of cellulose is shown in Figure 2.3. One end of its chain is a reducing end with a hemiacetal group that is in equilibrium with an aldehyde group, and the other is a non-reducing end with a pendant hydroxyl group. As can be seen from Figure 2.4,[11] a large number of intra- and inter-molecular hydrogen bonds exist in cellulose crystals which

contribute to their structure and give rise to polymorphs. Six crystal polymorphs have been identified, namely, I, II, III_I, III_{II}, IV_I, and IV_{II}. Interconversions between polymorphs are summarized in Figure 2.5.[13-14] Cellulose I is the main form found in nature and includes two suballomorphs, I_α and I_β. I_α is the dominant type in bacterial and algal celluloses, and I_β is prevalent in celluloses from higher plants. Different from the crystal structure of cellulose I with two parallel cellulose chains in a unit cell, cellulose II contains two chains in an antiparallel orientation in its unit cell, yielding a more stable structure. The conversion from cellulose I to cellulose II, which is usually considered irreversible, can be achieved by regeneration (dissolving cellulose I in a solvent followed by precipitation in water to yield cellulose II) or mercerization (swelling cellulose I in concentrated NaOH followed by removal of the swelling agent to give cellulose II). Celluloses III_I and III_{II} are reversibly formed from celluloses I and II, respectively, with the treatment of ammonia or various amines. Celluloses IV_I and IV_{II} can be obtained by heating celluloses III_I and III_{II} up to 206 ^oC in glycerol.

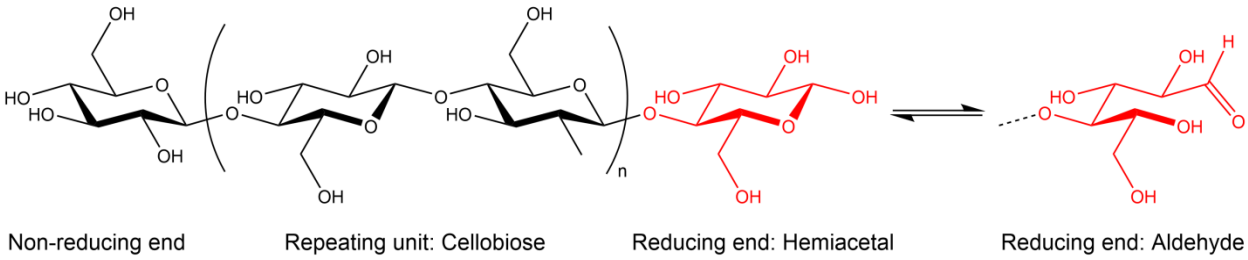

Figure 2.3 Molecular structure of cellulose with a non-reducing end group, cellobiose repeating units, and a reducing end group. The reducing end group, highlighted in red, can be either a hemiacetal or an aldehyde that are in equilibrium.

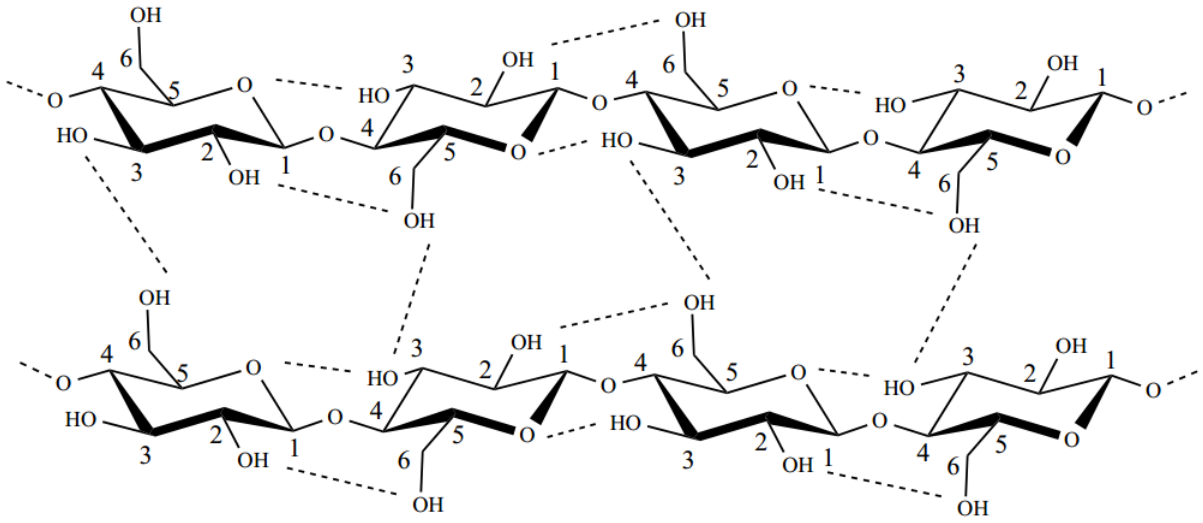

Figure 2.4 A representative intra- and inter-molecular hydrogen bonding network in celluloses. Reproduced from Zhang (Copyright 2014 Xiao Zhang).[11]

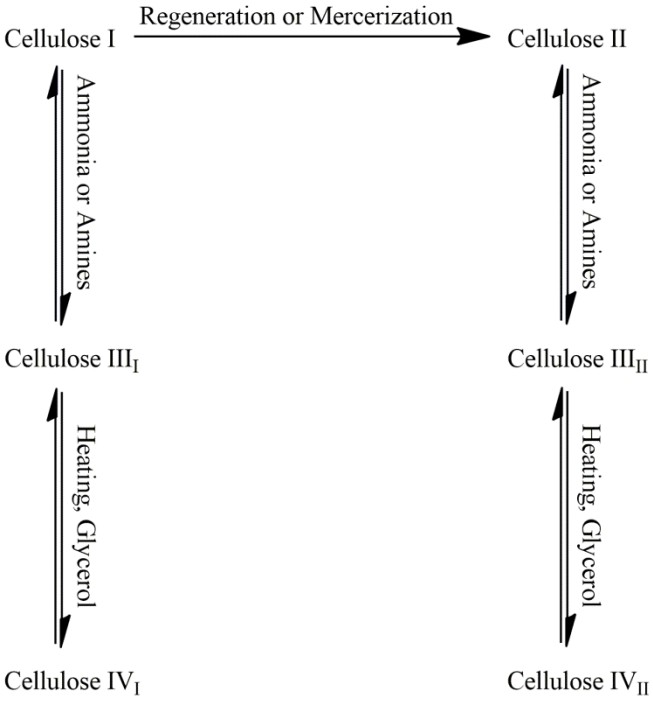

Figure 2.5 Interconversions between cellulose polymorphs.

2.2.3 Lignin

Lignin is one of the most abundant, naturally occurring biopolymers along with cellulose and

chitin, accounting for 15-35% of the dry weight of woody plants and about 30% of non-fossil organic carbon in the biosphere.[16] It provides mechanical support and rigidity to plants, helps bind adjacent cells together, protects against pathogens, and mediates internal transport of water and nutrients. These functions are attributed to its hydrophobicity relative to the polysaccharides in the cell wall.[17-18] Lignin can be found in all vascular plants, mostly between the tracheids and in the secondary cell walls.[19] It is an amorphous and crosslinked aromatic polymer with many functional groups, such as phenolic hydroxyl, aliphatic hydroxyl, and methoxy groups.[16, 19-20] Lignin is primarily derived from the dehydrogenative polymerization of three monolignols, namely, *p*-coumaryl alcohol, coniferyl alcohol, and sinapyl alcohol, as shown in Figure 2.6, and they correspond to *p*-hydroxyphenyl (H), guaiacyl (G), and syringyl (S) structural units of lignin, respectively.[10, 18] Two unconventional lignin units have been identified in recent years: catechyl (C) and 5-hydroxyguaiacyl (5H) units, originated from caffeyl and 5-hydroxyconiferyl alcohols, respectively. Lignin can be generally divided into three categories based on their sources: softwood, hardwood, and grass lignins. Their abundance follows the order of softwoods > hardwoods > grasses.[21] Softwood lignin mostly contains G units, and G and S units are the main components of hardwood lignin.[18, 22] Grass lignin is a mixture of H, G, and S units. C units primarily exist in the seed coats of vanilla orchids and several cactus species, and 5H units are present in some angiosperm plants. These structural units are connected by various bonds including carbon-carbon and ether linkages. Many efforts have been devoted to defining the actual structure of lignin. However, a full understanding of lignin remains elusive due to its complexity and structural changes caused by the isolation process. Figure 2.7 provides a schematic representation of a softwood lignin structure.[18]

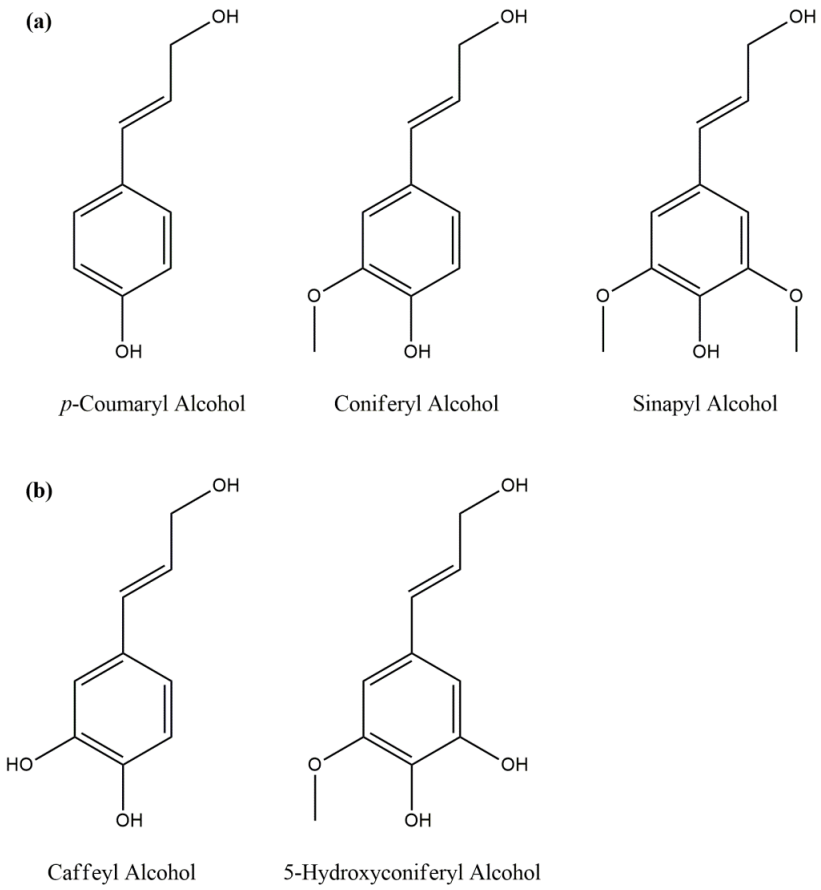

Figure 2.6 Molecular structures of (a) conventional and (b) unconventional monolignols.

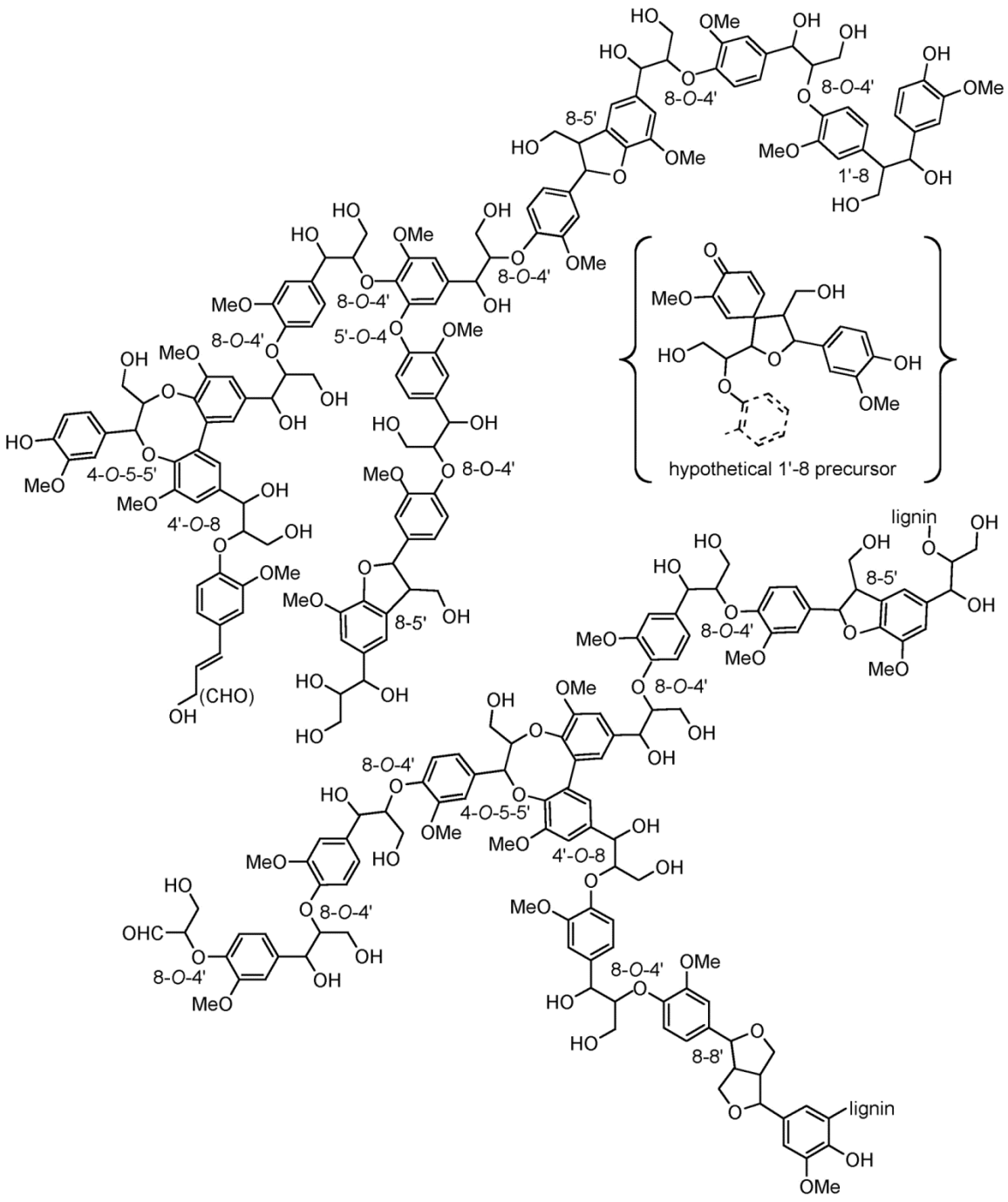

Figure 2.7 Representation of a softwood lignin structure. Reproduced from Tolbert et al. (Copyright 2014 Society of Chemical Industry and John Wiley & Sons, Ltd.).[18]

There are three different types of lignin on the basis of the most widely employed methods to isolate it from native biomass: milled wood lignin (MWL), cellulolytic enzyme lignin (CEL),

and enzymatic mild acidolysis lignin (EMAL).[18] The general trend for the molar mass of lignin obtained from these methods is EMAL > CEL > MWL. The biosynthesis of lignin can be divided into three steps: biosynthesis of monolignols, transport, and polymerization.[22] The monolignols are produced in the cytoplasm and transported to the apoplast after multiple reactions involving deamination, hydroxylation, methylation, and reduction. Lignin is then synthesized through the polymerization of the monolignols with the assistance of peroxidase and laccase in secondary cell walls. The as-prepared lignin is usually combined with cellulose and hemicelluloses to form lignin-carbohydrate complexes in plants. Most industrial lignins are Kraft lignin that are a byproduct of the Kraft pulping process in which wood chips are digested in an aqueous solution of sodium hydroxide and sodium sulfide to depolymerize the lignin.[18] Applications of lignin have been investigated in many areas, such as vanillin, lignosulfonates, additives for asphalt, and drilling fluids as an emulsification agent.[18]

2.2.3.1 Catechyl Lignin

A new naturally occurring lignin, catechyl lignin (C-lignin), was discovered in recent years in the seed coat tissues of vanilla orchids and several cactus species.[23-24] It is a linear homopolymer of catechyl units (C units) derived solely from caffeyl alcohol (C-alcohol) that are almost exclusively connected through benzodioxane linkages, as shown in Figure 2.8.[23-25] Its benzodioxane backbone consists of a *trans*/*cis*-isomeric mixture.[23] Compared to the β-*O*-4 bonds in conventional lignin, the benzodioxane structures without benzylic hydroxyl groups prevent the formation of benzyl carbocations, thus greatly alleviating their cleavage and condensation reactions under acidic conditions.[26-27] The lack of benzylic hydroxyl groups significantly mitigates the degradation of C-lignin by alkaline oxidation as well.[26] From these points of view, the C-lignin is more stable than the conventional lignin. Berstis et al.[28] studied the bond strengths

of C-lignin. The α-bond of the benzodioxane linkage with an average bond dissociation enthalpy of 56.5 kcal/mol is weaker than the conventional β-*O*-4 bond, while the β-bond is slightly stronger, averaging 65.4 kcal/mol. The difference in thermodynamic stability between the stereoisomers of C-lignin is small.

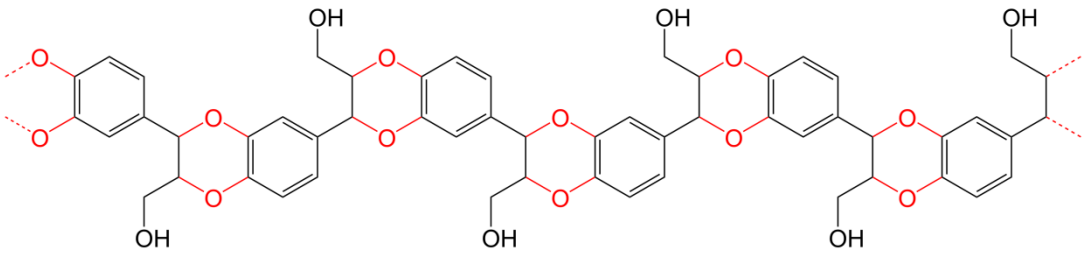

Figure 2.8 Molecular structure of C-lignin. Benzodioxane linkages, highlighted in red, give rise to a more linear structure relative to conventional lignin (Figure 2.7).

The synthesis of C-lignin from C-alcohol in vivo follows a combinatorial oxidative radical coupling process that is under simple chemical control, similar to the biosynthesis of conventional lignin, as shown in Figure 2.9.[23-24, 28-30] The C-alcohol and the growing C-lignin polymer are first oxidized by such enzymes as peroxidases and laccases to radicals. An end-wise β-*O*-4-type radical coupling reaction subsequently occurs between the C-alcohol radical at its β-position and the end catechol unit of the growing polymer at its 4-*O*-position. The generated quinone methide (QM) intermediate is then rearomatized to form a benzodioxane linkage via internal trapping through the 3-OH group on the end unit of the growing polymer which acts as a nucleophile. Density functional theory models have shown that there is no thermodynamic preference for the QM intermediates undergoing intramolecular ring closure to create benzodioxane linkages relative to hydration reaction to ultimately form β-*O*-4 linkages, and as a result, the almost complete benzodioxane linkage generation during C-lignin synthesis is presumably kinetically favored.

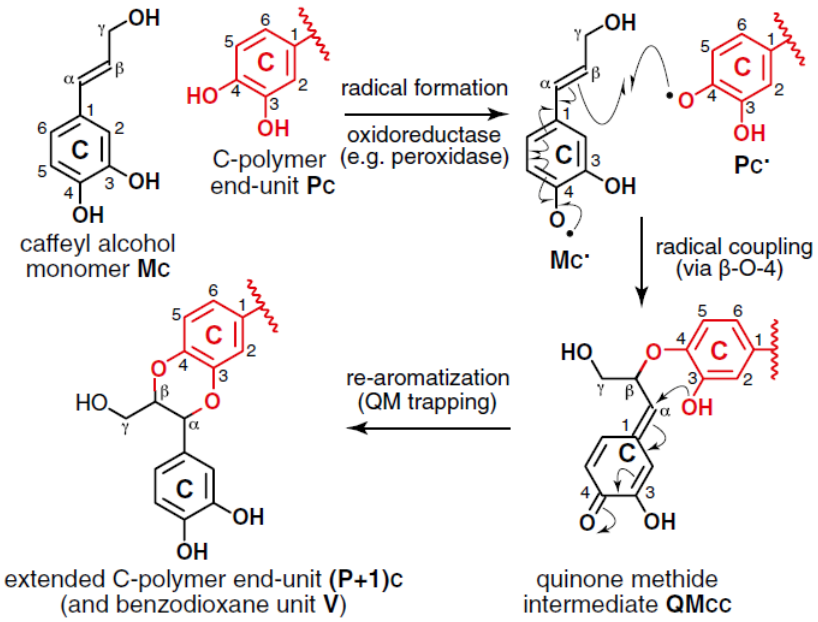

Figure 2.9 C-lignin formation via a combinatorial oxidative radical coupling mechanism. Reproduced from Chen et al. (Copyright 2012 Authors).[23]

The exact pathway for the biosynthesis of C-lignin is uncertain at this time, but all available studies report that the C-lignin formation is temporally or spatially separated from the production of conventional lignin in vivo.[29, 31] Figure 2.10 illustrated the biosynthesis of conventional lignin and C-lignin in plants. Several studies agree that the C-lignin biosynthesis involves down-regulation of transcripts encoding caffeoyl CoA 3-*O*-methyltransferase (CCoAOMT) and caffeic acid 3-*O*-methyltransferase (COMT).[29, 32-35] In addition, Wu et al.[36] observed a remarkable increase in the content of C-lignin in the brown midrib2 mutant of maize after the suppression of methylenetetrahydrofolate reductase (MTHFR).

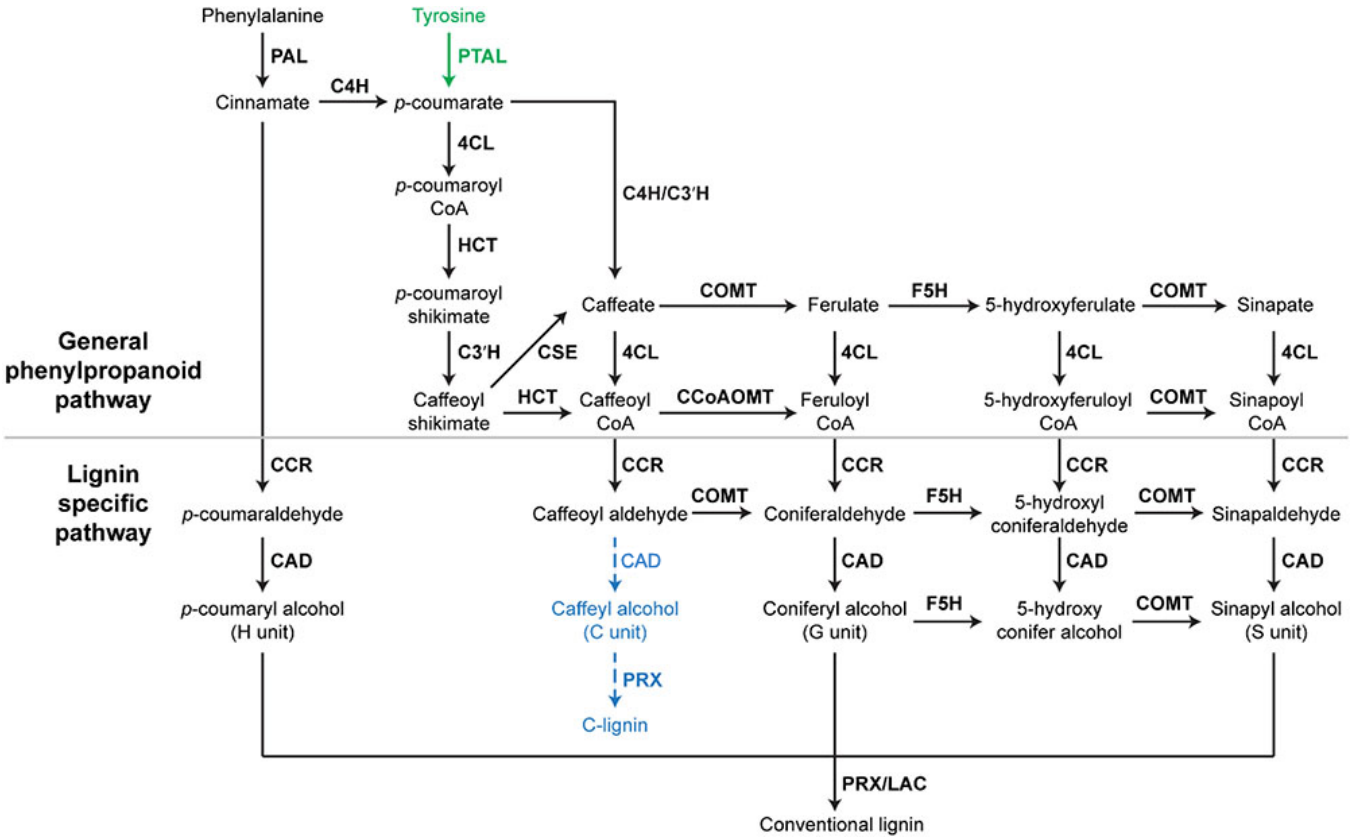

Figure 2.10 Simplified lignin biosynthesis pathway in plants. PAL, phenylalanine ammonia-lyase; C4H, cinnamate 4-hydroxylase; 4CL, 4-coumarate-CoA ligase; HCT, quinateshikimate *p*-hydroxycinnamoyltransferase; C3'H, *p*-coumaroylshikimate 3'-hydroxylase; CCoAOMT, caffeoyl-CoA *O*-methyltransferase; CCR, cinnamoyl-CoAreductase; F5H, ferulate 5-hydroxylase; CAD, cinnamyl alcohol dehydrogenase; COMT, caffeic acid *O*-methyltransferase; CSE, caffeoyl shikimate esterase; PRX, peroxidase; LAC, laccase. Adapted from Xie et al. (Copyright 2018 Authors).[31]

Besides natural C-lignin, a synthetic dehydrogenative polymer from C-alcohol (C-DHP) in vitro is widely regarded as a model compound. A general process to synthesize the C-DHP includes two separate solutions of C-alcohol in acetone/sodium phosphate buffer and hydrogen peroxide in water, which are slowly and continuously added into a sodium phosphate buffer

solution containing horseradish peroxidase at room temperature.[23, 26, 33] Chen et al.[23] carefully studied the structure of synthesized C-DHP, as shown in Figure 2.11. About 98% of the total identifiable dimeric units belonged to benzodioxane with non-existence of β-*O*-4 units. The ratio of *trans*- to *cis*-benzodioxane was 96:4, strikingly similar to the 97:3 for C-lignin from vanilla (*Vanilla planifolia*) seed coats. Nevertheless, the C-DHP had only a number-average degree of polymerization (DP_n) of ~8 which was much smaller than the isolated natural C-lignin whose DP_n were ~18 and 13 after extraction using DMSO and dioxane/water (96/4 v/v), respectively.

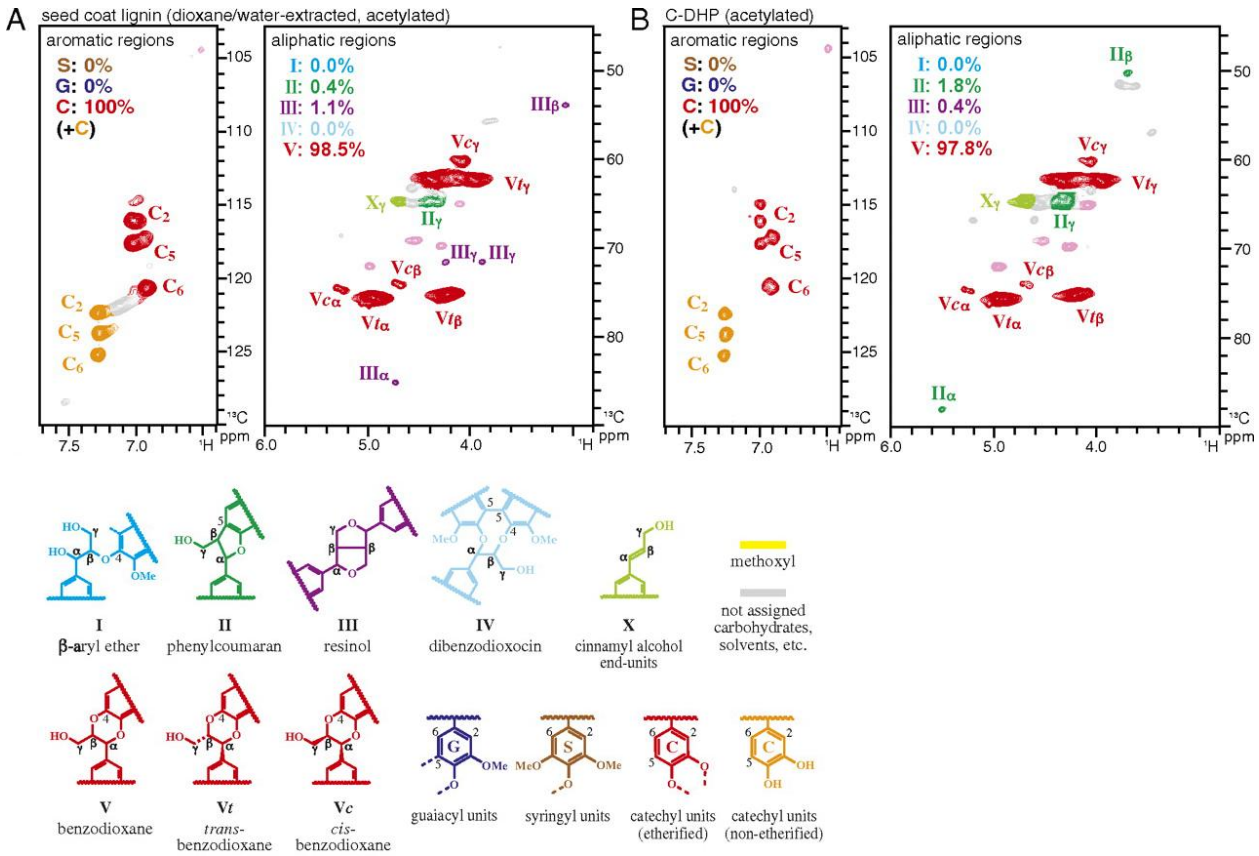

Figure 2.11 Short-range ^{13}C-^{1}H correlation spectra of (A) acetylated lignin isolated through extraction with dioxane/water (96/4 v/v) from *V. planifolia* seed coats and (B) acetylated C-DHP synthesized via horseradish peroxidase-catalyzed dehydrogenative polymerization of C-alcohol. Adapted from Chen et al. (Copyright 2012 Authors).[23]

Although various strategies have been developed to degrade conventional lignin, such as hydrogenolysis, oxidation, pyrolysis, liquefaction, and hydrolysis, the degradation of C-lignin is limited to a few reports on hydrogenolysis.[26-27, 30, 37-40] Li et al.[26] found the C-lignin from vanilla (*V. planifolia*) seed coats was quite stable even under harsh acidic conditions and both alkaline nitrobenzene oxidation and thioacidolysis were ineffective at depolymerization. Nevertheless, they successfully cleaved all of its benzodioxane structures under 40-bar H_2 at 200 ^oC, and 8 hydrogenolytic monomeric products were identified in which catechylpropanol and catechylpropane accounted for the majority. The distribution of monomeric products could be controlled by changing the catalyst (Pt/C, Pd/C, or Ru/C) and solvent (methanol, dioxane/water, or THF/water) combinations, as shown in Figure 2.12. Stone et al.[30] performed reductive catalytic fractionation (RCF) on pre-extracted vanilla (*V. planifolia*) seeds under H_2 at 190-250 ^oC in methanol using 15 wt% Ni/C as the catalyst to investigate the depolymerization of natural C-lignin. A depolymerization efficiency similar to that for hardwood lignin could be achieved with the generation of propyl catechol and propenyl catechol as the monomeric products. Both flow-through and batch RCFs demonstrated that the catalyst played roles in not only the cleavage of benzodioxane linkages but also the selectivity towards generating propyl catechol. Incomplete benzodioxane cleavage was observed due to the deactivation of catalyst caused by impurities, such as sugars, that were not removed from the pre-extracted vanilla seeds.

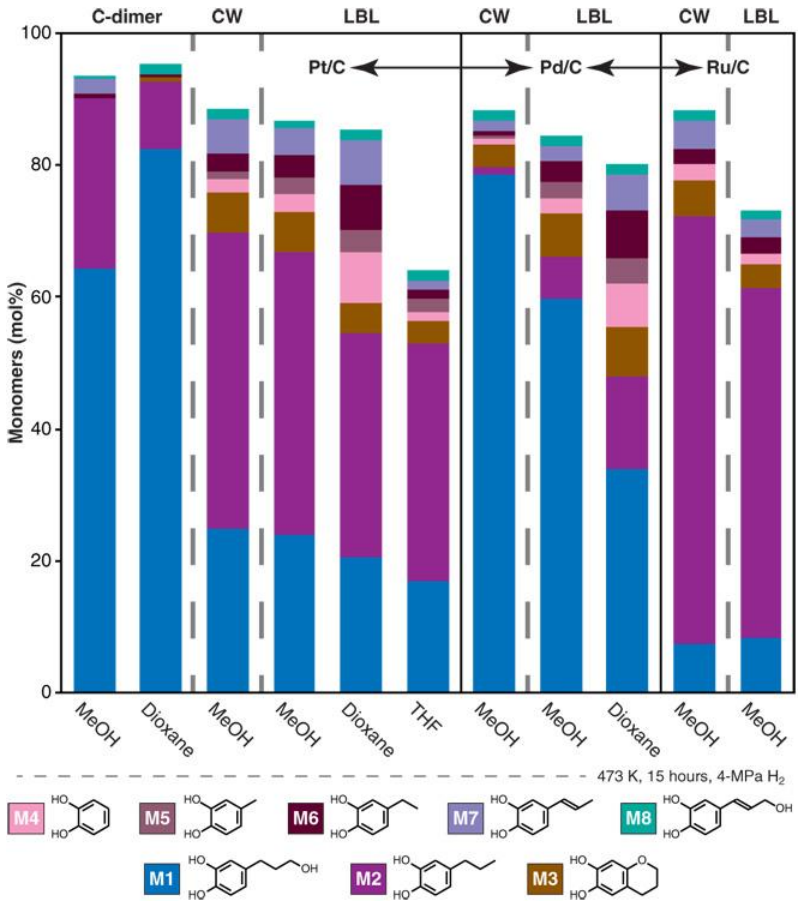

Figure 2.12 Products from hydrogenolysis of cell wall (CW) and acidic lithium bromide-pretreated C-lignin (LBL) from V. *planifolia* seed coats using different catalyst and solvent combinations. Reproduced from Li et al. (Copyright 2018 Authors).[26]

The unique structure and properties of C-lignin yield distinct characteristics that could be applied to various areas. For example, the biosynthesis of C-lignin may provide an alternative bioengineering approach to generate lignocellulosic biomass for bio-ethanol production with higher economic benefits due to its simple structure.[31, 41] In addition, the work from Li et al.,[26] Stone et al.,[30] and Liu et al.[27] has shown that the depolymerization products of C-lignin are a resource pool of catechols. Nar et al.[42] fabricated carbon fibers from C-lignin, taking advantage of its linear and homogeneous structure, as shown in Figure 2.13. They found that the C-lignin solution could be continuously electrospun into fine uniform fibers, while electrospun fibers

from Kraft lignin solution were only ~50.8 mm in length. Compared to carbon fibers derived from the Kraft lignin, the C-lignin carbon fibers had larger transverse and axial modulus, higher ratios of graphic structure, lower polydispersity indices, better thermal stability, and fewer impurities. Their research established the C-lignin as a promising renewable resource for effective carbon fibers of comparable quality to current market options.

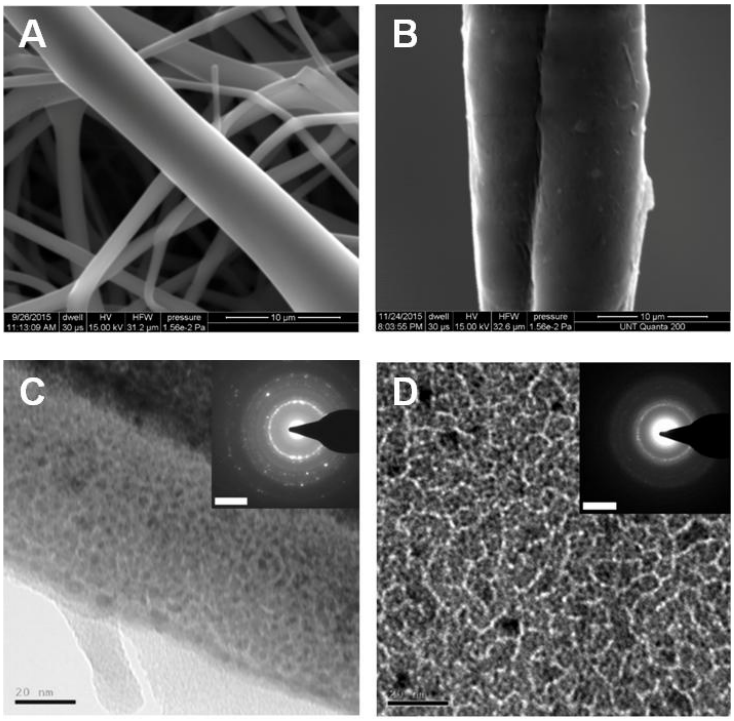

Figure 2.13 Environmental scanning electron microscopy (ESEM) images of carbon fibers derived from (A) Kraft lignin and (B) C-lignin, transmission electron microscopy (TEM) and electronic diffraction images of carbon fibers derived from (A) Kraft lignin and (B) C-lignin. Adapted from Nar et al. (Copyright 2016 Elsevier Ltd.).[42]

Although C-lignin has great potential for a variety of applications, its narrow distribution in nature severely limits its wider application. In view of that, some efforts have been made into converting β-*O*-4 units of conventional lignin to benzodioxanes via chemical treatment and incorporating C units into conventional lignin by genetically engineering the plants.[26, 32-33, 43] It is

generally believed that the C-lignin shows promise towards significantly improving lignin valorization.

2.2.4 Pectin

Pectin is mainly present in the middle lamella and primary cell wall with a gradual decrease in concentration from the middle lamella towards the plasma membrane. It is commonly deposited in the early stages of cell expansion and approximately accounts for one third of the biopolymers in cell walls.[44-45] Pectin plays important roles in cell wall formation and cell development contributing to integrity and rigidity of plant tissue, regulation of ion and water exchange, defense against pathogens and wounding, and determination of texture in fruits and vegetables during their growth and maturation.[44-46] Commercial pectin is primarily a homogalacturonan and mostly comes from citrus peel and apple pomace from which it is extracted at high temperature and under acidic conditions.[44] Pectin is widely used in the food industry as a gelling agent, thickener, stabilizer, emulsifier, and dietary fiber.[44-45] It can also be applied for drug delivery, wound healing, cigars, and cosmetics.

Pectins are among the most complicated macromolecules in nature. They possess as many as 17 different monosaccharides and over 20 different linkages.[45] Moreover, their structure depends upon the source and processing method. Basically, pectins are acidic structural heteropolysaccharides composed of α-(1-4)-linked D-galacturonic acid units in which varying portions of the uronic acid carboxyls are methyl esterified and a certain number of neutral sugars are contained as side chains.[44-45] Three main structural domains have been identified in pectin, namely, homogalacturonan and two highly branched rhamnogalacturonans designated as RG-I and RG-II. Many other structural domains also exist, such as xylogalacturonans, arabinogalactans, and arabinans, as shown in Figure 2.14.[44-45]

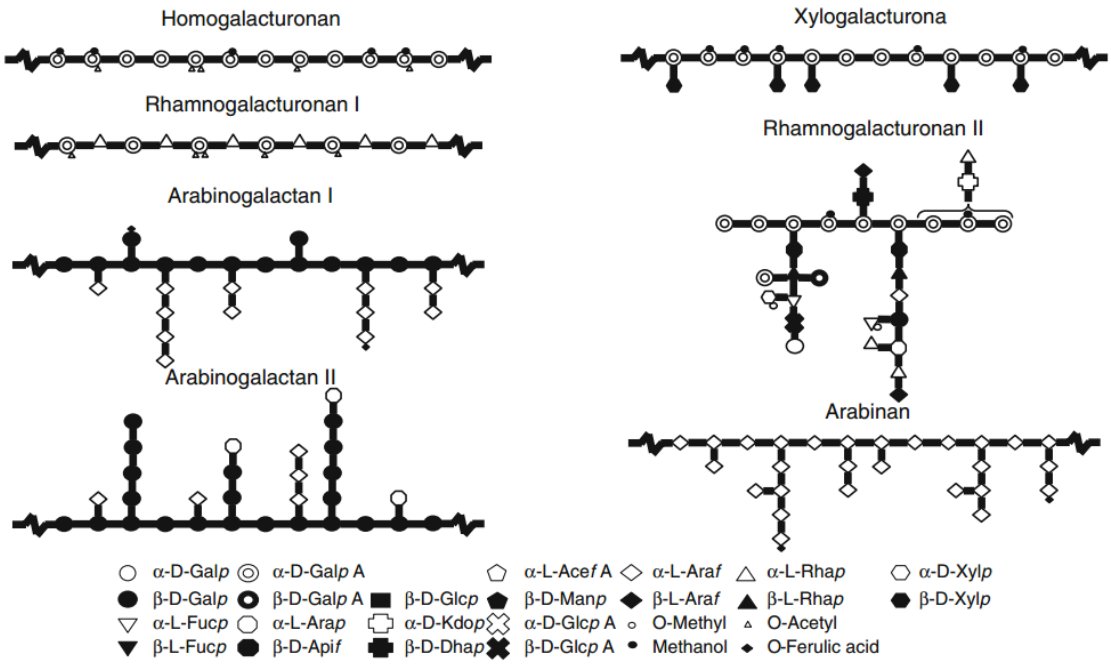

Figure 2.14 Structural domains in pectin. Reproduced from Voragen et al. (Copyright 2009 Authors).[45]

2.3 Main Polymers in Fungal Cell Walls

The cell wall is the outermost layer in fungi, external to the plasma membrane. Fungal cell walls play critical roles in resistance to osmotic pressure and other environmental stresses, maintenance of cell shape and preservation of cell integrity, recognition of external surfaces, reception of external stimuli, selective permeation of large molecules, and accumulation of molecules important to cell physiology.[47]

2.3.1 Structure of Fungal Cell Walls

Fungal cell walls primarily consist of chitin, glucans, and glycoproteins and have significantly different structures from plant cell walls. A typical fungal cell wall contains 50 to 60% glucans, 20 to 30% glycoproteins, and a small portion of chitin.[48-49] These components are extensively cross-linked to generate a complex three-dimensional network as the structural basis

of the fungal cell wall.[48-50] Chitin microfibrils are located next to the plasma membrane, and they covalently bind to β-1,3-glucans, which extend through the cell wall. Mannoproteins on the cell wall surface are linked to branched networks formed by β-1,3-glucans and β-1,6-glucans. The cell wall is a dynamic structure that varies with the developmental stage and growth conditions of fungi. Different fungal species usually have different cell wall structures as well, as depicted in Figure 2.15.[50] Basically, the inner cell wall is rich in carbohydrates that form a tensile and robust scaffold to provide mechanical support, whereas the outer cell wall is rich in proteins to achieve the physiological functions.[50-51] The inner and outer cell walls work together to form strong but flexible cell walls. Since many components of fungal cell walls are absent in human cells, they are an excellent target to develop antifungal agents.

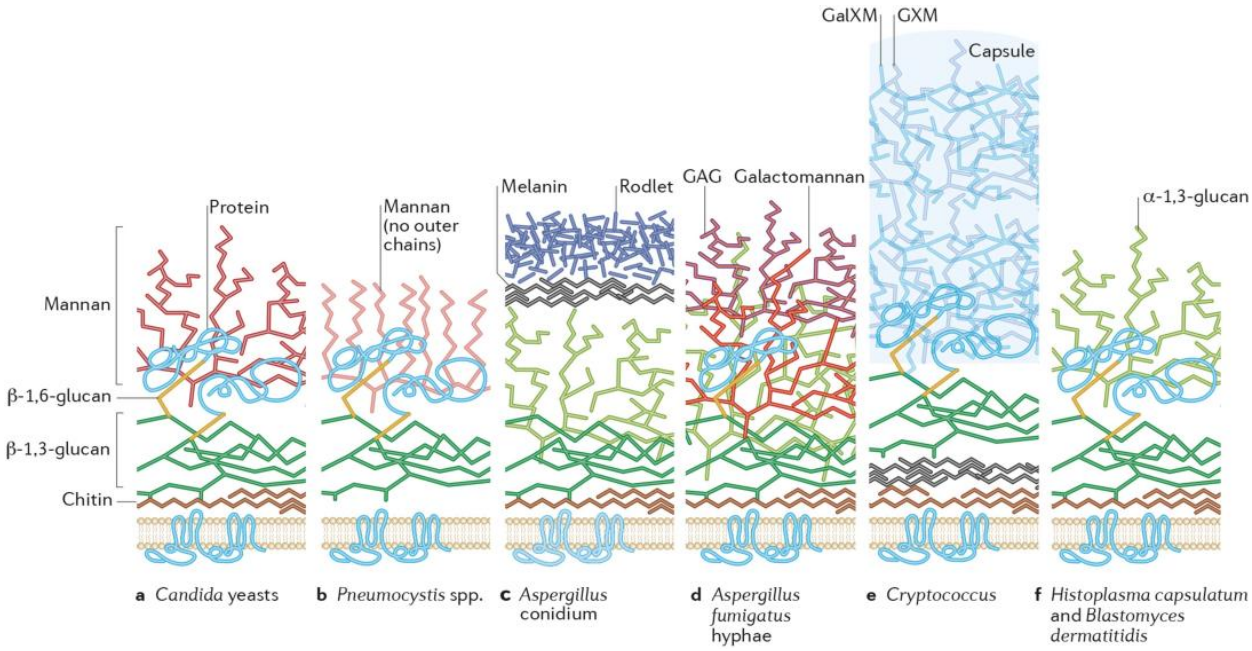

Figure 2.15 Cell wall structures of fungal pathogens. Reproduced from Gow et al. (Copyright 2017 American Society for Microbiology).[50]

2.3.2 Chitin

Chitin is the most abundant natural polymer after cellulose. It is widely distributed in cell

walls of fungi, exoskeletons of arthropods such as crustaceans and insects, radulae of mollusks, beaks of cephalopods, and scales of fish and lissamphibians.[52-54] The yeast cell wall contains only 1 to 2% chitin by dry weight, whereas chitin makes up 10 to 30% of the dry mass of the cell wall in filamentous fungi.[49] Chitin is a linear homopolysaccharide of *N*-acetyl-D-glucosamine that is connected by covalent β-(1→4) linkages, as shown in Figure 2.16. Structurally analogous to cellulose, chitin can be viewed as cellulose with the hydroxyl group at the C2 position on each monomer unit replaced with an acetamide group. The main roles of chitin are to provide organisms with support and protection and to prevent the loss of fluids in organisms. Chitin is not soluble in water, weak acids, and organic solvents, which is related to mixing entropy versus enthalpy and the strong inter- and intra-molecular hydrogen bonding interactions. It can be dissolved in some concentrated acids (e.g., formic acid), polar fluorinated solvents (e.g., hexafluoroisopropanol), DMAc/LiCl, aqueous alkali containing solvents (e.g., NaOH/urea), and ionic liquids.[10] The similar solubility between chitin and cellulose indicates some analogous reactions can be applied to them.

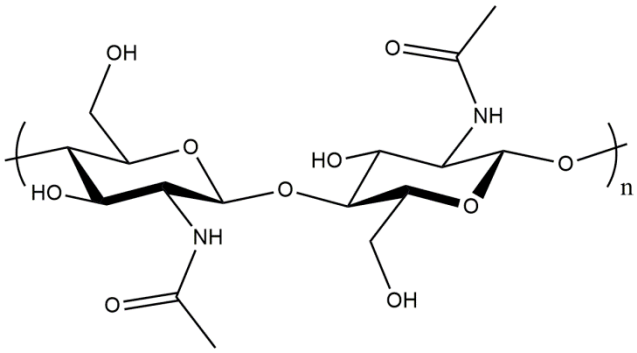

Figure 2.16 Molecular structure of chitin.

Chitin occurs as ordered crystalline microfibrils in nature. Pure chitin is translucent, pliable, resilient, and tough. However, it is always associated with many other materials to form composites in organisms. For example, chitin microfibrils cross-link glucans, glycoproteins, and

mannans to exist as a complex network in fungal cell walls. Chitin has two polymorphs, namely, α- and β-chitin. α-Chitin is rich in the cell walls of fungi, shells of lobsters and shrimps, and cuticles of insects, whereas the β-chitin mainly comes from the squid pens, tubes of pogonophorans and vestimentiferans, as well as spines of some diatoms.[52, 54] The unit cell of α-chitin consists of two antiparallel chains, and only one chitin chain is contained in the unit cell of β-chitin in a parallel arrangement.[54-55] Compared to β-chitin, α-chitin is much more abundant and thermodynamically stable. Under some conditions, such as acidic or alkaline processing, β-chitin can irreversibly convert to α-chitin. The most important derivative of chitin is chitosan which can be prepared by partial deacetylation of chitin. Chitin and chitosan are widely used in foods, cosmetics, and biomedical and pharmaceutical areas.[52]

2.3.3 Glucan

Glucans are the major structural component of fungal cell walls, accounting for 50 to 60% of the cell wall dry mass.[48-49] They are polysaccharides derived from D-glucose linked by glycosidic bonds and can be divided into α-glucans and β-glucans based on stereochemistry. α-Glucans are D-glucose polysaccharides linked through α-glycosidic bonds, while β-glucans consist of D-glucose monomers connected by β-glycosidic bonds.

β-Glucans, including β-1,3-glucan, β-1,4-glucan, and β-1,6-glucan, are the predominant glucans in fungal cell walls although some α-glucans, such as α-1,3-glucan and α-1,4-glucan, have been found. Among them, β-1,3-glucan makes up about 65 to 90% of the mass of the glucans in fungal cell walls, and the most abundant structure is present as a β-1,3-glucan backbone with β-1,6-glucan branches, as depicted in Figure 2.17.[49, 56-57] There is considerable structural variation between β-glucans from different sources which may differ in their molar mass, length of backbone, extent of branching, and position of branches.[58] These differences can

affect their physiological functions and physicochemical properties. β-Glucans offer a number of health benefits and are widely used in health care, foods, cosmetics, and animal feeds.[57]

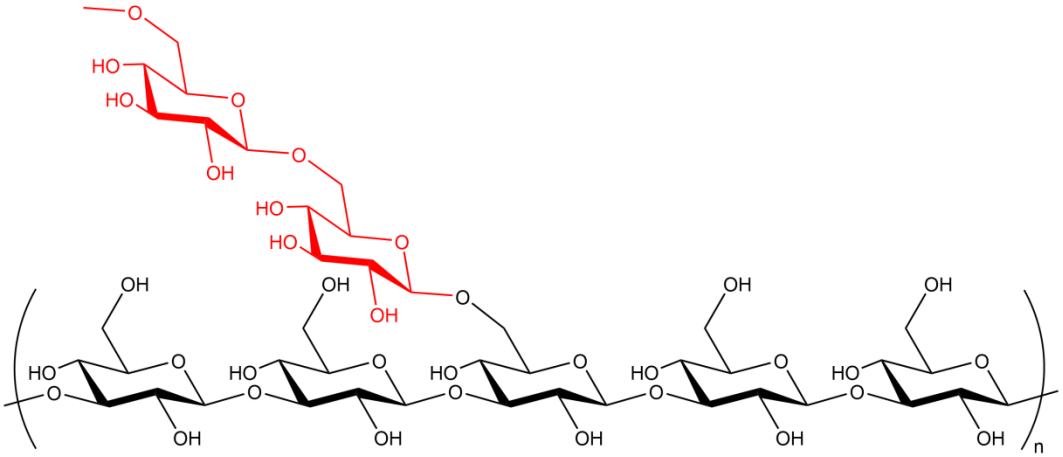

Figure 2.17 Structure of a β-1,3-glucan backbone with a β-1,6-glucan branch. The β-1,6-glucan is highlighted in red.

2.3.4 Glycoprotein

Glycoproteins are simply proteins with covalently attached carbohydrates, and they make up approximately 20 to 30% of the dry weight of the cell wall in filamentous fungi.[48-49, 59] Glycoproteins widely exist in almost all organisms, and the glycoproteins in the cell wall of fungi function for the preservation of cell shape, mediation of adhesion for cell migration and fusion, protection of cells from foreign substances, adjustment of absorption of molecules, transmission of intracellular signals from external stimuli, and synthesis of cell wall components.[49-50]

The carbohydrates on glycoproteins are short and usually branched molecules which may be simple sugars (e.g., glucose), amino sugars (e.g., *N*-acetylglucosamine), and acidic sugars (e.g., sialic acid). The connection between carbohydrates and proteins can be categorized into N-glycosylation, O-glycosylation, P-glycosylation, C-glycosylation, S-glycosylation, glypiation,

and glycation. N-linked glycoproteins, O-linked glycoproteins, and GPI-anchored glycoproteins that correspond to N-glycosylation, O-glycosylation, and glypiation, respectively, are usually present in fungal cell walls, as shown in Figure 2.18.[49, 59-61] N-glycosylation is the attachment of carbohydrate to nitrogen, typically on the amide side chain of asparagine. O-glycosylation refers to carbohydrate bond to oxygen, usually on serine or threonine, and sometimes on hydroxylysine or hydroxyproline. Glypiation is a glycophosphatidylinositol (GPI) glycolipid attached to the carbon terminus of a polypeptide. The glycoproteins are integrated into the fungal cell wall through the linkages between their carbohydrates and other components, such as glucan and chitin.

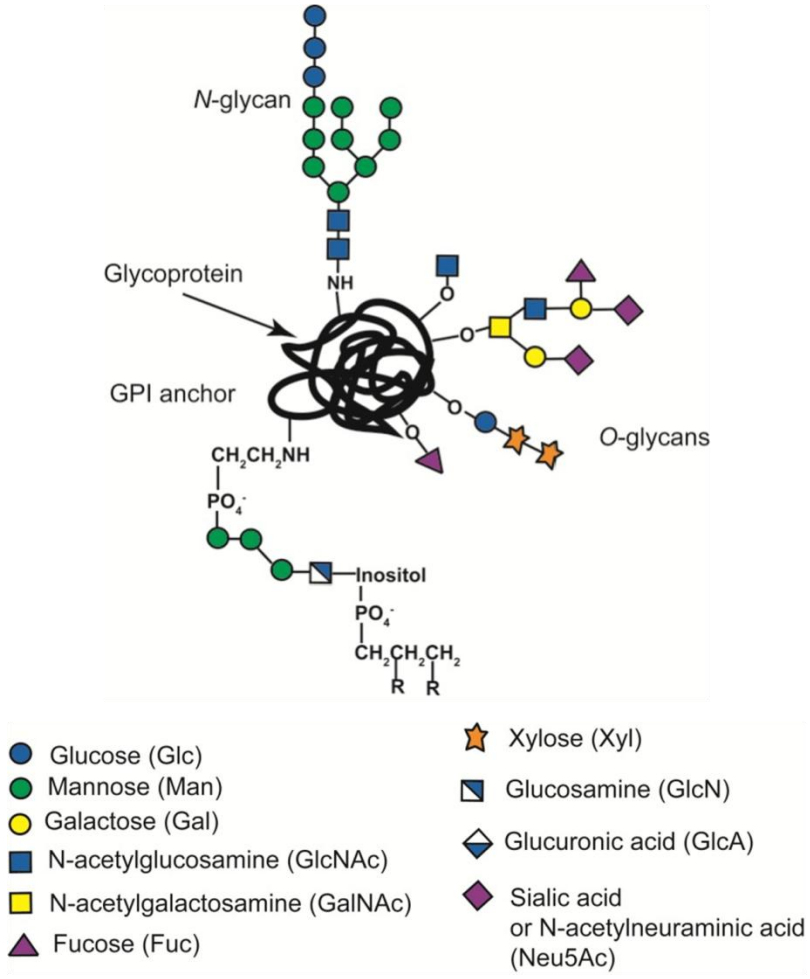

Figure 2.18 Symbolic representations of some glycosylations in glycoproteins. Adapted from Zandberg (Copyright 2010 Wesley F. Zandberg).[61]

2.4 Enzymes for Degradation of Polymers in Plant and Fungal Cell Walls

Biodegradability is a notable feature of natural polymers. The biodegradation of natural polymers is essential to maintain the carbon cycle in the biosphere. Most biopolymers in nature are degraded through the enzymatic action of microorganisms. An exploration of enzyme-biopolymer interactions is of vital importance to the application of biopolymers and related enzymes and understanding how cells and nature work.

2.4.1 Cellulases

Cellulases are a family of enzymes that catalyze the decomposition of cellulose and some related polysaccharides, which is actually a process of enzymatic hydrolysis of glycosidic linkages depolymerizing cellulose and other related cello-oligosaccharide derivatives to fermentable sugars.[62-63] Cellulases can be naturally produced by a wide spectrum of fungi, bacteria, and protozoans, and they are increasingly used in industries, such as textile, pulp and paper, detergent, food, animal feed, and the biorefinery.[63-64]

Complete hydrolysis of cellulose needs synergistic action of three principle types of cellulases, namely, endoglucanases, exoglucanases or cellobiohydrolases, and β-glucosidases, and their roles are exhibited in Figure 2.19.[62-63, 65] Endoglucanases preferentially break down glycosidic bonds in a random manner in the amorphous regions of the cellulose, generating long chain oligomers. Exoglucanase acts on the long chain oligomers from either the reducing or non-reducing ends, primarily liberating cellobiose. β-glucosidase further cleaves cellobiose and other cellodextrins with a low degree of polymerization into glucose. A few other cellulases have been identified. Cellulose is depolymerized by oxidative cellulase through free radical reactions, and cellulose phosphorylase decomposes cellulose by means of phosphates.[63]

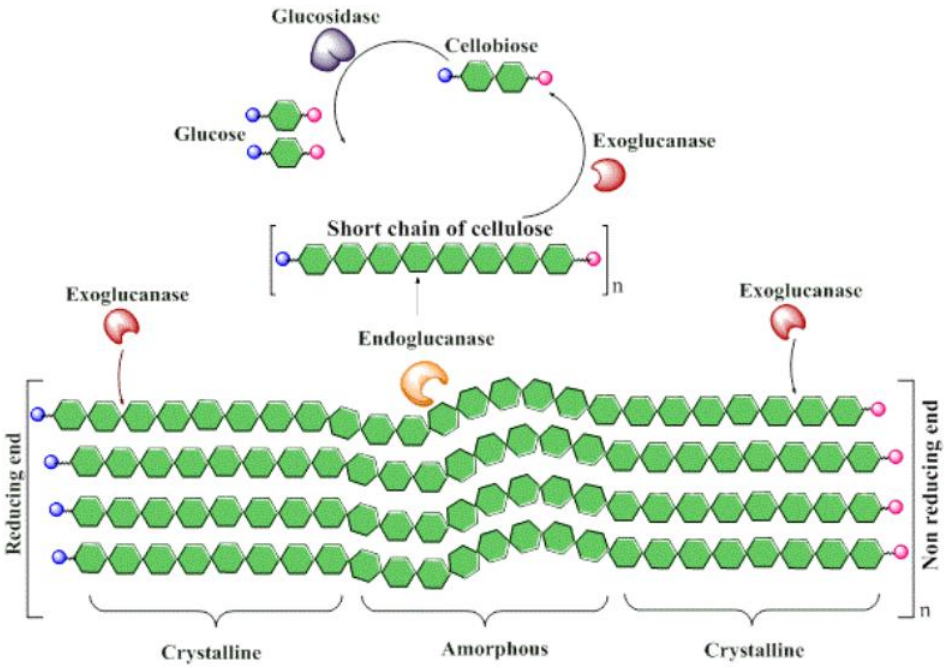

Figure 2.19 Enzymatic hydrolysis of cellulose. Reproduced from Sajith et al. (Copyright 2016 Authors).[62]

2.4.2 Ligninolytic Enzymes

Lignin is chemically recalcitrant to degradation due to its complex structure, and treating lignin with ligninolytic enzymes as an environmentally friendly method for lignin degradation has drawn much attention. Many ligninolytic enzymes can be found in various types of organisms, including plants, bacteria, insects, and fungi, of which white-rot fungi are the most well-known.[66] Ligninolytic enzymes are mainly used to reduce the content of lignin and some other substances, like phenolic compounds and furan derivatives, in biotechnological processes, and therefore, they are involved in the pulp and paper, animal feed, biofuel, laundry detergent, brewery and wine, and food industries, and for chemical pollutant remediation.[66-67]

Ligninolytic enzymes are generally a family of oxidative extracellular enzymes that primarily consist of laccase, lignin peroxidase (LiP), manganese peroxidase (MnP), and versatile

peroxidase (VP), as displayed in Figure 2.20.[68-71] Some other enzymes, such as veratryl alcohol oxidase, aryl alcohol dehydrogenase, quinone oxidoreductase, aromatic acid reductase, vanillate hydroxylase, dioxygenase, catalase, aromatic aldehyde oxidase, and glyoxal oxidase, can also participate in lignin degradation.[72] Laccases or phenol oxidases are multicopper-containing glycoproteins which preferably catalyze the oxidation of phenolic compounds. The peroxidases belong to heme glycoproteins and require H_2O_2 for their activity. LiPs possess high redox potential and can oxidize a wide number of phenolic, aromatic, and non-phenolic substrates. MnPs oxidize Mn(II) to Mn(III), which facilitates the degradation of phenolic structures.[66, 72-74] VPs are also known as hybrid peroxidases (manganese-lignin peroxidases). They have catalytic characteristics of LiP and MnP, and therefore, can oxidize substrates typical for both of them, such as Mn(II), phenolic lignin, and non-phenolic lignin.

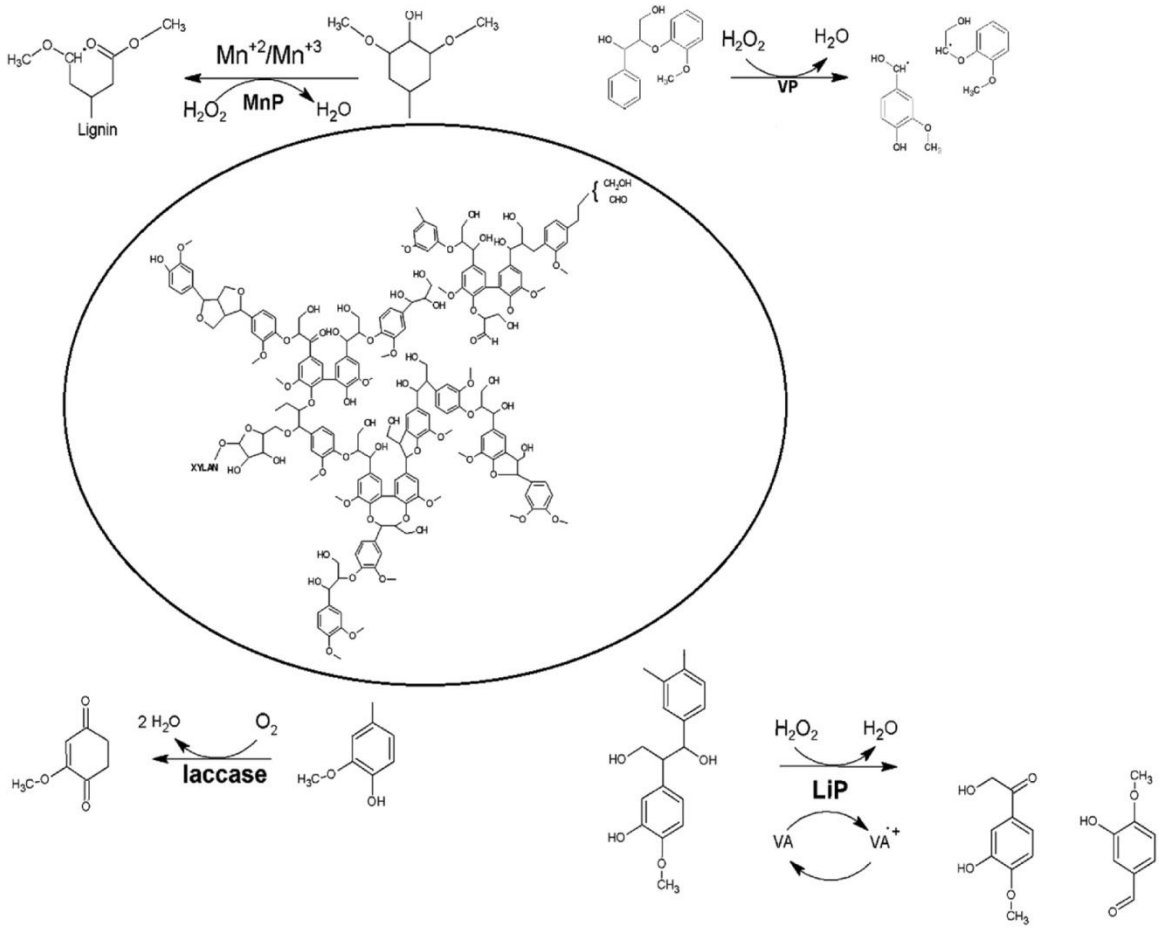

Figure 2.20 Degradation of lignin by laccase, LiP, MnP, and VP. Adapted from Kumar et al. (Copyright 2020 Authors).[68]

2.4.3 Pectinases

Pectinases are a collective term for enzymes that degrade pectin into simpler molecules like galacturonic acids. The main sources of pectinases are plants and microorganisms, and the most commonly used pectinase in industry is from *Aspergillus niger*.[75-76] Pectinases have extensive applications in fruit and vegetable processing, textile and wine industries, animal feed, vegetable oil extraction, tea and coffee fermentation, kraft pulp biobleaching, and waste management.[76-78]

Pectinases can be broadly classified into pectinesterases, depolymerizing enzymes, and protopectinases. The chemical processes by which pectinases break down pectin are depicted in

Figure 2.21.[78-80] Pectinesterases catalyze deesterification of methoxyl group of pectin, yielding pectic acids. Depolymerizing enzymes catalyze the cleavage of α-1,4-glycosidic bonds in pectin, and they include hydrolases (polygalacturonases and polymethylgalacturonases) and lyases (polygalacturonate lyases and polymethylgalacturonate lyases). Hydrolases depolymerize pectin through hydrolysis, whereas lyases break down pectin via a trans-elimination reaction. Protopectin can be dissolved in protopectinases to form highly polymerized soluble pectin.

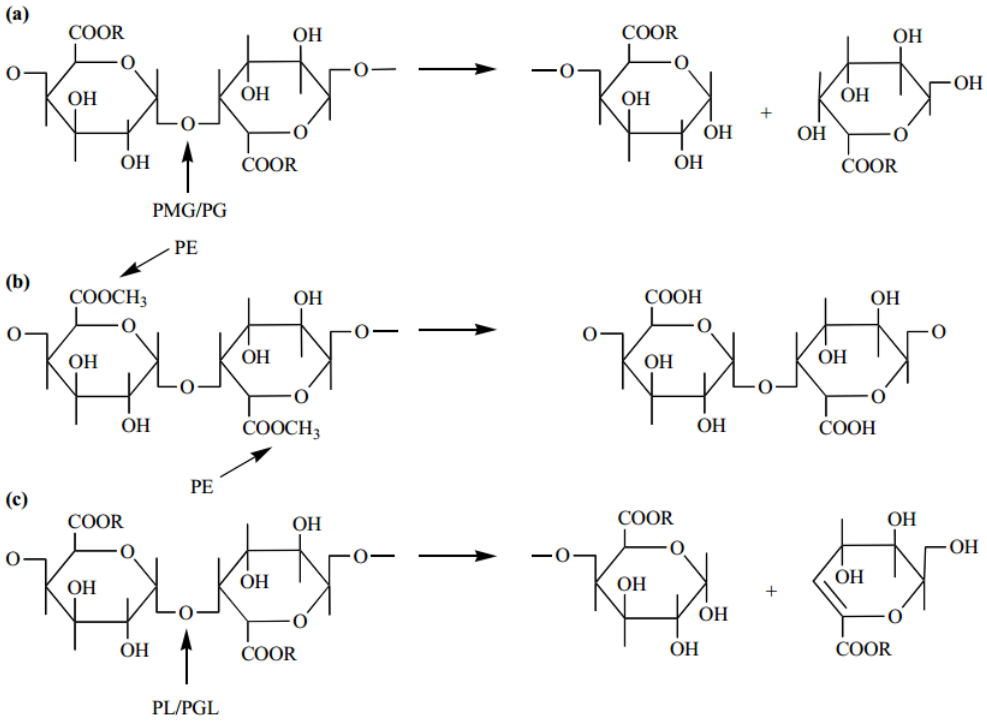

Figure 2.21 Enzymatic degradation of pectin. PMG, polymethylgalacturonases; PG, polygalacturonases; PE, pectinesterases; PL, pectin lyases; PGL, polygalacturonate lyases. Reproduced from Pedrolli et al. (Copyright 2009 Authors).[79]

2.4.4 Chitinases

Chitin does not accumulate in nature because of chitinases. They are hydrolytic enzymes that catalyze the degradation of chitin by breaking glycosidic bonds.[81] Chitinases have been found in various organisms, including bacteria, fungi, plants, invertebrates, and vertebrates. They are

attracting increased attention in the field of biotechnology applied to pest control, preparation of chitin-oligosaccharides, production of single-cell proteins, control of pathogenic fungi, isolation of protoplasts, and treatment of chitinous waste.[82]

Chitinases are broadly classified as endochitinases and exochitinases, containing both chitobiosidases and *N*-acetylglucosaminidases. The combination of these chitinases leads to a synergistic increase in the chitinolytic activity, as shown in Figure 2.22.[81, 83] Endochitinases can randomly cleave at internal sites in the chitin chain, generating dimer and low molar mass oligomers, such as chitobiose, chitotriose, and chitotetraose. Chitobiosidases act progressively on the non-reducing end of chitin to release chitobiose, and *N*-acetylglucosaminidases cleave the oligomers into *N*-acetylglucosamine units. Based upon the amino acid sequence and similarity, chitinases can also be categorized into the 18, 19, and 20 families.

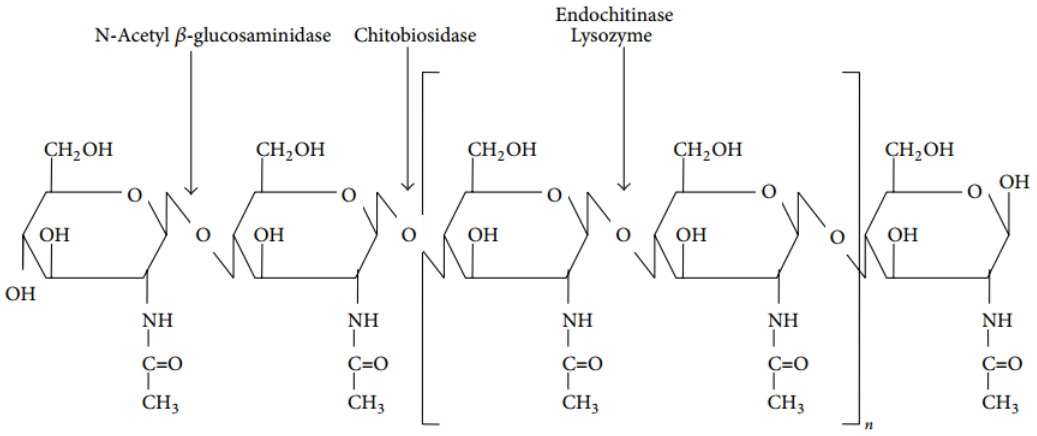

Figure 2.22 Enzymatic degradation of chitin. Reproduced from Rathore et al. (Copyright 2015 Authors).[81]

2.5 Polymer Surfaces and Natural Polymer Thin Films

The surfaces of natural polymers are critical to their properties and applications. They are well involved in diagnosis, therapy, tissue engineering, and cell growth, proliferation,

differentiation, migration, and invasion.[84] Numerous reactions in organisms occur at interfaces, and quantities of biopolymers are directly in contact with other components in nature. It is vital to understand these surfaces, and polymer thin films provide an excellent platform to investigate them.

2.5.1 Polymer Surfaces

Polymers are usually fixed to a solid substrate via adsorption or grafting. Adsorption is often a simple spontaneous physical process, while grafting generally refers to polymers attached chemically to the substrate surface.

2.5.1.1 Polymer Adsorption

If the polymers prefer the substrate to the solvent, they will form an adsorption layer at the substrate surface, as shown in Figure 2.23a.[11, 85-86] The volume fraction occupied by the polymers decreases with an increase in the distance from the substrate surface. Conversely, a depletion layer will be formed near the substrate surface if the interaction between the polymer and the substrate is smaller than the interaction of the polymer with the solvent, as displayed in Figure 2.23b.[11, 85-86] The polymer volume fraction increases as the distance from the substrate surface becomes large.

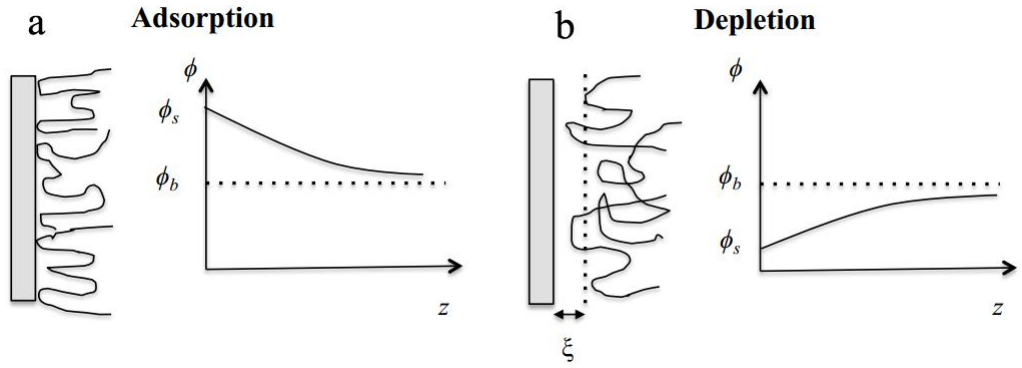

Figure 2.23 Polymer formation of (a) an adsorption layer and (b) a depletion layer at a solid substrate surface. ϕ, polymer volume fraction; z, distance from the substrate surface; ϕ_s, polymer volume fraction at the surface; ϕ_b, polymer volume fraction in the bulk solution. Adapted from Zhang (Copyright 2014 Xiao Zhang).[11]

The "loop-train-tail" model is commonly used to describe the conformation of an adsorbed polymer chain. The chain can be regarded as an assembly of loops, trains, and tails, as exhibited in Figure 2.24.[11, 87-89] Only some segments of the chain are in contact with the substrate, which are present in trains. Loops refer to desorbed chain segments that are separated by two trains, and tails are end segments with only one contact point with the substrate.

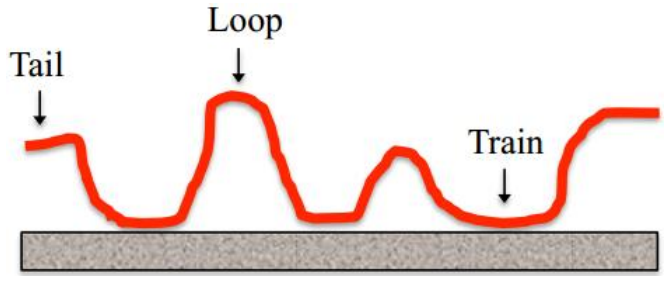

Figure 2.24 Conformation of an adsorbed neutral polymer chain. Reproduced from Zhang (Copyright 2014 Xiao Zhang).[11]

2.5.1.2 Polymer Grafting

Grafted polymer chains form laterally inhomogeneous cluster structures and thus generate a

flattened shape when their density on the substrate is low, as shown in Figure 2.25.[85, 90-92] With an increase in the density of polymer chains, they are obliged to stretch themselves, changing from mushrooms to brushes, due to space limitations.[85, 91-92] Consequently, the thickness of the polymer thin film increases.

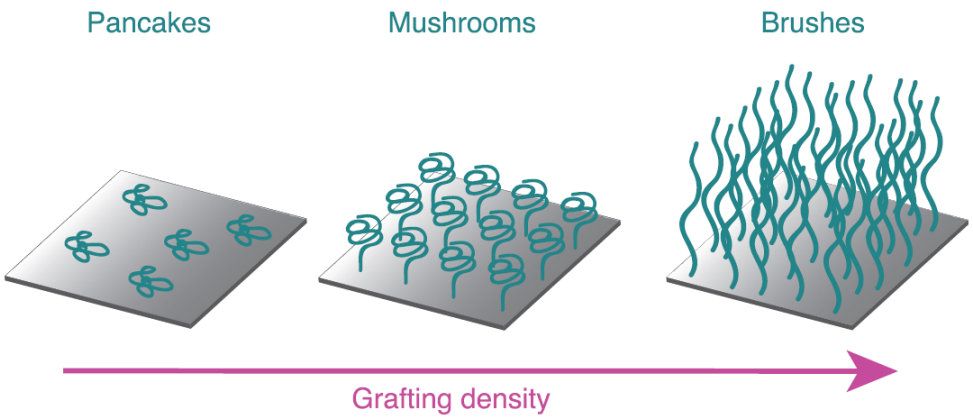

Figure 2.25 Changes in the conformation of grafted polymer chains with an increase in grafting density, from pancakes via mushrooms to brushes. Reproduced from Hildebrandt et al. (Copyright 2020 Authors).[93]

There are many factors that affect the conformation of grafted polymer chains, including the substrate, solvent, and architecture of polymers. These factors lead to the polymer surfaces with diverse properties. Generally, polymer chains tend to stretch in a good solvent and contract in a poor solvent. As the length of polymer chains increases, chain tilting gradually becomes significant, especially when shear flow is applied to the polymer, as depicted in Figure 2.26.[91, 94-95] The polymer chains may collapse if the shear forces exceed the threshold.

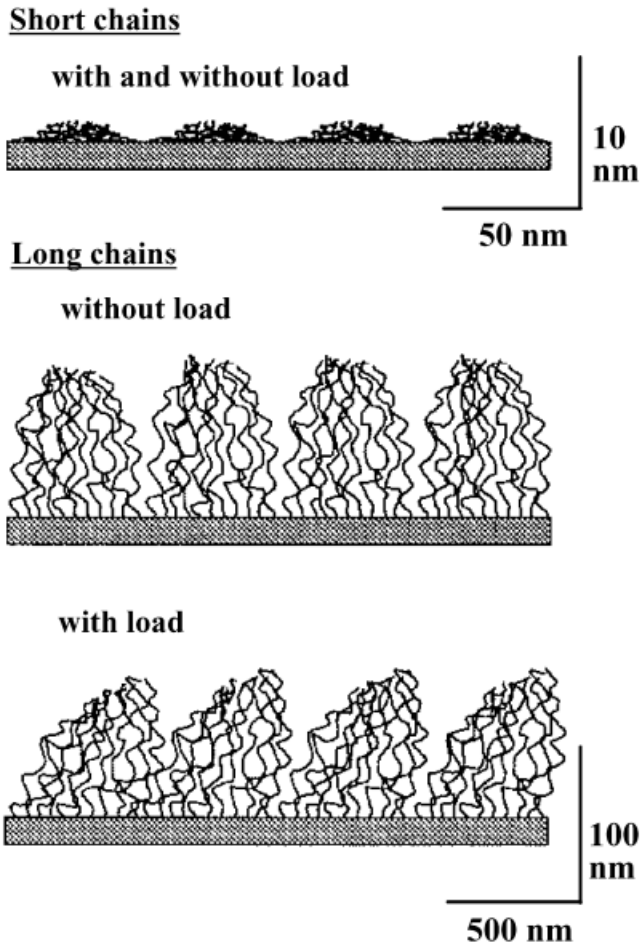

Figure 2.26 Polymer chain tilting and the effect of chain length. Reproduced from Kato et al. (Copyright 2003 Elsevier Science Ltd.).[91]

Ionic polymer chains on substrates have a different conformation from those described for neutral polymer chains, as displayed in Figure 2.27.[91, 96] The double layer and slipping plane are similar to a conventional rigid surface when the ionic polymer chains are short. As the ionic polymer chain length increases, the chains extend away from the substrate, resulting in a shift of the slipping plane and interweaving of ionic chains. Consequently, the movement of ionic polymer chains is restricted and the dissociation of ionic groups is suppressed.

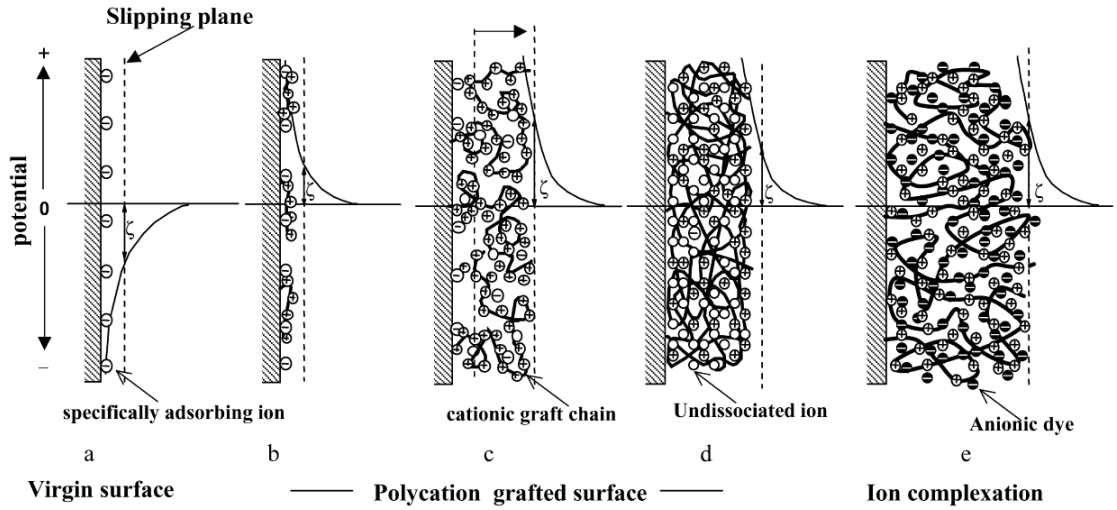

Figure 2.27 Structure of grafted polycation chains with different lengths. Reproduced from Kato et al. (Copyright 2003 Elsevier Science Ltd.).[91]

2.5.2 Natural Polymer Thin Films

Some usual methods to prepare thin films include solvent casting, dip-coating, spin-coating, and Langmuir-Blodgett (LB) deposition. Spin-coating and LB-deposition are the two methods mainly used for preparation of natural polymer thin films. Spin-coating utilizes centrifugal force created by a spinning substrate to spread a coating solution evenly over a surface to generate a uniform thin film.[10, 97] LB-deposition is a process in which the coating material spreads over a liquid (usually water) surface to form a Langmuir monolayer, and then the monolayer is transferred onto a solid substrate to generate the LB film.[10, 98] A multilayer film can be fabricated if the process is repeated.

2.5.2.1 Lignin Thin Films

Various techniques have been developed to fabricate lignin thin films, including spin-coating, LB-deposition, self-assembly, solvent casting, electrodeposition, and surface-initiated polymerization of monolignols. These techniques with different advantages and disadvantages

often bring about lignin thin films possessing diverse morphologies.

Spin-coating is the most common method to fabricate lignin thin films. Notley et al.[99] spin-coated a softwood Kraft lignin/ammonium hydroxide solution onto silica substrates at a spinning speed of 1500 rpm for 60 s. The prepared lignin thin film had a thickness of 60 to 75 nm and smooth surface with roughness in the range of 1 to 2 nm. Rahikainen et al.[100] utilized lignins from spruce and wheat straw with steam explosion and without pre-treatment to fabricate ultrathin lignin films by spin-coating under the same conditions. The steam explosion pre-treated lignin showed a higher enzyme (Cel7A of *Trichoderma reesei*) adsorption capacity and inhibitory effect on hydrolysis.

Fabrication of LB multilayer lignin films were first reported by Constantino et al. in 1996.[101] Tetrahydrofuran solutions of lignins from *Pinus caribaea hondurensis* and sugar cane bagasse were spread onto ultrapure water surfaces to form Langmuir monolayers followed by transfer onto aluminized glass slides. It was found that the thickness of both types of lignin films increased linearly with the number of deposited layers at a rate of 6 nm per layer. Martins et al.[102] adopted a similar procedure to prepare LB lignin films. Solutions of lignin in tetrahydrofuran were deposited onto water, and then Y-type LB films formed on substrates of gold interdigitated electrodes and indium-tin oxide coated glass, respectively.

Lignin can usually associate with cationic chemicals due to the numerous negatively charged functional groups. Taking advantage of this characteristic, a few papers reported the fabrication of lignin films by self-assembly. Maximova et al.[103] used mica and cellulose fibers, respectively, to adsorb lignin from aqueous solution in the presence of cationic polyelectrolytes to prepare lignin layers. Paterno et al.[104] studied the formation of lignin layers on the surface of poly(*o*-ethoxyaniline) at different pH.

Solvent casting is similar to self-assembly to some extent. The orientation and organization of lignin molecules on substrate surfaces varies with the chemical make-up of lignin and categories of substrates. Lignin can be oriented parallel to the substrate resulting in a flat surface or form aggregates perpendicular to the substrate. Micic et al.[105] dropped a lignin water suspension onto the surface of a cellulose-acetate film and then dried it at room temperature. Stergiou et al.[106] prepared a lignin film-modified glassy carbon electrode by dropping 10 or 20 μL of lignin in acetone solution onto the 3 mm diameter active surface of the electrode which was then left to air-dry.

Landaeta et al.[107] electrodeposited lignin onto a glassy carbon electrode in a solution of 0.25 mg/mL lignin and 0.5 M sulfuric acid by applying a cyclic potential between -0.6 and 1.0 V *vs.* Ag/AgCl/KCl at a scan rate of 100 mV/s for 20 cycles. The electrodeposited lignin film had a density of 1×10^{-9} mol/cm^2, which indicated a multilayer structure. Amare et al.[108] employed a mixed solution of lignin, sulfuric acid, and nitric acid to electrodeposit lignin films on the surface of glassy carbon electrodes potentiostatically at 0.9 V for 2 min.

Synthesis of lignin is another way to prepare lignin thin films. Wang et al.[109] polymerized monolignols via dehydrogenative polymerization that was catalyzed by horseradish peroxidase (HRP) physically immobilized on gold or silica surfaces. The type and concentration of monolignol and temperature had a great effect on the kinetics of the surface-immobilized HRP-initiated dehydrogenative polymerization and the morphologies of the resulting dehydrogenative polymer (DHP) thin films. Micic et al.[110] synthesized lignin on the surface of a cellulose diacetate film using a 120 W low-pressure mercury lamp to irradiate a solution of coniferyl alcohol in phosphate buffer at pH 7.6 for 2 h. The prepared lignin had a rough surface with many patches and holes.

Comparing the above methods, solvent casting is relatively simple to operate. However, the lignin films fabricated by it are usually thick and not smooth. Self-assembly can only be employed in certain situations and is not a general method. Electrodeposition may cause the prepared lignin films to have a large roughness due to the fact that lignin molecules sometimes prefer to be deposited onto some active sites of the electrode. Chemical synthesis is hard to handle, whereas the composition and structure of the lignin films can be well adjusted. LB-deposition often brings about ultrathin lignin films and the thickness is precisely controlled. Spin-coating is commonly used on account of the ease of operation and extensive applicability.

2.5.2.2 Chitin Thin Films

Chitin thin films have been widely studied, and the major methods for preparing them include spin-coating, chemical synthesis, solvent casting, dip-coating, and solvent exchange for coagulation.

Spin-coating is an effective way to produce chitin thin films. Gasteleijn et al.[111] dissolved chitin in a solution of dimethylacetamide and 5% lithium chloride at a concentration of 0.1% (w/v), and then spin-coated the solution onto bare gold surfaces or polystyrene-coated gold surfaces at a spinning speed of 3600 rpm for 1 min. The obtained chitin films on gold and polystyrene had similar thicknesses that were 1910 and 1790 nm in air (the chitin films were spin-coated and then dried), 49 to 189 and 26 to 156 nm in buffer (the chitin films were spin-coated, wetted with buffer, and then dried; buffer: 20 mM TEA, 1 mM EDTA, 1 mM DTT, 1 mM NaN_3, pH 8 at 25 ℃), respectively. A more uniform and stable structure was observed for the chitin film on polystyrene.

Spin-coating is combined with chemical synthesis to prepare chitin thin films in some reports. Kittle et al.[112] fabricated smooth, homogeneous, and ultrathin chitin films for the first time.

Solutions of trimethylsilyl chitin (TMSChi) in a mixture of chloroform/tetrachloroethane were spin-coated onto gold or silica substrates at 3000 rpm for 1 min, followed by exposing the obtained TMSChi film to the vapor of a 10% hydrochloric acid aqueous solution for 2 min to regenerate it to an amorphous chitin (RChi) film. The RChi films produced on gold surfaces had a thickness of ~15 nm with a roughness of ~1.2 nm, whereas the thickness of the RChi films on silica surfaces were ~21 nm.

The procedures of solvent casting and dip-coating are similar. Both of them utilize the evaporation of solvent to create chitin films. Ramirez-Wong et al.[113] prepared a solution of chitin in hexafluoroisopropanol at a concentration of 0.5% (w/w), and then simply poured it on a Teflon disc inside a petri dish. After the solvent evaporated at ambient temperature, chitin films were obtained. Montiel-Gonzalez et al.[114] employed dip-coating to fabricate chitin films with a thickness range of 120 to 200 nm by dipping silicon substrates into a solution of chitin in hexafluoroisopropanol at different substrate withdrawal speeds, followed by drying at 100 ^{o}C for 6 h in air. It was found that the thickness and refractive index of chitin films decreased with an increase in temperature.

A widely used method to prepare chitin films starts with solvent exchange to have chitin precipitate and coagulate, followed by applying different drying manners to create chitin films with diverse morphologies. This method can be viewed as a kind of solvent casting. Chakravarty et al.[115] dissolved chitin in 1-ethyl-3-methylimidazolium acetate ionic liquid at 80-90 ^{o}C to form a homogeneous and viscous solution of amber color. After that, the solution was transferred to a cultivation plate and submerged in deionized water for coagulation. Then, the cultivation plate was removed, and the coagulated chitin membrane was washed by water 6 to 8 times to completely wash away the ionic liquid. Finally, the chitin membrane was transferred to non-stick

parchment paper and dried via four different methods, namely air, press, methanol, and freeze drying. Compared to the other methods, the chitin membrane prepared by freeze drying was highly porous. King et al.[116] used a similar process to fabricate chitin films. They found that the drying methods significantly affected the strength, flexibility, morphology, and porosity of the films.

The characteristics of the methods to prepare chitin films are similar to those for the preparation of lignin films. The solvent exchange followed by drying solves the problem to some extent that the film fabricated through solvent casting is not uniform and smooth enough.

2.6 Quartz Crystal Microbalance with Dissipation Monitoring

Quartz crystal microbalance with dissipation monitoring (QCM-D) experiments are real-time and label-free methods for analyzing surface phenomena at the nanoscale. They can provide information about mass and structural changes in thin films. Mass changes as low as 0.5 ng/cm^2 and thickness changes ranging from ~1 Å to 1 μm can be detected. Due to these characteristics, the QCM-D is used for the study of a variety of processes (adsorption, desorption, binding, interactions, degradation, fouling, crosslinking, swelling, etc.) taking place on various molecules and entities (water molecules, lipids, proteins, surfactants, nanoparticles, polymers, cells, etc.).[10-11, 117-120] It can be applied to a broad range of areas, such as drug discovery, biomaterials, biophysics, coatings and materials, nanotechnology, cleaning and detergents, oil and gas, biofuels, and environmental science.[10-11, 117-120]

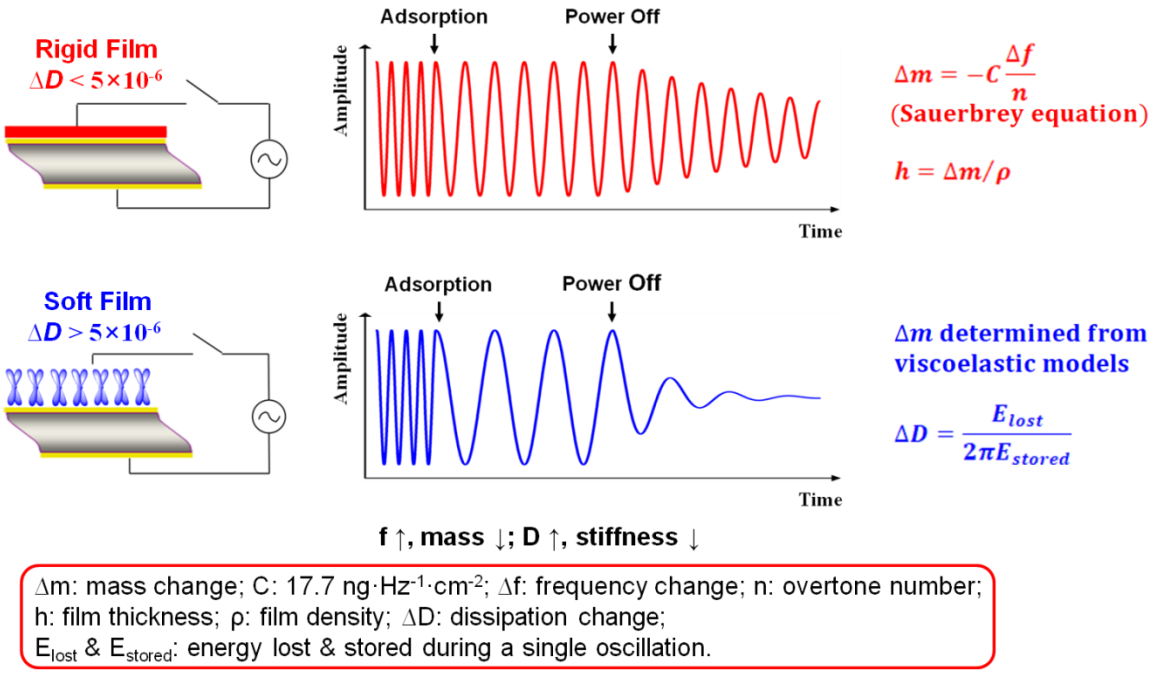

Figure 2.28 Mechanism for QCM-D. Adapted from Wang (Copyright 2014 Chao Wang).[10]

The QCM-D sensor comprises a thin quartz disc sandwiched between a pair of electrodes. Due to the piezoelectric properties of quartz, the sensor will oscillate when an alternating voltage is applied. The oscillation frequency relies on the total mass of the sensor. If a rigid film is deposited onto the sensor, the frequency will decrease, and the decreased frequency is proportional to the mass of the film that can be calculated through the Sauerbrey equation, as shown in Figure 2.28.[10-11] Furthermore, the thickness of the film can be calculated from the density. The oscillation of the sensor will be dampened if a soft film is attached. As a result, the Sauerbrey relation will underestimate the mass of the film which can be more accurately deduced from viscoelastic models.[10-11] The viscoelasticity of the film can be revealed by monitoring the energy dissipation during a single oscillation of the sensor after the driving power is switched off. Qualitatively, the frequency and dissipation decrease with an increase in mass of the film and rigidity, respectively, no matter how rigid or soft the film is.

2.7 References

1. Kaushik, K.; Sharma, R. B.; Agarwal, S., Natural polymers and their applications. *Int J Pharm Sci Rev Res* **2016,** *37*, 30-36.

2. Shanmugam, S.; Manavalan, R.; Venkappayya, D.; Sundaramoorthy, K.; Mounnissamy, V. M.; Hemalatha, S.; Ayyappan, T., Natural polymers and their applications. *Nat Prod Rad* **2005,** *4*, 478-481.

3. *Natural polymers: industry techniques and applications*; Olatunji, O., Ed.; Springer: 2016.

4. Ochoa-Villarreal, M.; Aispuro-Hernandez, E.; Vargas-Arispuro, I.; Martinez-Tellez, M. A. Plant cell wall polymers: function, structure and biological activity of their derivatives. IntechOpen: 2012; pp 63-86.

5. Palin, R. J. A comparison of cell wall properties of Arabidopsis thaliana. Ph.D. Dissertation, University of Birmingham, United Kingdom, 2011.

6. Timell, T. E.; Syracuse, N. Y., Recent progress in the chemistry of wood hemicelluloses. *Wood Sci Technol* **1967,** *1*, 45-70.

7. Zietsman, J. J. Investigating grape berry cell wall deconstruction by hydrolytic enzymes. Ph.D. Dissertation, Stellenbosch University, South Africa, 2015.

8. Cosgrove, D. J., Expansive growth of plant cell walls. *Plant Physiol Biochem* **2000,** *38*, 109-124.

9. Wang, T.; Yang, H.; Kubicki, J. D.; Hong, M., Cellulose structural polymorphism in plant primary cell walls investigated by high-field 2D solid-state NMR spectroscopy and density functional theory calculations. *Biomacromolecules* **2016,** *17*, 2210-2222.

10. Wang, C. Renewable natural polymer thin films and their interactions with biomacromolecules. Ph.D. Dissertation, Virginia Tech, Blacksburg, VA, 2014.

11. Zhang, X. Adsorption of biomacromolecules onto polysaccharide surfaces. Ph.D. Dissertation, Virginia Tech, Blacksburg, VA, 2014.

12. Klemm, D.; Heublein, B.; Fink, H. P.; Bohn, A., Cellulose: fascinating biopolymer and sustainable raw material. *Angew Chem Int Ed Engl* **2005,** *44*, 3358-3393.

13. Habibi, Y.; Lucia, L. A.; Rojas, O. J., Cellulose nanocrystals: chemistry, self-assembly, and applications. *Chem Rev* **2010,** *110*, 3479-3500.

14. O'Sullivan, A. C., Cellulose: the structure slowly unravels. *Cellulose* **1997,** *4*, 173-207.

15. Liebert, T. Cellulose solvents - remarkable history, bright future. In *Cellulose solvents: for analysis, shaping and chemical modification*; Liebert, T. F., Heinze, T. J., Edgar, K. J., Eds.; American Chemical Society: Washington, DC, 2010; pp 3-54.

16. Xiong, W.; Qiu, X.; Zhong, R.; Yang, D., Characterization of the adsorption properties of a phosphorylated kraft lignin-based polymer at the solid/liquid interface by the QCM-D approach. *Holzforschung* **2016,** *70*, 937-945.

17. Aadil, K. R.; Barapatre, A.; Meena, A. S.; Jha, H., Hydrogen peroxide sensing and cytotoxicity activity of *Acacia* lignin stabilized silver nanoparticles. *Int J Biol Macromol* **2016,** *82*, 39-47.

18. Tolbert, A.; Akinosho, H.; Khunsupat, R.; Naskar, A. K.; Ragauskas, A. J., Characterization and analysis of the molecular weight of lignin for biorefining studies. *Biofuels, Bioprod Biorefin* **2014,** *8*, 836-856.

19. Notley, S. M.; Norgren, M., Adsorption of a strong polyelectrolyte to model lignin surfaces.

Biomacromolecules **2009,** *9*, 2081-2086.

20. Saarinen, T.; Orelma, H.; Gronqvist, S.; Andberg, M.; Holappa, S.; Laine, J., Adsorption of different laccases on cellulose and lignin surfaces. *BioResources* **2009,** *4*, 94-110.

21. Zakzeski, J.; Bruijnincx, P. C. A.; Jongerius, A. L.; Weckhuysen, B. M., The catalytic valorization of lignin for the production of renewable chemicals. *Chem Rev* **2010,** *110*, 3552-3599.

22. Liu, Q.; Luo, L.; Zheng, L., Lignins: biosynthesis and biological functions in plants. *Int J Mol Sci* **2018,** *19*, 335.

23. Chen, F.; Tobimatsu, Y.; Havkin-Frenkel, D.; Dixon, R. A.; Ralph, J., A polymer of caffeyl alcohol in plant seeds. *Proc Natl Acad Sci USA* **2012,** *109*, 1772-1777.

24. Chen, F.; Tobimatsu, Y.; Jackson, L.; Nakashima, J.; Ralph, J.; Dixon, R. A., Novel seed coat lignins in the Cactaceae: structure, distribution and implications for the evolution of lignin diversity. *Plant J* **2013,** *73*, 201-211.

25. Rawal, T. B.; Zahran, M.; Dhital, B.; Akbilgic, O.; Petridis, L., The relation between lignin sequence and its 3D structure. *Biochim Biophys Acta Gen Subj* **2020,** *1864*, 129547.

26. Li, Y.; Shuai, L.; Kim, H.; Motagamwala, A. H.; Mobley, J. K.; Yue, F.; Tobimatsu, Y.; Havkin-Frenkel, D.; Chen, F.; Dixon, R. A.; Luterbacher, J. S.; Dumesic, J. A.; Ralph, J., An "ideal lignin" facilitates full biomass utilization. *Sci Adv* **2018,** *4*, eaau2968.

27. Liu, C.; Wang, S.; Wang, B.; Song, G., Catalytic hydrogenolysis of castor seeds C-lignin in deep eutectic solvents. *Ind Crop Prod* **2021,** *169*, 113666.

28. Berstis, L.; Elder, T.; Crowley, M.; Beckham, G. T., Radical nature of C-lignin. *ACS Sustainable Chem Eng* **2016,** *4*, 5327-5335.

29. Tobimatsu, Y.; Chen, F.; Nakashima, J.; Escamilla-Trevino, L. L.; Jackson, L.; Dixon, R. A.; Ralph, J., Coexistence but independent biosynthesis of catechyl and guaiacyl/syringyl lignin polymers in seed coats. *Plant Cell* **2013,** *25*, 2587-2600.

30. Stone, M. L.; Anderson, E. M.; Meek, K. M.; Reed, M.; Katahira, R.; Chen, F.; Dixon, R. A.; Beckham, G. T.; Roman-Leshkov, Y., Reductive catalytic fractionation of C-lignin. *ACS Sustainable Chem Eng* **2018,** *6*, 11211-11218.

31. Xie, M.; Zhang, J.; Tschaplinski, T. J.; Tuskan, G. A.; Chen, J. G.; Muchero, W., Regulation of lignin biosynthesis and its role in growth-defense tradeoffs. *Front Plant Sci* **2018,** *9*, 1427.

32. Zhuo, C. L.; Rao, X. L.; Azad, R.; Pandey, R.; Xiao, X. R.; Harkelroad, A.; Wang, X. Q.; Chen, F.; Dixon, R. A., Enzymatic basis for C-lignin monomer biosynthesis in the seed coat of *Cleome hassleriana*. *Plant J* **2019,** *99*, 506-520.

33. Wagner, A.; Tobimatsu, Y.; Phillips, L.; Flint, H.; Torr, K.; Donaldson, L.; Pears, L.; Ralph, J., CCoAOMT suppression modifies lignin composition in *Pinus radiata*. *Plant J* **2011,** *67*, 119-129.

34. Rao, X.; Krom, N.; Tang, Y.; Widiez, T.; Havkin-Frenkel, D.; Belanger, F. C.; Dixon, R. A.; Chen, F., A deep transcriptomic analysis of pod development in the vanilla orchid (*Vanilla planifolia*). *BMC Genom* **2014,** *15*, 964.

35. Elder, T.; Berstis, L.; Beckham, G. T.; Crowley, M. F., Coupling and reactions of 5-hydroxyconiferyl alcohol in lignin formation. *J Agric Food Chem* **2016,** *64*, 4742-4750.

36. Wu, Z.; Ren, H.; Xiong, W.; Roje, S.; Liu, Y.; Su, K.; Fu, C., Methylenetetrahydrofolate reductase modulates methyl metabolism and lignin monomer methylation in maize. *J Exp Bot* **2018,** *69*, 3963-3973.

37. Barta, K.; Warner, G. R.; Beach, E. S.; Anastas, P. T., Depolymerization of organosolv lignin to aromatic compounds over Cu-doped porous metal oxides. *Green Chem* **2014,** *16*, 191-196.

38. Ouyang, X.-P.; Tan, Y.-D.; Qiu, X.-Q., Oxidative degradation of lignin for producing monophenolic compounds. *J Fuel Chem Technol* **2014,** *42*, 677-682.

39. Lan, W.; Amiri, M. T.; Hunston, C. M.; Luterbacher, J. S., Protection group effects during α,γ-diol lignin stabilization promote high-selectivity monomer production. *Angew Chem Int Ed Engl* **2018,** *57*, 1356-1360.

40. Dai, J.; Patti, A. F.; Saito, K., Recent developments in chemical degradation of lignin: catalytic oxidation and ionic liquids. *Tetrahedron Lett* **2016,** *57*, 4945-4951.

41. Xu, Z.; Lei, P.; Zhai, R.; Wen, Z.; Jin, M., Recent advances in lignin valorization with bacterial cultures: microorganisms, metabolic pathways, and bio-products. *Biotechnol Biofuels* **2019,** *12*, 32.

42. Nar, M.; Rizvi, H. R.; Dixon, R. A.; Chen, F.; Kovalcik, A.; D'Souza, N., Superior plant based carbon fibers from electrospun poly-(caffeyl alcohol) lignin. *Carbon* **2016,** *103*, 372-383.

43. Li, N.; Li, Y.; Yoo, C. G.; Yang, X.; Lin, X.; Ralph, J.; Pan, X., An uncondensed lignin depolymerized in the solid state and isolated from lignocellulosic biomass: a mechanistic study. *Green Chem* **2018,** *20*, 4224-4235.

44. Lara-Espinoza, C.; Carvajal-Millan, E.; Balandran-Quintana, R.; Lopez-Franco, Y.; Rascon-Chu, A., Pectin and pectin-based composite materials: beyond food texture. *Molecules* **2018,** *23*, 942.

45. Voragen, A. G. J.; Coenen, G.-J.; Verhoef, R. P.; Schols, H. A., Pectin, a versatile polysaccharide present in plant cell walls. *Struct Chem* **2009,** *20*, 263-275.

46. Harholt, J.; Suttangkakul, A.; Vibe Scheller, H., Biosynthesis of pectin. *Plant Physiol* **2010,** *153*, 384-395.

47. Ruiz-Herrera, J. Introduction. *Fungal cell wall: structure, synthesis, and assembly*, 2nd ed.; CRC Press: Boca Raton, 2016; pp 1-5.

48. Kang, X.; Kirui, A.; Muszynski, A.; Widanage, M. C. D.; Chen, A.; Azadi, P.; Wang, P.; Mentink-Vigier, F.; Wang, T., Molecular architecture of fungal cell walls revealed by solid-state NMR. *Nat Commun* **2018,** *9*, 2747.

49. Bowman, S. M.; Free, S. J., The structure and synthesis of the fungal cell wall. *Bioessays* **2006,** *28*, 799-808.

50. Gow, N. A. R.; Latge, J. P.; Munro, C. A., The fungal cell wall: structure, biosynthesis, and function. *Microbiol Spectr* **2017,** *5*, FUNK-0035-2016.

51. Free, S. J., Fungal cell wall organization and biosynthesis. *Adv Genet* **2013,** *81*, 33-82.

52. Rinaudo, M., Chitin and chitosan: properties and applications. *Prog Polym Sci* **2006,** *31*, 603-632.

53. Raabe, D.; Sachs, C.; Romano, P., The crustacean exoskeleton as an example of a structurally and mechanically graded biological nanocomposite material. *Acta Mater* **2005,** *53*, 4281-4292.

54. Saito, Y.; Okano, T.; Gaill, F.; Chanzy, H.; Putaux, J.-L., Structural data on the intra-crystalline swelling of β-chitin. *Int J Biol Macromol* **2000,** *28*, 81-88.

55. Saito, Y.; Putaux, J.-L.; Okano, T.; Gaill, F.; Chanzy, H., Structural aspects of the swelling of β chitin in HCl and its conversion into α chitin. *Macromolecules* **1997,** *30*, 3867-3873.

56. Camilli, G.; Tabouret, G.; Quintin, J., The complexity of fungal beta-glucan in health and disease: effects on the mononuclear phagocyte system. *Front Immunol* **2018,** *9*, 673.

57. Zhu, F.; Du, B.; Xu, B., A critical review on production and industrial applications of beta-glucans. *Food Hydrocoll* **2016,** *52*, 275-288.

58. Akramiene, D.; Kondrotas, A.; Didziapetriene, J.; Kevelaitis, E., Effects of β-glucans on the immune system. *Medicina* **2007,** *43*, 597-605.

59. Sharon, N., Nomenclature of glycoproteins, glycopeptides and peptidoglycans. *Pure & Appl Chem* **1988,** *60*, 1389-1394.

60. Dell, A.; Morris, H. R., Glycoprotein structure determination by mass spectrometry. *Science* **2001,** *291*, 2351-2356.

61. Zandberg, W. F. Glycoproteins: biosynthesis, structure and biological functions. Ph.D. Dissertation, Simon Fraser University, British Columbia, Canada, 2010.

62. Sajith, S.; Priji, P.; Sreedevi, S.; Benjamin, S., An overview on fungal cellulases with an industrial perspective. *J Nutr Food Sci* **2016,** *6*, 1000461.

63. Juturu, V.; Wu, J. C., Microbial cellulases: engineering, production and applications. *Renew Sust Energ Rev* **2014,** *33*, 188-203.

64. Kuhad, R. C.; Gupta, R.; Singh, A., Microbial cellulases and their industrial applications. *Enzyme Res* **2011,** *2011*, 280696.

65. Baldrian, P.; Voriskova, J.; Dobiasova, P.; Merhautova, V.; Lisa, L.; Valaskova, V., Production of extracellular enzymes and degradation of biopolymers by saprotrophic microfungi from the upper layers of forest soil. *Plant Soil* **2010,** *338*, 111-125.

66. Placido, J.; Capareda, S., Ligninolytic enzymes: a biotechnological alternative for bioethanol production. *Bioresour Bioprocess* **2015,** *2*, 23.

67. Usha, K. Y.; Praveen, K.; Reddy, B. R., Enhanced production of ligninolytic enzymes by a mushroom *Stereum ostrea*. *Biotechnol Res Int* **2014,** *2014*, 815495.

68. Kumar, A.; Chandra, R., Ligninolytic enzymes and its mechanisms for degradation of lignocellulosic waste in environment. *Heliyon* **2020,** *6*, e03170.

69. Chen, Y. R.; Sarkanen, S.; Wang, Y. Y., Lignin-degrading enzyme activities. *Methods Mol Biol* **2012,** *908*, 251-268.

70. Wang, X.; Yao, B.; Su, X., Linking enzymatic oxidative degradation of lignin to organics detoxification. *Int J Mol Sci* **2018,** *19*, 3373.

71. Hofrichter, M., Review: lignin conversion by manganese peroxidase (MnP). *Enzyme Microb Technol* **2002,** *30*, 454-466.

72. Niladevi, K. N. Ligninolytic enzymes. In *Biotechnology for agro-industrial residues utilisation*; Nigam, P. S., Pandey, A., Eds.; Springer: Dordrecht, 2009; pp 397-414.

73. Wong, D. W., Structure and action mechanism of ligninolytic enzymes. *Appl Biochem Biotechnol* **2009,** *157*, 174-209.

74. Chen, M.; Zeng, G.; Tan, Z.; Jiang, M.; Li, H.; Liu, L.; Zhu, Y.; Yu, Z.; Wei, Z.; Liu, Y.; Xie, G., Understanding lignin-degrading reactions of ligninolytic enzymes: binding affinity and interactional profile. *PLoS One* **2011,** *6*, e25647.

75. Oumer, O. J.; Abate, D., Screening and molecular identification of pectinase producing microbes from coffee pulp. *Biomed Res Int* **2018,** *2018*, 2961767.

76. Dhembare, A. J.; Kakad, S. L.; Rana, R., Effect of pH, temperature and kinetics of pectinase enzyme using *Aspergillus niger* by solid-state of fermentation. *Der Pharmacia Sinica* **2015,** *6*, 1-5.

77. Verma, H.; Narnoliya, L. K.; Jadaun, J. S., Pectinase: a useful tool in fruit processing industries. *Nutri Food Sci Int J* **2018,** *5*, 555673.

78. Garg, G.; Singh, A.; Kaur, A.; Singh, R.; Kaur, J.; Mahajan, R., Microbial pectinases: an ecofriendly tool of nature for industries. *3 Biotech* **2016,** *6*, 47.

79. Pedrolli, D. B.; Monteiro, A. C.; Gomes, E.; Carmona, E. C., Pectin and pectinases: production, characterization and industrial application of microbial pectinolytic enzymes. *Open Biotechnol J* **2009,** *3*, 9-18.

80. Tapre, A. R.; Jain, R. K., Pectinases: enzymes for fruit processing industry. *Int Food Res J* **2014,** *21*, 447-453.

81. Rathore, A. S.; Gupta, R. D., Chitinases from bacteria to human: properties, applications, and future perspectives. *Enzyme Res* **2015,** *2015*, 791907.

82. Fleuri, L. F.; Kawaguti, H. Y.; Sato, H. H., Production, purification and application of extracellular chitinase from *Cellulosimicrobium cellulans* 191. *Braz J Microbiol* **2009,** *40*, 623-630.

83. Thompson, S. E.; Smith, M.; Wilkinson, M. C.; Peek, K., Identification and characterization of a chitinase antigen from *Pseudomonas aeruginosa* strain 385. *Appl Environ Microbiol* **2001,** *67*, 4001-4008.

84. Delaittre, G.; Greiner, A. M.; Pauloehrl, T.; Bastmeyer, M.; Barner-Kowollik, C., Chemical approaches to synthetic polymer surface biofunctionalization for targeted cell adhesion using

small binding motifs. *Soft Matter* **2012,** *8*, 7323-7347.

85. de Gennes, P. G., Polymers at an interface; a simplified view. *Adv Colloid Interface Sci* **1987,** *27*, 189-209.

86. de Gennes, P. G., Polymer solutions near an interface. 1. Adsorption and depletion layers. *Macromolecules* **1981,** *14*, 1637-1644.

87. Manciu, M.; Ruckenstein, E., Loops, tails and trains: a simple model for structural transformations of grafted adsorbing neutral polymer brushes. *J Colloid Interface Sci* **2011,** *354*, 61-69.

88. Welch, D.; Lettinga, M. P.; Ripoll, M.; Dogic, Z.; Vliegenthart, G. A., Trains, tails and loops of partially adsorbed semi-flexible filaments. *Soft Matter* **2015,** *11*, 7507-7514.

89. Scheutjens, J. M. H. M.; Fleer, G. J., Statistical theory of the adsorption of interacting chain molecules. 2. Train, loop, and tail size distribution. *J Phys Chem* **1980,** *84*, 178-190.

90. Uchida, E.; Iwata, H.; Ikada, Y., Surface structure of poly(ethylene terephthalate) film grafted with poly(methacrylic acid). *Polymer* **2000,** *41*, 3609-3614.

91. Kato, K.; Uchida, E.; Kang, E.-T.; Uyama, Y.; Ikada, Y., Polymer surface with graft chains. *Prog Polym Sci* **2003,** *28*, 209-259.

92. Stuart, M. A. C.; Fleer, G. J.; Lyklema, J.; Norde, W.; Scheutjens, J. M. H. M., Adsorption of ions, polyelectrolytes and proteins. *Adv Colloid Interface Sci* **1991,** *34*, 477-535.

93. Hildebrandt, M.; Shin, E. Y.; Yang, S.; Ali, W.; Altinpinar, S.; Gutmann, J. S., Investigation of roughness correlation in polymer brushes via X-ray scattering. *Polymers (Basel)* **2020,** *12*, 2101.

94. Rabin, Y.; Alexander, S., Stretching of grafted polymer layers. *Europhys Lett* **1990,** *13*, 49-54.

95. Miao, L.; Guo, H.; Zuckermann, M. J., Conformation of polymer brushes under shear: chain tilting and stretching. *Macromolecules* **1996,** *29*, 2289-2297.

96. Uchida, E.; Uyama, Y.; Ikada, Y., Zeta potential of polycation layers grafted onto a film surface. *Langmuir* **1994,** *10*, 1193-1198.

97. Tyona, M. D., A theoritical study on spin coating technique. *Adv Mater Res* **2013,** *2*, 195-208.

98. Oliveira, O. N., Langmuir-Blodgett films - properties and possible applications. *Braz J Phys* **1992,** *22*, 60-69.

99. Notley, S. M.; Norgren, M., Adsorption of a strong polyelectrolyte to model lignin surfaces. *Biomacromolecules* **2008,** *9*, 2081-2086.

100. Rahikainen, J. L.; Martin-Sampedro, R.; Heikkinen, H.; Rovio, S.; Marjamaa, K.; Tamminen, T.; Rojas, O. J.; Kruus, K., Inhibitory effect of lignin during cellulose bioconversion: the effect of lignin chemistry on non-productive enzyme adsorption. *Bioresour Technol* **2013,** *133*, 270-288.

101. Constantino, C. J. L.; Juliani, L. P.; Botaro, V. R.; Balogh, D. T.; Pereira, M. R.; Ticianelli, E. A.; Curvelo, A. A. S.; Oliveira, O. N., Langmuir-Blodgett films from lignins. *Thin Solid Films* **1996,** *284-285*, 191-194.

102. Martins, G. F.; Pereira, A. A.; Straccalano, B. A.; Antunes, P. A.; Pasquini, D.; Curvelo, A. A. S.; Ferreira, M.; Riul Jr., A.; Constatino, C. J. L., Ultrathin films of lignins as a potential transducer in sensing applications involving heavy metal ions. *Sens Actuators B* **2008,** *129*, 525-

530.

103. Maximova, N.; Osterberg, M.; Laine, J.; Stenius, P., The wetting properties and morphology of lignin adsorbed on cellulose fibres and mica. *Colloids Surf A: Physicochem Eng Aspects* **2004,** *239*, 65-75.

104. Paterno, L. G.; Mattoso, L. H. C., Effect of pH on the preparation of self-assembled films of poly(*o*-ethoxyaniline) and sulfonated lignin. *Polymer* **2001,** *42*, 5239-5245.

105. Micic, M.; Radotic, K.; Jeremic, M.; Leblanc, R. M., Study of self-assembly of the lignin model compound on cellulose model substrate. *Macromol Biosci* **2003,** *3*, 100-106.

106. Stergiou, D. V.; Veltsistas, P. G.; Prodromidis, M. I., An electrochemical study of lignin films degradation: proof-of-concept for an impedimetric ozone sensor. *Sens Actuators B* **2008,** *129*, 903-908.

107. Landaeta, E.; Schultz, Z. D.; Burgos, A.; Schrebler, R.; Isaacs, M., Enhanced photostability of cuprous oxide by lignin films on glassy carbon electrodes in the transformation of carbon dioxide. *Green Chem* **2018,** *20*, 2356-2364.

108. Amare, M.; Aklog, S., Electrochemical determination of caffeine content in Ethiopian coffee samples using lignin modified glassy carbon electrode. *J Anal Methods Chem* **2017,** *2017*, 3979068.

109. Wang, C.; Qian, C.; Roman, M.; Glasser, W. G.; Esker, A. R., Surface-initiated dehydrogenative polymerization of monolignols: a quartz crystal microbalance with dissipation monitoring and atomic force microscopy study. *Biomacromolecules* **2013,** *14*, 3964-3972.

110. Micic, M.; Radotic, K.; Benitez, I.; Ruano, M.; Jeremic, M.; Moy, V.; Mabrouki, M.; Leblanc, R. M., Topographical characterization and surface force spectroscopy of the

photochemical lignin model compound. *Biophys Chem* **2001,** *94*, 257-263.

111. Casteleijn, M. G.; Richardson, D.; Parkkila, P.; Granqvist, N.; Urtti, A.; Viitala, T., Spin coated chitin films for biosensors and its analysis are dependent on chitin-surface interactions. *Colloids Surf A* **2018,** *539*, 261-272.

112. Kittle, J. D.; Wang, C.; Qian, C.; Zhang, Y.; Zhang, M.; Roman, M.; Morris, J. R.; Moore, R. B.; Esker, A. R., Ultrathin chitin films for nanocomposites and biosensors. *Biomacromolecules* **2012,** *13*, 714-718.

113. Ramirez-Wong, D. G.; Ramirez-Cardona, M.; Sanchez-Leija, R. J.; Rugerio, A.; Mauricio-Sanchez, R. A.; Hernandez-Landaverde, M. A.; Carranza, A.; Pojman, J. A.; Garay-Tapia, A. M.; Prokhorov, E.; Mota-Morales, J. D.; Luna-Barcenas, G., Sustainable-solvent-induced polymorphism in chitin films. *Green Chem* **2016,** *18*, 4303-4311.

114. Montiel-Gonzalez, Z.; Luna-Barcenas, G.; Mendoza-Galvan, A., Thermal behaviour of chitosan and chitin thin films studied by spectroscopic ellipsometry. *Phys Stat Sol C* **2008,** *5*, 1434-1437.

115. Chakravarty, J.; Rabbi, M. F.; Bach, N.; Chalivendra, V.; Yang, C. L.; Brigham, C. J., Fabrication of porous chitin membrane using ionic liquid and subsequent characterization and modelling studies. *Carbohydr Polym* **2018,** *198*, 443-451.

116. King, C.; Shamshina, J. L.; Gurau, G.; Berton, P.; Khan, N. F. A. F.; Rogers, R. D., A platform for more sustainable chitin films from an ionic liquid process. *Green Chem* **2017,** *19*, 117-126.

117. Kittle, J. D. Characterization of cellulose and chitin thin films and their interactions with bio-based polymers. Ph.D. Dissertation, Virginia Tech, Blacksburg, VA, 2012.

118. Du, X. Adsorption studies of polysaccharides and phospholipids onto cellulose. Ph.D. Dissertation, Virginia Tech, Blacksburg, VA, 2011.

119. Chen, Q.; Xu, S.; Liu, Q.; Masliyah, J.; Xu, Z., QCM-D study of nanoparticle interactions. *Adv Colloid Interface Sci* **2016,** *233,* 94-114.

120. Dixon, M. C., Quartz crystal microbalance with dissipation monitoring: enabling real-time characterization of biological materials and their interactions. *J Biomol Tech* **2008,** *19,* 151-158.

Chapter 3: Activities of Family 18 Chitinases on Amorphous Regenerated Chitin Thin Films and Dissolved Chitin Oligosaccharides: Comparison with Family 19 Chitinases

3.1 Abstract

Family 18 chitinases are widely distributed in nature, and their actions on chitin play important roles in the life cycle of fungi. Changes in mass and viscoelasticity of chitin layers in fungal cell walls during chitinase attack can considerably deepen our understanding of the mechanisms for bacterial invasion of and human defense against fungi, thereby promoting advances in agriculture and biotechnology. In this work, regenerated chitin (RChitin) thin films simulated the chitin layers in fungal cell walls and facilitated studies of degradation by family 18 chitinases from *Trichoderma viride* (*T. viride*) and family 19 chitinases from *Streptomyces griseus* (*S. griseus*) which possess chitin-binding domains (CBDs) that are absent in the family 18 chitinases at various pH and temperatures. Degradation was monitored via a quartz crystal microbalance with dissipation monitoring (QCM-D) in real time. Compared to substrates of colloidal chitin or dissolved chitin derivatives and analogues, the degradation of RChitin films was deeply affected by chitinase adsorption. While the family 18 chitinases had greater solution activity on chitin oligosaccharides, the family 19 chitinases exhibited greater activity on RChitin films, illustrating the importance of the CBD for insoluble substrates.

3.2 Introduction

Bacteria and fungi widely exist in nature, and they are found sharing microhabitats in nearly every ecosystem. Interactions between them range from mutualism to antagonism and play important roles in ecological balance, agricultural production, and biotechnology development.[1-3] Take the fungus *Rhizopus microsporus* (*R. microspores*) and its endosymbiont bacterium *Burkholderia rhizoxinica* (*B. rhizoxinica*) as an example.[2] The *R. microspores* harbors the

endofungal bacterium, while the *B. rhizoxinica* assists its host in producing phytotoxin rhizoxin to kill rice plants. In order to enter the *R. microspores* cell, the *B. rhizoxinica* will secrete chitinases to locally soften and loosen the fungal cell wall by degrading chitin which is one of the major structural components. Furthermore, fungal diseases are a global health problem. More than two million people currently suffer from life-threatening fungal infections throughout the world.[4] Worldwide, cryptococcal meningitis caused by the fungus *Cryptococcus neoformans* affects about 220,000 people with HIV/AIDS annually, resulting in nearly 181,000 deaths.[5] Humans encode two active chitinases: chitotriosidase and acidic mammalian chitinase.[6] Chitinase levels in humans increase in response to invasive fungal infections.[7-8] The release of small chitin fragments generated from the digestion of chitin layers in the fungal cell walls via the chitinases leads to chitin recognition by our immune system and that triggers immune responses. Clearly, chitinases are closely related to fungal activities, and an exploration of chitin-chitinase interactions can greatly help us understand how fungi and nature work.

Chitin is a linear homopolysaccharide composed of *N*-acetyl-D-glucosamine (GlcNAc) units that are connected through covalent β-(1→4) linkages in which every unit is rotated 180^{o} relative to the preceding GlcNAc unit. One end of its chain is a reducing end with a hemiacetal group, and the other is a non-reducing end with a pendant hydroxyl group. Chitin cannot be dissolved in water or common organic solvents partly due to the strong inter- and intra-molecular hydrogen bonding interactions among its molecules.[9-10] In fungal cell walls, chitin molecules pack into microfibrils which are located next to the plasma membrane. The chitin layer usually has a thickness of a few nanometers and provides the fungal cell wall with indispensable structural integrity.[11-13] Chitinases are a group of hydrolytic enzymes that catalyze the degradation of chitin by breaking its glycosidic bonds. Based upon the amino acid sequence and similarity, most

chitinases can be categorized into family 18 and 19. Family 18 chitinases are primarily distributed in bacteria, fungi, viruses, animals, humans, and some plants, while family 19 chitinases mostly exist in plants and a few microorganisms.[14-16] The chitinases isolated from nature are usually a mixture of endochitinases and exochitinases.[17-18] Exochitinases further contain chitobiosidases and *N*-acetylglucosaminidases. Endochitinases randomly cleave at internal sites in the chitin chain. Chitobiosidases and *N*-acetylglucosaminidases act progressively on the non-reducing end of chitin to release chitobioses and GlcNAc monomers, respectively. The combination of these chitinases leads to synergistic increases in chitinolytic activity, as shown in Figure 3.1.

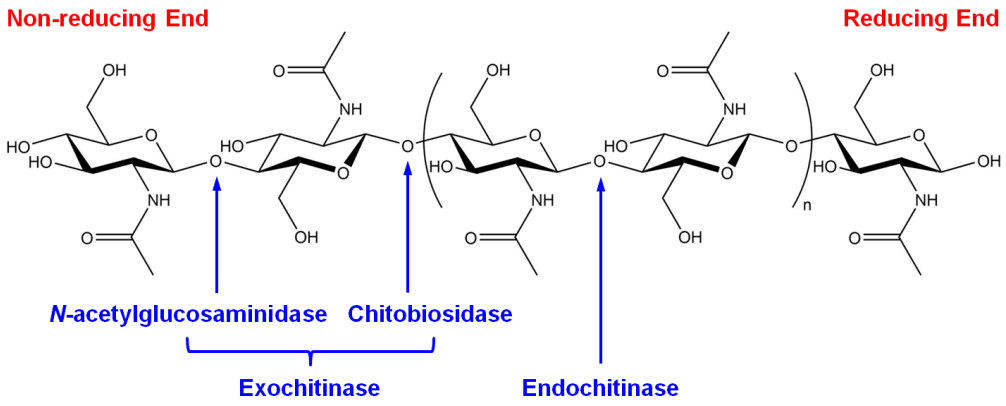

Figure 3.1 Enzymatic actions of different chitinases on chitin.

Some researchers have studied the activity of family 18 chitinases.[19-24] Berini et al.[19] employed three dissolved fluorimetric chitin oligosaccharides, 4-methylumbelliferyl *N*-acetyl-*β*-D-glucosaminide, 4-methylumbelliferyl *N,N′*-diacetyl-*β*-D-chitobioside, and 4-methylumbelliferyl *N,N′,N″*-triacetyl-*β*-D-chitotrioside, as substrates to quantify the activities of *N*-acetylglucosaminidase, chitobiosidase, and endochitinase in family 18 chitinases from *Trichoderma viride* (*T. viride*). Omumasaba et al.[20] assayed the chitinolytic activities of a purified chitinase from *T. viride* on partially deacetylated chitin, colloidal chitin, glycol chitin,

and chitosan, respectively, using a colorimetric method. However, all of these reports focus on the enzymatic degradation of colloidal chitin or dissolved chitin derivatives and analogues in solution, and the activity of family 18 chitinases on thin chitin films has never been reported. It is presumed that the chitinases could exhibit different activities on chitin films than colloidal chitin (where the total surface area of substrate would be greater) or dissolved chitin derivatives and analogues (with much higher substrate concentrations). In addition, the thin chitin film geometry is comparable to chitin layers in fungal cell walls, and changes in mass and viscoelasticity during degradation are anticipated to inform our understanding of how the chitinase softens the fungal cell wall to facilitate bacterium penetration.

In this work, amorphous regenerated chitin (RChitin) thin films were prepared via chemical conversion and spin-coating, and family 18 chitinases from *T. viride* were employed to degrade RChitin films at various temperatures and pH. Results were compared to family 19 chitinases from *Streptomyces griseus* (*S. griseus*). The chitinolytic activity was assayed using a quartz crystal microbalance with dissipation monitoring (QCM-D) which monitored the mass and viscoelasticity changes of the chitin films in real time. Through this study, the structural characteristics of the family 18 chitinases, the different roles of endochitinase and exochitinase, and the effects of adsorption on hydrolysis rates were revealed.

3.3 Experimental Section

3.3.1 Materials

Family 18 chitinases from *T. viride* (lyophilized powder, ≥ 600 units/g solid), family 19 chitinases from *S. griseus* (lyophilized powder, ≥ 200 units/g solid), α-chitin from shrimp shells (practical grade, ≥ 95% acetylated), hydrogen peroxide (30 wt% in H_2O), 1,1,2,2-tetrachloroethane (≥ 98%), and chitin oligosaccharides (4-nitrophenyl *N*-acetyl-*β*-D-

glucosaminide (4-NP-GlcNAc), 4-nitrophenyl *N,N′*-diacetyl-*β*-D-chitobioside [4-NP-$(GlcNAc)_2$], and 4-nitrophenyl *N,N′N″*-triacetyl-*β*-D-chitotrioside [4-NP-$(GlcNAc)_3$]) were purchased from Sigma-Aldrich. Chloroform (HPLC grade), ammonium hydroxide (30% NH_3 in H_2O), and hydrochloric acid (HCl, 37%) were supplied by Fisher Scientific. Sodium phosphate monobasic monohydrate, sodium phosphate dibasic heptahydrate, sodium hydroxide, and phosphoric acid (≥ 85%) were obtained from Sigma-Aldrich and used to prepare 50 mM phosphate buffer solutions at pH 4, 6, 7, and 8, respectively. Nitrogen (N_2, ultrahigh purity) was supplied by Airgas. Ultrapure water (Millipore Milli-Q, 18.2 MΩ·cm) was used for all experiments.

3.3.2 Preparation of Amorphous RChitin Thin Films

Due to its low solubility, chitin was first converted to trimethylsilyl chitin (TMSChitin) as previously reported.[25-26] Then, the TMSChitin was dissolved in a mixed solvent of chloroform and 1,1,2,2-tetrachloroethane (4:1 v/v) at a concentration of 0.7 wt%. After that, the TMSChitin solution was filtered by a syringe filter (0.45 μm in pore size and PTFE membrane), and the filtrate was used as the spin-coating solution.

Gold-coated QCM-D sensors (QSX 301 from Biolin Scientific) were employed as the substrates for spin-coating. Prior to use, the sensors were cleaned by UV/ozone for 20 min, heated in a 5:1:1 v/v mixture of ultrapure water : hydrogen peroxide (30%) : ammonium hydroxide (30%) at 80 ^{o}C for 1 h, rinsed via ultrapure water, and dried under N_2 gas. A thin TMSChitin film was fabricated through spin-coating 100 μL of the filtered TMSChitin solution onto a cleaned sensor surface at a spin speed of 3000 rpm for 1 min. The prepared TMSChitin film was placed face down 25 mm above the surface of a 10 wt% HCl aqueous solution for 2 min to regenerate chitin. Then, the regenerated chitin (RChitin) film was rinsed with ultrapure water and dried under N_2 gas.

3.3.3 Enzymatic Degradation of RChitin Films via a QCM-D

The kinetics of RChitin film degradation was monitored using a QCM-D (QSense E4, Biolin Scientific). The QCM-D sensors with RChitin films were loaded into flow modules. Then, 50 mM phosphate buffer was introduced into the system at a flow rate of 0.1 mL/min until the baseline became stable. Next, chitinases in phosphate buffer solution at a concentration of 0.2 mg/mL were injected into the system at 0.1 mL/min. After 30 min, the flow was stopped and the degradation proceeded in the absence of flow. The changes in frequency (Δf) and energy dissipation (ΔD) at the fundamental frequency and 6 odd overtones (n = 3, 5, 7, …, 13) were recorded. When $\Delta f/n$ and ΔD versus time curves became flat, which indicated either all available RChitin was exhausted or the chitinases lost their activities, phosphate buffer was flowed into the system again to wash away residual and reversibly adsorbed chitinases and degradation products. Four temperatures (20, 30, 35, and 40 ^{o}C) and four pH values (4, 6, 7, and 8) were investigated, and data from the fifth overtone (n = 5) were used for analysis.

For QCM-D measurements, if the mass on the sensor surface is evenly distributed, rigidly attached, and small relative to the mass of the quartz crystal, surface concentration Γ_{QCM} (mass per area) can be quantified using the Sauerbrey equation:[27-29]

$$\Gamma_{\mathrm{QCM}} = -C\left(\frac{\Delta f}{n}\right) \tag{3.1}$$

where C = 0.177 mg m^{-2} Hz^{-1}. The decrease in frequency is proportional to the mass.

For viscoelastic films, the Sauerbrey equation will underestimate the mass of the film. The softness of the film is related to energy dissipation (D) of the sensor, and D is defined as:[27-29]

$$D = \frac{E_{\mathrm{lost}}}{2\pi E_{\mathrm{stored}}} \tag{3.2}$$

where E_{lost} and E_{stored} are the energy lost and stored during a single oscillation, respectively. As

the film becomes softer, *D* increases.

3.3.4 Enzymatic Degradation of Chitin Oligosaccharides in Solution

The activities of chitinases on three dissolved substrates, 4-NP-GlcNAc, 4-NP-$(GlcNAc)_2$, and 4-NP-$(GlcNAc)_3$ in solution were assayed through a colorimetric method. The substrates were dissolved in 50 mM phosphate buffer (pH 6) at concentrations of 1 mg/mL for 4-NP-GlcNAc, 0.5 mg/mL for 4-NP-$(GlcNAc)_2$, and 0.2 mg/mL for 4-NP-$(GlcNAc)_3$. The chitinases in 50 mM phosphate buffer (pH 6) solution were prepared with a concentration of 0.01 or 1 mg/mL. Then, 100 μL of the substrate solution and 50 μL of the chitinase solution were sequentially added to a 96 well microplate (polystyrene, clear, and flat bottom) which was subsequently incubated in a shaker (Innova 42 from New Brunswick Scientific) at 20 ^{o}C and 160 rpm. The reaction was stopped by the addition of 200 μL of 4 wt% sodium carbonate aqueous solution. The enzymatic hydrolysis of the substrate liberated 4-nitrophenol which exhibited a yellow color under alkaline conditions that was measured with a microplate reader (Synergy Mx from BioTek Instruments) at 405 nm. A blank reaction was run, in which the chitinase solution was replaced with pure 50 mM phosphate buffer at pH 6. The activity of the chitinases was represented by the difference in absorbance between the chitinase solutions and the control.

3.3.5 Atomic Force Microscopy (AFM) Measurements

The QCM-D sensors were imaged by a Bruker Dimension Icon atomic force microscope in ScanAsyst mode using a ScanAsyst-Air probe under ambient conditions (22 ^{o}C and 50% relative humidity). RChitin films were measured before, during, and after treatment by the family 18 chitinases. Films were removed from the flow modules, washed gently with water, and dried under N_2 prior to measurements. Height images with 2 μm × 2 μm scan area were collected, and their root-mean-square (RMS) roughnessnes were reported. The surfaces of bare gold-coated

QCM-D sensors were imaged under the same conditions as a control.

3.3.6 Ellipsometry Measurements

Ellipsometry measurements were performed via a VASE ellipsometer (J.A. Woollam Co.) at multiple-angles-of-incidence (60 ºto 80 ºat 2 ºintervals) in a spectral range of 250 to 800 nm. The resulting data were modeled using WVASE 32 software, and the thickness of the RChitin films was determined to be 19.8 ± 0.8 nm.

3.4 Results and Discussion

3.4.1 Activity of Family 18 Chitinases on RChitin Films

The enzymatic degradation of RChitin films by chitinases is a hydrolytic reaction, and Figure 3.2 shows typical QCM-D responses for this hydrolytic process. The dry RChitin film behaved as a rigid layer on the sensor surface, and it was hydrated and swelled upon contact with the phosphate buffer, as shown in Figure 3.2a. After the $\Delta f/n$ and ΔD baselines reached a steady state, solutions of family 18 chitinases flowed over the RChitin film. A large decrease in frequency attributed to the enzyme adsorption was observed, and the small fluctuations of frequency and dissipation at the beginning of the injection of enzyme solution was believed to be caused by temporary changes in flow pressure on the sensor,[30] as displayed in the inset of Figure 3.2. Once the $\Delta f/n$ vs. t curve reached a minimum, it started to increase, as the RChitin film was hydrolyzed into soluble GlcNAc monomers, chitobioses, and chitooligosaccharides. The slope in Figure 3.2 represented an apparent hydrolysis rate. The process for the film was different from colloidal chitin and dissolved chitin derivatives and analogues, where hydrolysis was fastest at the start of the experiment. For RChitin films, the maximum hydrolysis rate (the largest slope of the $\Delta f/n$ vs. t curve) occurred in the middle of the degradation process. Based upon previous studies on

cellulose and others,[31-32] the amorphous RChitin film should be porous to water but not to chitinase molecules whose molecular weights range between 30 and 80 kDa.[19] In other words, the chitinase molecules would be confined to the surface of the RChitin film initially, as depicted in Figure 3.2b. As a result, the hydrolysis rate was restricted by the limited number of non-reducing ends of RChitin chains on the film surface. Since endochitinases acted upon internal bonds of the RChitin chains, more non-reducing ends were created and exochitinase access to the film was enhanced, as shown in Figure 3.2c. Consequently, the hydrolysis rate increased with time. After the inflection point where the maximum hydrolysis rate was achieved, the slope of the $\Delta f/n$ vs. t curve gradually decreased and plateaued. The reduced slope was due to the depletion of the RChitin film, and the plateau indicated available RChitin was totally exhausted or the chitinases lost their activities, as displayed in Figure 3.2d. Pure phosphate buffer was flowed over the sensor to wash away reversibly adsorbed chitinases and degradation products, resulting in an additional small increase in frequency, as shown in Figure 3.2e.

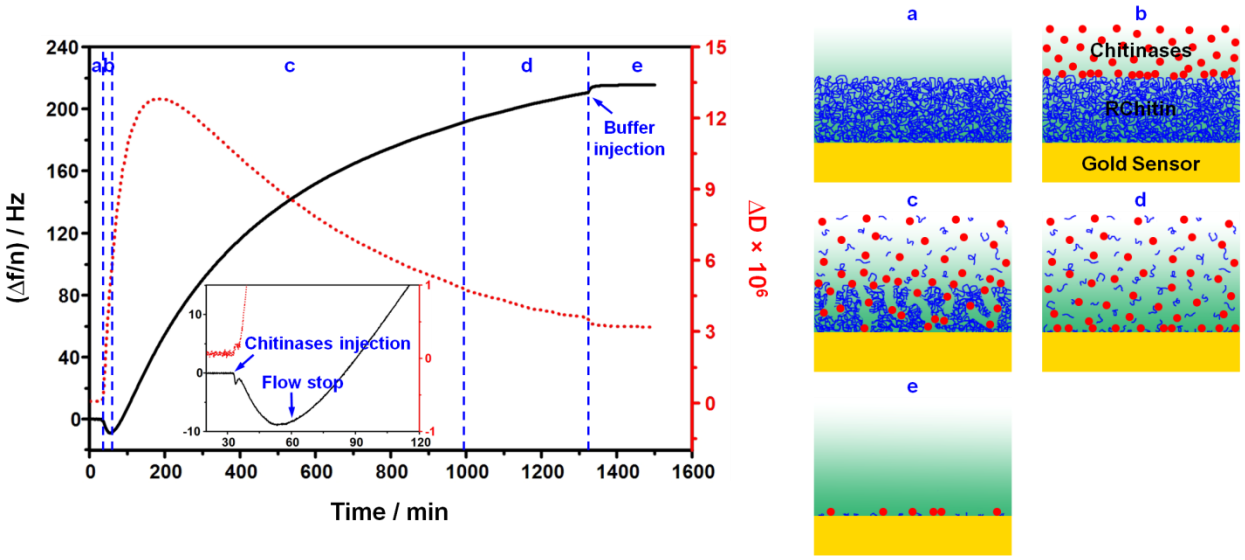

Figure 3.2 Representative Δ*f*/*n* (solid line) and Δ*D* (dotted line) versus time for the activity of family 18 chitinases on the ~20 nm thick RChitin film at 20 °C and pH 6, and a scheme for the changes in the film during this process.

The Δ*D* vs. *t* curve reflected changes in the viscoelasticity of the RChitin film. The adsorption of chitinases and their coupled water led to an instantaneous increase in dissipation after the introduction of the chitinase solution. As the enzymatic hydrolysis took place, the endochitinase rapidly penetrated into the bulk of the film through digestion of linkages between RChitin chain ends, which caused an increase in the number of chain ends and greater hydration and swelling of the film. As a result, the film became softer with greater energy dissipation. The maximum dissipation might suggest the largest accessibility of the RChitin film to chitinase attack that usually coincided with the maximum hydrolysis rate.[33-36] After that, the dissipation began to decrease due to the depletion of the RChitin film, and a plateau was reached once available RChitin was completely exhausted or the chitinases lost their activities, similar to the Δ*f*/*n* vs. *t* curve. The final wash further reduced the dissipation, and Δ*D* was ~3×10^{-6} (larger than 0 in the beginning), indicating there might be some chitinases, degradation products, or

undegraded RChitin left on the sensor surface.

Representative morphological changes of RChitin films during degradation by the family 18 chitinases obtained from AFM are provided in Figure 3.3. A smooth and homogeneous RChitin film was fabricated with a RMS roughness of ~3.0 nm, as shown in Figure 3.3b. As some of the RChitin film was degraded, its surface became rougher and the RMS roughness increased to ~5.6 nm (Figure 3.3c), in line with Figure 3.2c. After hydrolysis and a buffer wash, the RMS roughness decreased to ~3.0 nm (Figure 3.3d), an indication that most of the RChitin was degraded. Since the RMS roughness in Figure 3.3d was higher than that in Figure 3.3a, there must be some chitinases, degradation products, or undegraded RChitin left on the sensor surface after the buffer wash, which was consistent with the residual ΔD in the QCM-D data in Figure 3.2.

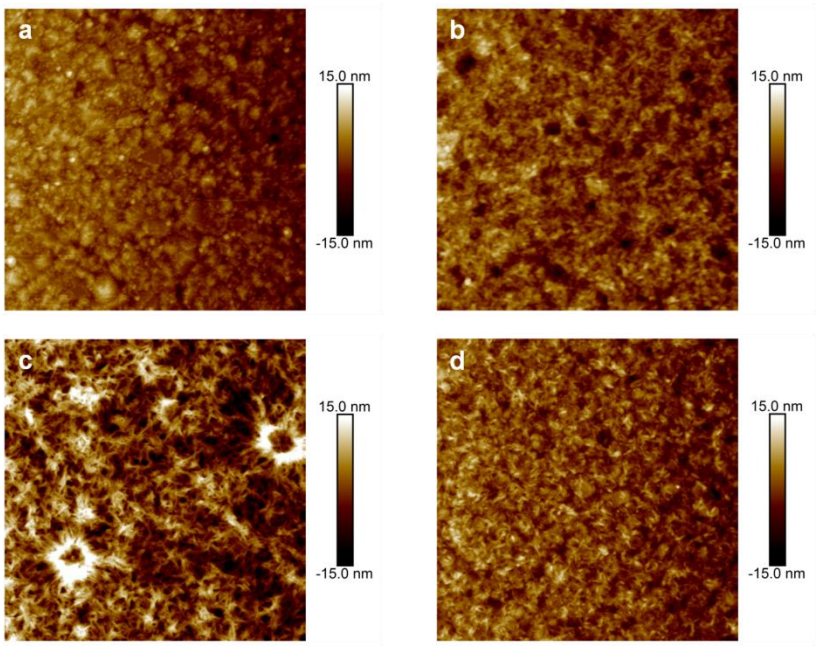

Figure 3.3 Representative AFM height images (2 μm × 2 μm) of (a) a bare gold-coated QCM-D sensor and (b-d) RChitin films before, during, and after treatment by the family 18 chitinases. RMS roughnesses were (a) ~2.3 nm, (b) ~3.0 nm, (c) ~5.6 nm, and (d) ~3.0 nm.

Actually, the frequency and dissipation changes throughout the incubation period were the result of a variety of simultaneous factors. The substrate degradation accompanied the enzyme adsorption process, while the enzyme adsorption/desorption was concurrent with the substrate degradation process. Variations in the density and viscosity of the bulk solution surrounding the sensor could also alter the response of the QCM-D. While these factors masked the true adsorption and hydrolysis rates, the entire incubation process was clearly divided into three stages, as displayed in Figure 3.4. The first stage was dominated by enzyme adsorption and corresponded to a decrease in frequency and an increase in dissipation. Both the frequency and dissipation increased in the second stage and that was interpreted as enzyme penetration and hydrolysis. An increase in frequency coincided with a decrease in dissipation in the final stage and that was attributed to hydrolytic removal of the substrate. Compared to the enzyme adsorption and substrate degradation, QCM-D responses caused by changes of the liquid properties that resulted from alternation of pure buffer and enzyme solution were negligible.[33-35] Since the true values were convoluted, the adsorbed amount and hydrolysis rate were always regarded as apparent in our discussion.

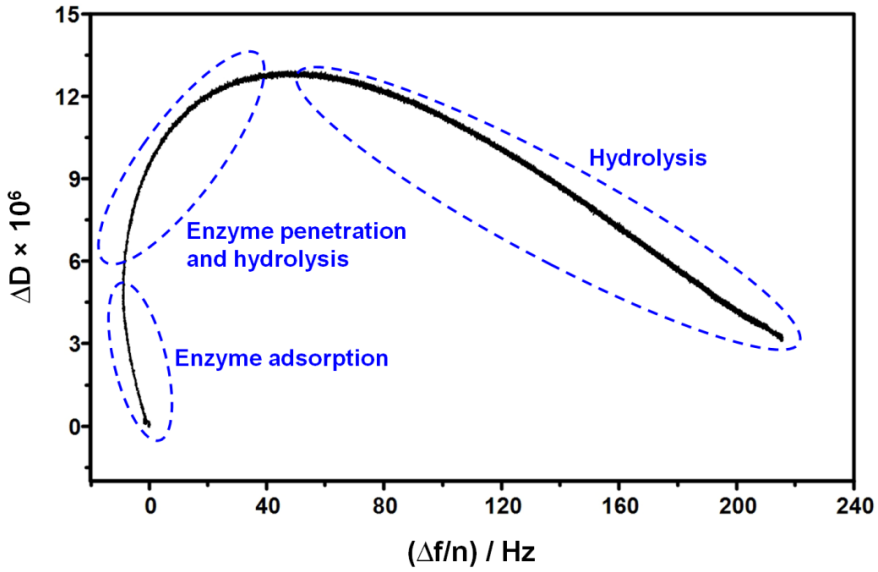

Figure 3.4 Representative ΔD vs. $\Delta f/n$ for the activity of family 18 chitinases on the ~20 nm thick RChitin film at 20 ^{o}C and pH 6.

The synergistic actions of exochitinase and endochitinase facilitated the degradation of RChitin films, but their effects on QCM-D responses were different. The exochitinase acted progressively on the non-reducing ends of RChitin chains and released soluble chitobioses and GlcNAc monomers and their associated coupled water. Hence, the exochitinase caused substantial mass loss and thickness decrease which were reflected in the frequency increase. However, the exochitinase did not increase the number of chain ends, and therefore, its contribution to the change in the viscoelasticity of the RChitin film during the enzyme penetration and hydrolysis stage was limited. In the long run, the exochitinase led to a slow decrease in dissipation during the final hydrolysis stage as the RChitin film was gradually consumed. On the other hand, the endochitinase rapidly penetrated and digested within the bulk of the RChitin film through cleavage at internal sites in the RChitin chains, and brought about significant increases in the number of chain ends and water content of the film. Consequently, the RChitin film became softer and the dissipation increased during the enzyme penetration and

hydrolysis stage in Figure 3.4. Nevertheless, the endochitinase contribution to mass loss was negligible due to the compensation from the increased water content of the film and the low probability that the cleaved chitin chains were of small enough molar mass to be soluble. In summary, the exochitinases were mainly responsible for the increase in $\Delta f/n$, while the endochitinases were primarily responsible for the increase in ΔD.

3.4.2 Effect of pH on the Activity of Family 18 Chitinases on RChitin Films

Figure 3.5a depicts the effect of pH on the activity of family 18 chitinases on thin RChitin films. As the pH increased from 4 to 8, the hydrolysis rates decreased in accordance with the smaller slopes of the $\Delta f/n$ vs. t curves. Moreover, the plateau $\Delta f/n$ values were also smaller at the end of the incubation period as pH increased, which indicated lesser degradation of the RChitin films. At pH 8, the RChitin film barely underwent any hydrolysis over the incubation time. It could be seen from Figure 3.5a that the minimum in $\Delta f/n$ became more negative, an indication of increased adsorbed chitinases with a rise in pH. This was thought to be caused by a diminished activity of exochitinases that consumed lesser amounts of RChitin during the enzyme adsorption stage in Figure 3.4. The slopes in Figure 3.5a and the values of the plateaus for $\Delta f/n$ both decreased as pH increased. These observations indicated that exochitinase activity decreased with increasing pH and were consistent with greater enzyme adsorption.

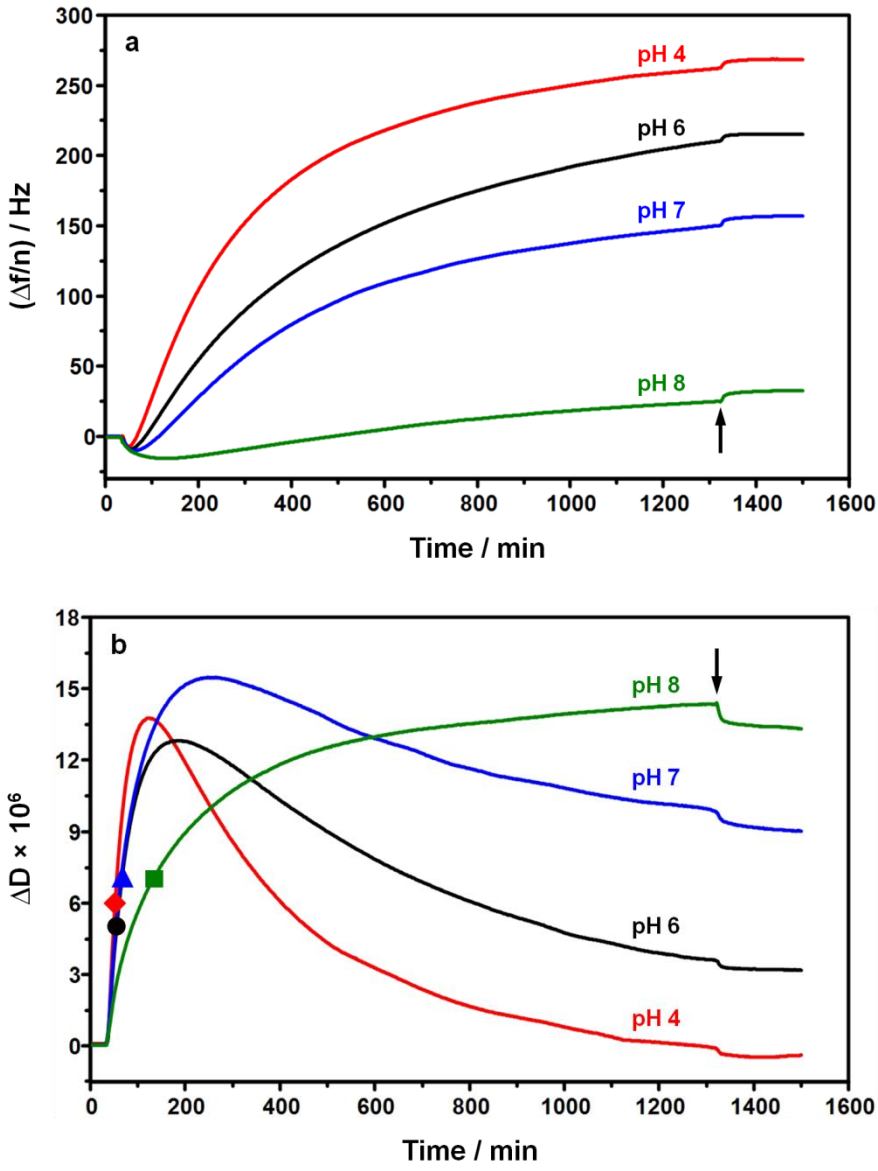

Figure 3.5 Representative (a) Δ*f*/*n* vs. *t* and (b) Δ*D* vs. *t* for the activity of family 18 chitinases on the ~20 nm thick RChitin film at 20 ^{o}C and various pH. The solid symbols correspond to the time when the frequency reached its minimum, for (●) pH 4, (◆) pH 6, (▲) pH 7, and (■) pH 8. The arrows indicate where fresh buffer was introduced into the system at the end of the incubation.

In Figure 3.5b, Δ*D* was plotted as a function of time for different pH. All the maximums in Δ*D* at different pH were similar in magnitude ~13 to 15 ×10^{-6} and non-zero, an indication of

stable endochitinase activity across the pH range. The slopes of the ΔD vs. t curves were in the order pH 4 > 6 ≈ 7 >> 8, a trend that reflected the convolution with exochitinase activity at low pH. For pH 4 through 7, there was a decrease in ΔD that corresponded to the third stage (hydrolysis) in Figure 3.4 where exochitinases depleted the RChitin film. The ΔD vs. t curve dropped faster for the trend pH 4 > 6 > 7 and was consistent with decreased exochitinase activity as pH increased. The exochitinases lost almost all of their activity at pH 8 based upon Figure 3.5a, and thus ΔD exhibited a plateau rather than a decline.

Our results that the family 18 chitinases from *T. viride* performed best in a mildly acidic environment were consistent with previous studies on colloidal chitin and dissolved chitin derivatives and analogues.[19-22] It was found in our experiments that the family 18 chitinases quickly dissolved in pH 8 phosphate buffer, but soon became cloudy, which was probably caused by enzyme denaturation. This explained the low hydrolytic activity of family 18 chitinases under alkaline conditions. The degradation of chitin by chitinases from *T. viride* is believed to follow a substrate-assisted retaining mechanism.[37-39] In this mechanism, the glycosidic oxygen of chitin was first protonated by the carboxyl group of glutamic acid on the chitinase. Then, the formed oxazoline ion intermediate was stabilized by the *N*-acetyl group of chitin that acted as a nucleophile. Next, the glycosidic bond broke and water molecules were introduced to complete the hydrolysis reaction. Based upon this mechanism, the glutamic acid on the chitinase which has a pK_a of 4.25, was essential for catalysis, and therefore, a mildly acidic environment promoted glycosidic oxygen protonation. Consequently, the chitinase exhibited a relatively high chitinolytic activity under mildly acidic conditions.

3.4.3 Effect of Temperature on the Activity of Family 18 Chitinases on RChitin Films

The QMC-D responses to temperature variations are shown in Figure 3.6. The $\Delta f/n$ vs. t

curves in Figure 3.6a exhibited shallower minima in $\Delta f/n$ below 100 min as temperature decreased, an indication that lesser amounts of chitinases were adsorbed. This observation might have arisen as the surface of the RChitin film became rougher and broader as the RChitin film expanded and swelled with an increase in the temperature. Moreover, higher $\Delta f/n$ plateaus were observed at the end of the experiment for 20 and 30 ^{o}C than for 35 and 40 ^{o}C, which indicated greater exochitinase activity at 20 and 30 ^{o}C with higher degrees of RChitin film degradation. Although the hydrolysis rate at 35 ^{o}C was initially comparable to or even faster than that at 20 ^{o}C or 30 ^{o}C based upon the slopes of the $\Delta f/n$ vs. t curves between ~60 and ~200 min, $\Delta f/n$ plateaued at a smaller value, which was attributed to reduced exochitinase stability at higher temperature. By 40 ^{o}C, there was an even more pronounced effect of temperature. The minimum in $\Delta f/n$ was deeper, and the plateau in $\Delta f/n$ at the end of the incubation was ~1/3 the value at 20 and 30 ^{o}C.

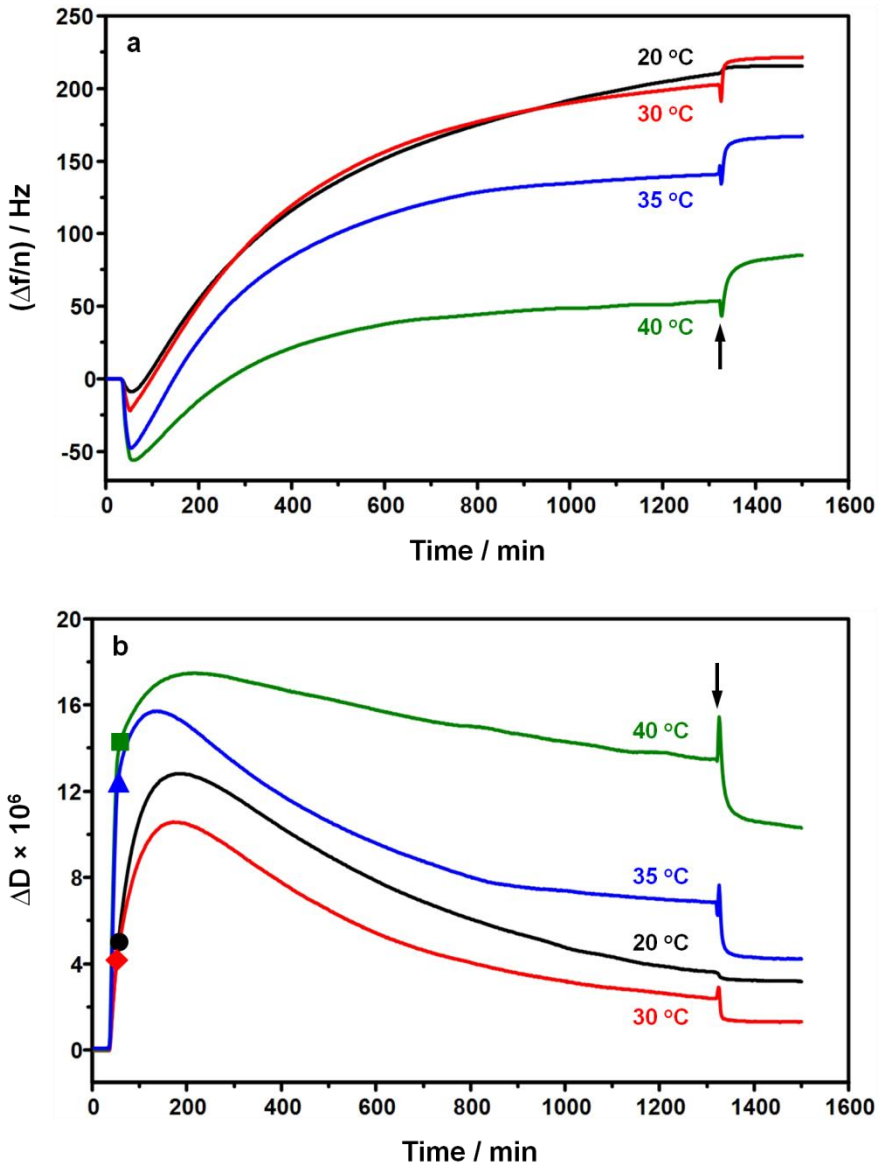

Figure 3.6 Representative (a) Δ*f*/*n* vs. *t* and (b) Δ*D* vs. *t* for the activity of family 18 chitinases on the ~20 nm thick RChitin film at pH 6 and various temperatures. The solid symbols correspond to the time when the frequency reached its minimum, for (●) 20 °C, (◆) 30 °C, (▲) 35 °C, and (■) 40 °C. The arrows indicate where fresh buffer was introduced into the system at the end of the incubation.

The plots of Δ*D* vs. *t* in Figure 3.6b had three major features. The first feature was an instantaneous increase in Δ*D* with a slope that roughly increased with temperature. This region

of the plot corresponded to the enzyme adsorption portion of the curve in Figure 3.4 and ended at the solid symbol which corresponded to the minimum in $\Delta f/n$ in Figure 3.6a. Next, Figure 3.6b transitioned into a broad maximum in ΔD that corresponded to the enzymatic penetration and hydrolysis region of Figure 3.4. Finally, there was a long decay in ΔD after the maximum in Figure 3.6b which corresponded to the hydrolysis phase of Figure 3.4. The data for 20 and 30 ^{o}C showed larger decreases in ΔD after the maximum that were consistent with higher degrees of film hydrolysis discussed for Figure 3.6a. At 35 and 40 ^{o}C, ΔD ended at much higher values which would be consistent with exochitinase inactivation at higher temperature and incomplete hydrolysis. Another interesting observation was that the ΔD increased more significantly during the enzymatic penetration and hydrolysis stage at 20 and 30 ^{o}C than at 35 and 40 ^{o}C. A possible reason was that the endochitinase "hopped" around on the surface of the RChitin film more easily at higher temperature, which resulted in more digestion near the surface prior to penetration deep into the film.[40] The dissipation declined after its maximum as a result of the depletion of the RChitin film by the exochitinase.

As the temperature increased, greater changes in frequency and dissipation were observed when the pure phosphate buffer flowed over the sensor at the end of the incubation, as shown in Figure 3.6. This observation was attributed to greater desorption of chitinases and degradation products from the sensor surface on account of unfavorable adsorption at higher temperature. Compared to literature reports where the optimum temperature for the family 18 chitinases from *T. viride* on colloidal chitin or dissolved chitin derivatives and analogues in solution was ~40 ^{o}C,[19, 21] our findings revealed a lower optimum temperature, and the discrepancy between them was believed to result from the impacts of the stability and adsorption of the chitinases at higher temperature on the insoluble substrate.

3.4.4 Activity of Family 19 Chitinases on RChitin Films

A comparison of activity between family 18 chitinases and family 19 chitinases on thin RChitin films is provided in Figure 3.7. The family 19 chitinases showed much greater activity on the RChitin films. Starting with Figure 3.7a, the initial slope for $\Delta f/n$ vs. t after the minimum was greater and a higher $\Delta f/n$ plateau value was achieved for family 19 chitinases. These results indicated the RChitin film was degraded faster and more completely by the family 19 chitinases. Furthermore, there were substantial differences in the ΔD vs. t plots for family 18 and 19 chitinases. Family 19 chitinases had a larger ΔD maximum that was achieved more quickly and decayed to the plateau value more quickly than family 18 chitinases. In addition, the minimum for $\Delta f/n$ of family 19 chitinases was deeper and achieved faster, an indication that the family 19 chitinases were adsorbed more rapidly in greater quantity during the enzyme adsorption stage in Figure 3.4. The reason for the difference in their QCM-D responses was thought to be that family 18 chitinases from *T. viride* lacked chitin-binding domains (CBDs) in their structure, whereas family 19 chitinases from *S. griseus* possessed CBDs.[20, 41] The CBDs significantly facilitated the adsorption of chitinases onto RChitin films, thus enhancing the hydrolysis rate. An enzymatic reaction normally begins with the enzyme binding to the substrate to form an enzyme-substrate complex, which is then broken down into the product and the original enzyme. Based upon the Michaelis-Menten kinetics model, a low concentration of enzyme-substrate complex or a low rate of enzyme-substrate complex formation can seriously retard reaction rates. Larger adsorption and faster digestion of insoluble substrates have also been reported by Cheng et al.[40] for cellulases. Cellulases with carbohydrate-binding modules (CBMs) exhibited greater activity on insoluble cellulose than cellulases without CBMs. The studies by Cheng et al. for cellulases were consistent with greater family 19 chitinase activity than family 18 chitinase activity on

RChitin films.

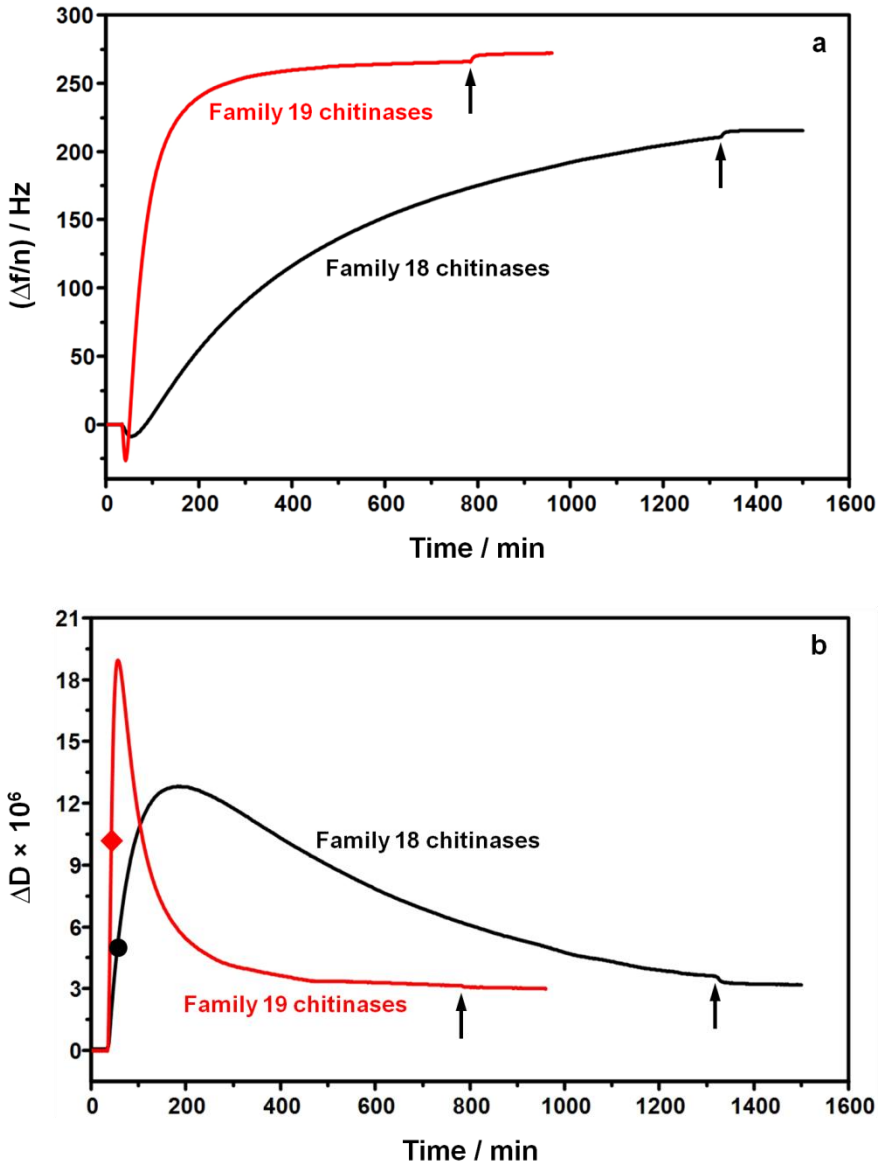

Figure 3.7 Representative (a) Δ*f*/*n* vs. *t* and (b) Δ*D* vs. *t* for the activity of family 18 and 19 chitinases on the ~20 nm thick RChitin film at 20 ^{o}C and pH 6. The solid symbols correspond to the time when the frequency reached its minimum, for (●) family 18 chitinases and (◆) family 19 chitinases. The arrows indicate where fresh buffer was introduced into the system at the end of the incubation.

3.4.5 Activity of Chitinases on Dissolved Chitin Oligosaccharides

Three soluble chitin oligosaccharides of different lengths, 4-NP-GlcNAc, 4-NP-$(GlcNAc)_2$, and 4-NP-$(GlcNAc)_3$, were employed to assay the chitinolytic activities of family 18 and 19 chitinases in solution. They served as dimeric, trimeric, and tetrameric substrates, respectively, and contained a 4-nitrophenol group that connected to the chitooligosaccharide through a β-(1→4) linkage at the reducing end of the chitin oligosaccharide. Upon cleavage, the 4-nitrophenol exhibited a yellow color. Based upon their mechanisms of action, *N*-acetylglucosaminidases, chitobiosidases, and endochitinases required at least a dimer, trimer, and tetramer, respectively, for the observation of hydrolytic activity. Therefore, 4-NP-GlcNAc could only be degraded by *N*-acetylglucosaminidases, both chitobiosidases and *N*-acetylglucosaminidases could act on 4-NP-$(GlcNAc)_2$, and all three kinds of chitinases could participate in the hydrolysis of 4-NP-$(GlcNAc)_3$.[42-43] Accordingly, the degradation of the 4-NP-$(GlcNAc)_3$ most closely resembled the activity of the family 18 or 19 chitinase mixtures on actual chitin.

Table 3.1 shows representative absorbance data for 4-nitrophenol released from 4-NP-GlcNAc, 4-NP-$(GlcNAc)_2$, and 4-NP-$(GlcNAc)_3$ upon incubation with equal amounts of family 18 and 19 chitinases. The absorbance observed for the activity of family 19 chitinases from *S. griseus* at a concentration of 0.01 mg/mL on 4-NP-GlcNAc solution was about 0 after incubation for 30 min, an indication of low *N*-acetylglucosaminidase activity, and therefore, the hydrolysis of 4-NP-$(GlcNAc)_2$ with an absorbance of 0.052 after 30 min was primarily achieved by the chitobiosidases in the family 19 chitinases. Since the absorbance for the 4-NP-$(GlcNAc)_3$ was nearly 0 as well after a 30 min incubation, the endochitinases in the family 19 chitinases must have a low activity, given that chitobiosidase action on 4-NP-$(GlcNAc)_3$ could not release 4-

nitrophenol. In contrast, family 18 chitinases from *T. viride* exhibited stronger activity on all three substrates within 30 min. For 4-NP-GlcNAc and 4-NP-$(GlcNAc)_3$, the concentration of the family 19 chitinase solution was increased by a factor of 100, and still no activity was detected in 30 min. Only after a 24 h incubation time with 1 mg/mL solutions of family 19 chitinases was appreciable activity observed on 4-NP-GlcNAc and 4-NP-$(GlcNAc)_3$ (roughly half of what was observed for ~30 and ~270 min reaction times with family 18 chitinases, respectively). These results indicated the family 19 chitinases had very low *N*-acetylglucosaminidase and endochitinase activity in solution relative to the family 18 chitinases. With the exception of family 18 chitinases in 4-NP-$(GlcNAc)_3$ solution, all other solutions showed absorbances that increased at a steady or slowing rate over the time range investigated. In contrast, the 4-NP-$(GlcNAc)_3$ solution with family 18 chitinases exhibited a lag phase followed by an acceleration in the growth rate of absorbance, which might be caused by substrate inhibition in the initial stage of degradation.[44]

Table 3.1 Absorbance of 4-nitrophenol released from hydrolysis of chitin oligosaccharides.

Substrate	Chitinases	Absorbance (Hydrolysis Time)	
4-NP-GlcNAc	Family 18	0.694 ± 0.024 (30 min) [a]	0.416 ± 0.009 (18 min) [a]
	Family 19	0 ± 0.003 (30 min) [a]	0.385 ± 0.005 (24 h) [b]
4-NP-$(GlcNAc)_2$	Family 18	0.145 ± 0.015 (30 min) [a]	0.341 ± 0.037 (90 min) [a]
	Family 19	0.052 ± 0.006 (30 min) [a]	0.338 ± 0.088 (270 min) [a]
4-NP-$(GlcNAc)_3$	Family 18	0.047 ± 0.010 (30 min) [a]	0.733 ± 0.093 (270 min) [a]
	Family 19	0 ± 0.003 (30 min) [a]	0.337 ± 0.004 (24 h) [b]

The concentrations of the family 18 and 19 chitinases before added to the 96 well microplate were [a] 0.01 mg/mL and [b] 1 mg/mL. Error bars represent one standard deviation.

While it was difficult to distinguish the relative activities of endochitinases and exochitinases in family 18 chitinases from *T. viride* and family 19 chitinases from *S. griseus* because most of the substrates were acted upon by more than one type of enzyme, absorbance and time data clearly showed that the family 18 chitinases had greater activity on all three substrates after the same 30 min of incubation and the activity of family 19 chitinases never caught up at later reaction times, which was exactly opposite of the observation on RChitin films. These studies clearly showed the family 18 chitinases did not possess inherently weaker activity at equivalent concentration and that greater family 19 chitinase activity on RChitin films must arise from a different source. Thus, the existence of CBDs in family 19 chitinases was strongly suspected as the cause of the enhanced activity.

3.5 Conclusions

This work highlighted the chitinolytic activity of family 18 chitinases from *T. viride* on thin RChitin films at various pH and temperatures using QCM-D which monitored the changes in mass and viscoelasticity of the films in real time throughout the degradation process. Based upon the frequency and dissipation changes, the degradation process in a typical experiment could be divided into three stages, enzyme adsorption, enzyme penetration and hydrolysis, and hydrolysis. The variations in the activity of the family 18 chitinases along with the changes in pH were consistent with literature reports that they preferred an acidic environment, but our work also found that the endochitinase was clearly more stable than the exochitinase in terms of activity at different pH. The optimum temperature for the activity of the family 18 chitinases was around 30 ^{o}C which was lower than that reported in the literature for the degradation of colloidal chitin or dissolved chitin derivatives and analogues, which might result from the differences in stability and adsorption of chitinases at high temperature on different substrates. Compared to family 19

chitinases from *S. griseus*, the chitinases from *T. viride* exhibited a relatively low activity on thin RChitin films even though they possessed a much greater activity on dissolved chitin oligosaccharides in solution. This difference in solution versus surface activity was attributed to the lack of CBDs in their structures, indicating the importance of CBDs for chitinase activity on insoluble substrates. These results are expected to provide insights into chitinase activity on fungal cell walls.

3.6 References

1. Deveau, A.; Bonito, G.; Uehling, J.; Paoletti, M.; Becker, M.; Bindschedler, S.; Hacquard, S.; Herve, V.; Labbe, J.; Lastovetsky, O. A.; Mieszkin, S.; Millet, L. J.; Vajna, B.; Junier, P.; Bonfante, P.; Krom, B. P.; Olsson, S.; van Elsas, J. D.; Wick, L. Y., Bacterial-fungal interactions: ecology, mechanisms and challenges. *FEMS Microbiol Rev* **2018,** *42*, 335-352.

2. Moebius, N.; Uzum, Z.; Dijksterhuis, J.; Lackner, G.; Hertweck, C., Active invasion of bacteria into living fungal cells. *Elife* **2014,** *3*, e03007.

3. Kruger, W.; Vielreicher, S.; Kapitan, M.; Jacobsen, I. D.; Niemiec, M. J., Fungal-bacterial interactions in health and disease. *Pathogens* **2019,** *8*, 70.

4. Kang, X.; Kirui, A.; Muszynski, A.; Widanage, M. C. D.; Chen, A.; Azadi, P.; Wang, P.; Mentink-Vigier, F.; Wang, T., Molecular architecture of fungal cell walls revealed by solid-state NMR. *Nat Commun* **2018,** *9*, 2747.

5. Rajasingham, R.; Smith, R. M.; Park, B. J.; Jarvis, J. N.; Govender, N. P.; Chiller, T. M.; Denning, D. W.; Loyse, A.; Boulware, D. R., Global burden of disease of HIV-associated cryptococcal meningitis: an updated analysis. *Lancet Infect Dis* **2017,** *17*, 873-881.

6. Ohno, M.; Togashi, Y.; Tsuda, K.; Okawa, K.; Kamaya, M.; Sakaguchi, M.; Sugahara, Y.;

Oyama, F., Quantification of chitinase mRNA levels in human and mouse tissues by real-time PCR: species-specific expression of acidic mammalian chitinase in stomach tissues. *PLoS One* **2013,** *8*, e67399.

7. Wiesner, D. L.; Specht, C. A.; Lee, C. K.; Smith, K. D.; Mukaremera, L.; Lee, S. T.; Lee, C. G.; Elias, J. A.; Nielsen, J. N.; Boulware, D. R.; Bohjanen, P. R.; Jenkins, M. K.; Levitz, S. M.; Nielsen, K., Chitin recognition via chitotriosidase promotes pathologic type-2 helper T cell responses to cryptococcal infection. *PLoS Pathog* **2015,** *11*, e1004701.

8. Vega, K.; Kalkum, M., Chitin, chitinase responses, and invasive fungal infections. *Int J Microbiol* **2012,** *2012*, 920459.

9. Wang, C. Renewable natural polymer thin films and their interactions with biomacromolecules. Ph.D. Dissertation, Virginia Tech, Blacksburg, VA, 2014.

10. Rinaudo, M., Chitin and chitosan: properties and applications. *Prog Polym Sci* **2006,** *31*, 603-632.

11. Bowman, S. M.; Free, S. J., The structure and synthesis of the fungal cell wall. *Bioessays* **2006,** *28*, 799-808.

12. Gow, N. A. R.; Latge, J. P.; Munro, C. A., The fungal cell wall: structure, biosynthesis, and function. *Microbiol Spectr* **2017,** *5*, FUNK-0035-2016.

13. Free, S. J., Fungal cell wall organization and biosynthesis. *Adv Genet* **2013,** *81*, 33-82.

14. Eijsink, V.; Hoell, I.; Vaaje-Kolstada, G., Structure and function of enzymes acting on chitin and chitosan. *Biotechnol Genet Eng Rev* **2010,** *27*, 331-366.

15. Kawase, T.; Yokokawa, S.; Saito, A.; Fujii, T.; Nikaidou, N.; Miyashita, K.; Watanabe, T., Comparison of enzymatic and antifungal properties between family 18 and 19 chitinases from *S.*

coelicolor A3(2). *Biosci Biotechnol Biochem* **2006,** *70*, 988-998.

16. Garcia-Casado, G.; Collada, C.; Allona, I.; Casado, R.; Pacios, L. F.; Aragoncillo, C.; Gomez, L., Site-directed mutagenesis of active site residues in a class I endochitinase from chestnut seeds. *Glycobiology* **1998,** *8*, 1021-1028.

17. Rathore, A. S.; Gupta, R. D., Chitinases from bacteria to human: properties, applications, and future perspectives. *Enzyme Res* **2015,** *2015*, 791907.

18. Liu, J. Studies of macromolecule/molecule adsorption and activity at solid surfaces. Ph.D. Dissertation, Virginia Tech, Blacksburg, VA, 2019.

19. Berini, F.; Caccia, S.; Franzetti, E.; Congiu, T.; Marinelli, F.; Casartelli, M.; Tettamanti, G., Effects of *Trichoderma viride* chitinases on the peritrophic matrix of Lepidoptera. *Pest Manag Sci* **2016,** *72*, 980-989.

20. Omumasaba, C. A.; Yoshida, N.; Ogawa, K., Purification and characterization of a chitinase from *Trichoderma viride*. *J Gen Appl Microbiol* **2001,** *47*, 53-61.

21. Jenifer, S.; Jeyasree, J.; Laveena, D. K.; Manikandan, K., Purification and characterization of chitinase from *Trichoderma viride* N9 and its antifungal activity against phytopathogenic fungi. *World J Pharm Pharm Sci* **2014,** *3*, 1604-1611.

22. da Silva, L. C.; Honorato, T. L.; Cavalcante, R. S.; Franco, T. T.; Rodrigues, S., Effect of pH and temperature on enzyme activity of chitosanase produced under solid stated fermentation by *Trichoderma* spp. *Indian J Microbiol* **2012,** *52*, 60-65.

23. Mallikharjuna Rao, K. L.; Siva Raju, K.; Ravisankar, H., Cultural conditions on the production of extracellular enzymes by *Trichoderma* isolates from tobacco rhizosphere. *Braz J Microbiol* **2016,** *47*, 25-32.

24. Ekundayo, E. A.; Ekundayo, F. O.; Bamidele, F., Production, partial purification and optimization of a chitinase produced from *Trichoderma viride*, an isolate of maize cob. *Mycosphere* **2016,** *7*, 786-793.

25. Kurita, K.; Sugita, K.; Kodaira, N.; Hirakawa, M.; Yang, J., Preparation and evaluation of trimethylsilylated chitin as a versatile precursor for facile chemical modifications. *Biomacromolecules* **2005,** *6*, 1414-1418.

26. Kittle, J. D.; Wang, C.; Qian, C.; Zhang, Y.; Zhang, M.; Roman, M.; Morris, J. R.; Moore, R. B.; Esker, A. R., Ultrathin chitin films for nanocomposites and biosensors. *Biomacromolecules* **2012,** *13*, 714-718.

27. Dixon, M. C., Quartz crystal microbalance with dissipation monitoring: enabling real-time characterization of biological materials and their interactions. *J Biomol Tech* **2008,** *19*, 151-158.

28. Zhang, X. Adsorption of biomacromolecules onto polysaccharide surfaces. Ph.D. Dissertation, Virginia Tech, Blacksburg, VA, 2014.

29. Chen, Q.; Xu, S.; Liu, Q.; Masliyah, J.; Xu, Z., QCM-D study of nanoparticle interactions. *Adv Colloid Interface Sci* **2016,** *233*, 94-114.

30. Rojas, O. J.; Jeong, C.; Turon, X.; Argyropoulos, D. S. Measurement of cellulase activity with piezoelectric resonators. In *Materials, chemicals, and energy from forest biomass*; Argyropoulos, D. S., Ed.; American Chemical Society: Washington, DC, 2007; pp 478-494.

31. Kittle, J. D.; Qian, C.; Edgar, E.; Roman, M.; Esker, A. R., Adsorption of xyloglucan onto thin films of cellulose nanocrystals and amorphous cellulose: film thickness effects. *ACS Omega* **2018,** *3*, 14004-14012.

32. Kittle, J. D.; Du, X.; Jiang, F.; Qian, C.; Heinze, T.; Roman, M.; Esker, A. R., Equilibrium

water contents of cellulose films determined via solvent exchange and quartz crystal microbalance with dissipation monitoring. *Biomacromolecules* **2011,** *12*, 2881-2887.

33. Wang, C.; Kittle, J. D.; Qian, C.; Roman, M.; Esker, A. R., Chitinase activity on amorphous chitin thin films: a quartz crystal microbalance with dissipation monitoring and atomic force microscopy study. *Biomacromolecules* **2013,** *14*, 2622-2628.

34. Hu, G.; Heitmann, J. A.; Rojas, O. J., In situ monitoring of cellulase activity by microgravimetry with a quartz crystal microbalance. *J Phys Chem B* **2009,** *113*, 14761-14768.

35. Turon, X.; Rojas, O. J.; Deinhammer, R. S., Enzymatic kinetics of cellulose hydrolysis: a QCM-D study. *Langmuir* **2008,** *24*, 3880-3887.

36. Liu, J.; Zhu, Y.; Wang, C.; Goodell, B.; Esker, A. R., Chelator-mediated biomimetic degradation of cellulose and chitin. *Int J Biol Macromol* **2020,** *153*, 433-440.

37. Brameld, K. A.; Shrader, W. D.; Imperiali, B.; Goddard, W. A., Substrate assistance in the mechanism of family 18 chitinases: theoretical studies of potential intermediates and inhibitors. *J Mol Biol* **1998,** *280*, 913-923.

38. Tews, I.; Terwisscha van Scheltinga, A. C.; Perrakis, A.; Wilson, K. S.; Dijkstra, B. W., Substrate-assisted catalysis unifies two families of chitinolytic enzymes. *J Am Chem Soc* **1997,** *119*, 7954-7959.

39. Oyeleye, A.; Normi, Y. M., Chitinase: diversity, limitations, and trends in engineering for suitable applications. *Biosci Rep* **2018,** *38*, BSR2018032300.

40. Cheng, G.; Datta, S.; Liu, Z.; Wang, C.; Murton, J. K.; Brown, P. A.; Jablin, M. S.; Dubey, M.; Majewski, J.; Halbert, C. E.; Browning, J. F.; Esker, A. R.; Watson, B. J.; Zhang, H.; Hutcheson, S. W.; Huber, D. L.; Sale, K. L.; Simmons, B. A.; Kent, M. S., Interactions of

endoglucanases with amorphous cellulose films resolved by neutron reflectometry and quartz crystal microbalance with dissipation monitoring. *Langmuir* **2012,** *28*, 8348-8358.

41. Itoh, Y.; Watanabe, J.; Fukada, H.; Mizuno, R.; Kezuka, Y.; Nonaka, T.; Watanabe, T., Importance of Trp59 and Trp60 in chitin-binding, hydrolytic, and antifungal activities of *Streptomyces griseus* chitinase C. *Appl Microbiol Biotechnol* **2006,** *72*, 1176-1184.

42. Tronsmo, A.; Harman, G. E., Detection and quantification of *N*-acetyl-β-D-glucosaminidase, chitobiosidase, and endochitinase in solutions and on gels. *Anal Biochem* **1993,** *208*, 74-79.

43. Haran, S.; Schickler, H.; Oppenheim, A.; Chet, I., New components of the chitinolytic system of *Trichoderma harzianum*. *Mycol Res* **1995,** *99*, 441-446.

44. *Manual of clinical enzyme measurements*; Worthington Biochemical Corporation: Freehold, NJ, 1972.

Chapter 4: Surface-Initiated Synthesis and Degradation of C-Lignin Films: Comparison with G- and H-Lignin Films

4.1 Abstract

A new naturally occurring lignin, catechyl lignin (C-lignin), was recently discovered in the seed coat tissues of vanilla orchids and several cactus species. Compared to conventional lignin which has a crosslinked and heterogeneous structure, the C-lignin is a linear homopolymer derived solely from caffeyl alcohol (C-alcohol) that is almost exclusively connected through benzodioxane linkages. Due to these characteristics, the C-lignin is promising to tackle the challenge of lignin valorization and circumvent the issue of lignin recalcitrance to degradation in the lignocellulosic biorefinery. In this work, C-DHP films were synthesized on gold surfaces via surface-immobilized horseradish peroxidase (HRP)-catalyzed dehydrogenative polymerization of C-alcohol in various solvents. The films were then degraded through different Fenton systems under mild conditions with the degradation monitored using a quartz crystal microbalance with dissipation monitoring (QCM-D) and atomic force microscopy (AFM). Results for C-DHP films were compared with conventional DHP films. During polymerization, the reaction rate and yield for C-DHP was lower than DHPs synthesized from coniferyl alcohol (G-alcohol) and *p*-coumaryl alcohol (H-alcohol) under the same conditions. The C-DHP films underwent complete Fenton mediated degradation in contrast to the G-DHP and H-DHP films regardless of their thickness. This work revealed differences in synthetic and degradation processes of C-lignin films from conventional lignin films.

4.2 Introduction

Lignin is one of the most abundant, naturally occurring biopolymers, accounting for 15 to 35% of the dry weight of woody plants and about 30% of non-fossil organic carbon in the

biosphere.[1-2] It provides mechanical support and rigidity to plants, helps bind adjacent cells together, protects against pathogens, and mediates internal transport of water and nutrients.[3-4] Lignin can be found in all vascular plants, mostly between the tracheids and in the secondary cell walls.[5] Conventional lignin is an amorphous, crosslinked, and heterogeneous aromatic polymer that is primarily derived from the dehydrogenative polymerization of *p*-coumaryl alcohol (H-alcohol), coniferyl alcohol (G-alcohol), and sinapyl alcohol (S-alcohol).[1-2, 4-6] These three monolignols form *p*-hydroxyphenyl (H), guaiacyl (G), and syringyl (S) structural units of lignin, respectively, which are linked together through a variety of bonds, such as β-*O*-4 (usually more than 50% of total linkages), α-*O*-4, 4-*O*-5, β-1, β-β, β-5, and 5-5.[7-8]

Lignocellulosic biomass is widely utilized in agro-industries to produce pulp, biofuels, and biocomposites due to its inherent renewability and sustainability. However, the recalcitrance of lignin to degradation arising from its complex structure largely impedes the economical efficiency of biorefining processes. Moreover, the decomposition of lignin usually leads to a wide distribution of products owing to the heterogeneity of lignin, which greatly increases the separation and purification costs. A new naturally occurring lignin, catechyl lignin (C-lignin), may overcome those challenges. It was discovered in the seed coat tissues of vanilla orchids and several cactus species in recent years and is a linear homopolymer derived solely from caffeyl alcohol (C-alcohol) that is almost exclusively connected through benzodioxane linkages.[8-10]

Although C-lignin promises to be an ideal substrate for lignin valorization, there have only been limited studies. It is generally accepted that the C-lignin is biosynthesized via combinatorial oxidative radical coupling, a mechanism analogous to that for classic lignification.[10-14] The end units of growing C-lignin polymer chains are oxidized by plant peroxidases and/or laccases to phenolic radicals, and then cross-coupled with the monolignol radicals in a chemically controlled

manner. Chen et al.[10] synthesized a dehydrogenative polymer from C-alcohol (C-DHP) in vitro through horseradish peroxidase (HRP)-catalyzed polymerization with the assistance of hydrogen peroxide (H_2O_2) in an acetone/sodium phosphate buffer solution. The structure of the C-DHP was carefully studied with about 98% benzodioxane units and small amounts of β-5, β-β, and other units. The C-DHP structure was strikingly similar to that of isolated C-lignin from *Vanilla planifolia* seed coats. However, the polymerization kinetics of C-alcohol and the differences between the synthesis of C-lignin and conventional lignin have never been reported.

Many strategies have been developed to degrade conventional lignin, such as hydrogenolysis, oxidation, pyrolysis, liquefaction, and hydrolysis, but the degradation of C-lignin is limited to reports on hydrogenolytic approaches which are performed at high temperature and H_2 pressure.[13, 15-19] Li et al.[19] found C-lignin was quite stable even under harsh acidic conditions and gained extremely low yields of monomeric products when two traditional lignin degradative methods, alkaline nitrobenzene oxidation and thioacidolysis, were applied to C-lignin. Nevertheless, they completely depolymerized the C-lignin via hydrogenolysis under 40 bar H_2 at 200 ^{o}C. Through optimization of catalyst (Pt/C, Pd/C, or Ru/C) and solvent (methanol, dioxane/water, or THF/water) combination, a better product yield and selectivity were obtained than for the depolymerization of conventional lignin. Furthermore, C-lignin yielded a narrower distribution of degradation products relative to conventional lignin, but new approaches for effective C-lignin degradation under mild conditions are desired.

In this work, C-DHP films were prepared on gold surfaces in an “end-wise” approach via surface-immobilized HRP-catalyzed dehydrogenative polymerization of C-alcohol for the first time. Effects of different solvents on the polymerization kinetics were investigated, and the synthesis of C-DHP films was compared with that of conventional G-DHP and H-DHP films.

Enzymatic and chemical degradation of the synthesized C-DHP films were further studied, and it was found that Fenton chemistry quickly and completely degraded the C-DHP films under mild conditions. The changes in the mass of the C-DHP films during degradation were monitored in real time via a quartz crystal microbalance with dissipation monitoring (QCM-D), and the morphologies of the C-DHP film before and after degradation were imaged by atomic force microscopy (AFM). The differences in degradation between the C-DHP films and conventional DHP films were explored upon treatment with Fenton reagents. This study developed an approach for the synthesis and degradation of C-lignin films under mild conditions and revealed differences from conventional lignin.

4.3 Experimental Section

4.3.1 Materials

Caffeyl alcohol (C-alcohol, ≥ 95%) was synthesized by Syntame Ltd. in Ningbo, China. G- and H-alcohols were synthesized in our lab following published procedures.[2] Horseradish peroxidase (HRP, type I, essentially salt-free, lyophilized powder) and H_2O_2 (30 wt% in H_2O) were purchased from Sigma-Aldrich. Ammonium hydroxide (30% NH_3 in H_2O), acetone (≥ 99.9%), and methanol (≥ 99.9%) were supplied by Fisher Scientific. Lignin peroxidase (LiP), manganese peroxidase (MnP, from white-rot fungus (*Phanerochaete chrysosporium*)), manganese (II) sulfate monohydrate ($MnSO_4 \cdot H_2O$), iron(II) sulfate heptahydrate ($FeSO_4 \cdot 7H_2O$), and iron(III) chloride hexahydrate ($FeCl_3 \cdot 6H_2O$) were obtained from Sigma-Aldrich. 2,3-Dihydroxybenzoic acid (DHBA) was purchased from TCI America. L-(+)-Tartaric acid and sodium hydroxide were supplied by Sigma-Aldrich and used for the preparation of 10 mM sodium tartrate buffer solutions at pH 3.0 and 4.5. Sodium phosphate monobasic monohydrate and sodium phosphate dibasic heptahydrate were purchased from Sigma-Aldrich to prepare 100

mM phosphate buffer solution at pH 6.5. A 100 mM pH = 4.0 acetate buffer solution was prepared using sodium acetate and acetic acid that were obtained from Sigma-Aldrich. Nitrogen (N_2, ultrahigh purity) was supplied by Airgas, and ultrapure water (Millipore Milli-Q, 18.2 MΩ cm) was used in all experiments.

4.3.2 Preparation of DHP Films

The DHP films were synthesized directly on gold-coated QCM-D sensor (QSX 301 from Biolin Scientific) surfaces via dehydrogenative polymerization, and the process was monitored in real time through QCM-D (QSense E4 Analyzer, Biolin Scientific). Prior to synthesis, the sensors were cleaned by treating with UV/ozone for 20 min, and then immersion in a solution of H_2O_2/ammonium hydroxide/ultrapure water (1/1/5 v/v) at 80 ^oC for 1 h, followed by a rinse with ultrapure water and drying under N_2 gas.

Once the cleaned sensors were loaded into the flow modules of the QCM-D, ultrapure water was flowed over them at a rate of 0.1 mL/min until a stable baseline was reached. Then, an aqueous solution of HRP at a concentration of 1.0 mg/mL was injected into the flow modules at the same flow rate for 25 min. After that, the flow was changed to water to wash away the reversibly adsorbed HRP. Next, monolignol aqueous solution containing 20 mM H_2O_2 was introduced into the flow modules at 0.1 mL/min for polymerization. After 90 min, the flow was switched to water again for the removal of reversibly adsorbed monolignol and low molecular weight DHP. The synthesis of C-DHP films was also performed using 100 mM sodium phosphate buffer (pH 6.5) and a mixture of acetone/water (2/98 v/v) as solvents instead of pure water for comparison.

4.3.3 Enzymatic Degradation of C-DHP Films by Ligninolytic Enzymes

After polymerization, the sensors loaded with C-DHP films were equilibrated in 10 mM sodium tartrate buffer (pH = 3.0 for LiP and 4.5 for MnP) at a flow rate of 0.1 mL/min for 60 min. Then, MnP (with 0.5 mM $MnSO_4$) or LiP buffered solution at a concentration of 0.3 mg/mL containing 2 mM H_2O_2 was introduced into the flow modules at the same flow rate. After 50 min, the flow was stopped and the degradation proceeded in the absence of flow. When the frequency reached a plateau, pure buffer followed by ultrapure water were flowed over the sensors for the removal of reversibly adsorbed molecules, such as degradation products and the ligninolytic enzyme.

4.3.4 Chemical Degradation of DHP Films by Fenton Chemistry

After polymerization, the sensors loaded with DHP films were equilibrated in 100 mM pH = 4.0 acetate buffer at a flow rate of 0.1 mL/min for 60 min. Next, $FeSO_4$ or $FeCl_3$ buffered solution at a concentration of 10 mM were introduced into the flow modules at the same flow rate for 50 min. The flow was then switched to 0.4 M H_2O_2 buffered solution with or without 5 mM DHBA, and after 8 min when the frequency began to increase, the flow was stopped and the degradation proceeded in the absence of flow. Once the frequency reached a plateau, pure buffer followed by ultrapure water were flowed through the flow modules for the removal of reversibly adsorbed molecules, such as degradation products. Similar procedures were used for the degradation of HRP without the polymerization of C-alcohol.

4.3.5 AFM Measurements

The DHP films on QCM-D sensors after synthesis or degradation were removed from the flow modules, rinsed gently with water, and dried under N_2 flow. They were then imaged in

ScanAsyst mode via a Bruker Dimension Icon atomic force microscope with a ScanAsyst-Air probe under ambient conditions (22 ^{o}C and 50% relative humidity). Height images of 2 μm × 2 μm areas and their root-mean-square (RMS) roughnesses were collected. The surfaces of bare gold-coated QCM-D sensors were imaged under the same conditions.

4.3.6 Mass Spectrometry (MS) Measurements

Solution that flowed out of the QCM-D during the polymerization process was collected and dried at 60 ^{o}C in a vacuum oven. MS samples were prepared by dissolving the recovered solids in methanol at a concentration of 1.0 mg/mL. MS measurements were performed with Agilent 6220 Accurate Mass TOF LC/MS. The samples were injected by an Agilent 1311 HPLC pump and a 1367B autosampler. The HPLC was operated in isocratic mode using methanol/H_2O (65/35 v/v) containing 0.1% formic acid as the mobile phase at a flow rate of 0.5 mL/min. Results were obtained using both positive and negative modes.

4.3.7 QCM-D Analysis

All QCM-D experiments, including both the synthesis and degradation of DHP films, were conducted at 20 ^{o}C. Frequency (Δf) and energy dissipation (ΔD) changes at the fundamental frequency and 6 odd overtones (n = 3, 5, 7, …, 13) were monitored simultaneously. Data presented in this work corresponded to the fifth overtone (n = 5).

If the film was thin, rigid, and firmly attached to the sensor surface, the mass change followed the Sauerbrey equation:[20-22]

$$\Delta \mathrm{m} = -C\left(\frac{\Delta f}{n}\right) \tag{4.1}$$

where C = 0.177 mg m^{-2} Hz^{-1}.

Nevertheless, the Sauerbrey relation will underestimate the mass if the film is soft.

Viscoelasticity changes were reflected in energy dissipation (D):[20-22]

$$D = \frac{E_{\text{lost}}}{2\pi E_{\text{stored}}} \tag{4.2}$$

where E_{lost} and E_{stored} were the energy dissipated and stored per oscillation, respectively. Qualitatively, as the frequency increased, the mass of the film decreased, and an increase in dissipation meant the film became softer.

4.4 Results and Discussion

4.4.1 Synthesis of C-DHP Films in Water

Figure 4.1 provides a representative plot of $\Delta f/n$ vs. t for the synthesis of C-DHP. After the initial equilibration of the bare gold sensor in water, HRP aqueous solution was introduced. An instantaneous decrease in frequency was observed as HRP and its coupled water were adsorbed onto the gold surface. This process usually reached equilibrium within 20 min, and then the frequency increased slightly with the injection of water which washed away reversibly adsorbed HRP. Once the C-alcohol aqueous solution containing H_2O_2 flowed over the sensor, the frequency immediately decreased, which was attributed to the formation of C-DHP via HRP-catalyzed dehydrogenative polymerization of C-alcohol in the presence of H_2O_2. The reaction rate could be represented by the slope of $\Delta f/n$ versus time, i.e. $d(\Delta f/n) / dt$. A large negative slope indicated the mass of the C-DHP layer increased rapidly. As the C-DHP chains grew, it became more difficult for them to be oxidized by the HRP, and the reaction rate gradually decreased to zero. The C-DHP layer was finally rinsed with water for the removal of soluble low molecular weight C-DHP and reversibly adsorbed C-alcohol, which led to a small increase in frequency. The ΔD vs. t curve reflected viscoelasticity changes. An increase in the dissipation was observed for HRP adsorption and C-DHP formation, while the dissipation decreased slightly as water was

introduced at the end of the experiment. It seemed that the generated C-DHP layer was soft in the aqueous environment, based upon the dissipation plateau value (> 5×10^{6}) after polymerization.

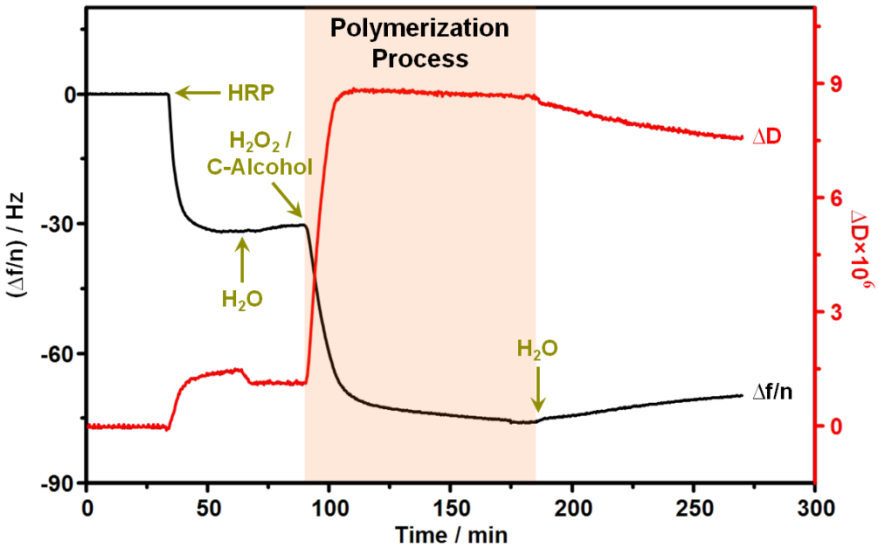

Figure 4.1 Representative $\Delta f/n$ and ΔD versus time for the synthesis of C-DHP films in H_2O through surface-immobilized HRP-catalyzed dehydrogenative polymerization of 0.5 mg/mL C-alcohol in the presence of H_2O_2.

Since the C-alcohol aqueous solution flowed over the sensor during the entire polymerization process, it was believed that some synthesized C-DHP with a low molecular weight was soluble in water and flowed out of the QCM-D. Therefore, the solution that flowed out of the QCM-D during the polymerization process was collected, processed, and analyzed via MS. As seen in Figure 4.2, a large peak for the C-DHP dimer existed, which demonstrated successful coupling of C-alcohol.

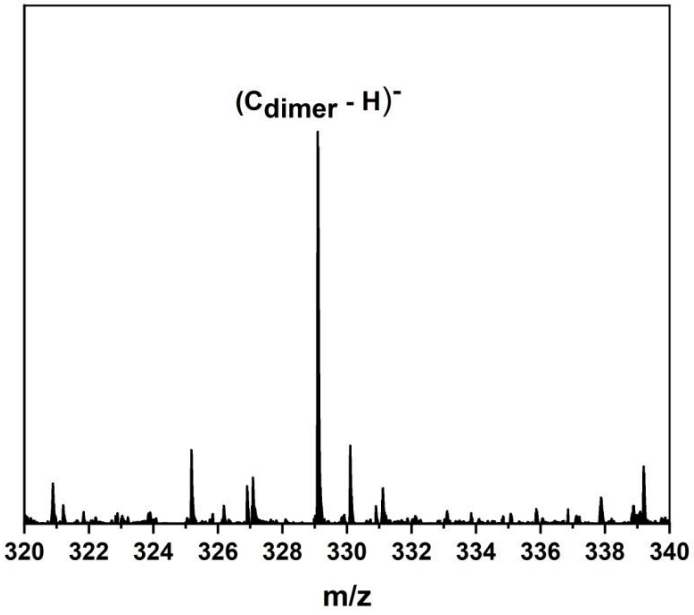

Figure 4.2 A representative mass spectrum for solids recovered from the solution that flowed out of the QCM-D during the process of 0.5 mg/mL C-alcohol polymerization in the presence of H_2O_2 in H_2O.

4.4.2 Effects of Solvents on the Synthesis of C-DHP Films

Although there have been a few reports on the synthesis of bulk C-DHP in solution,[10, 19, 23] the C-DHP film was directly synthesized for the first time in this study. The synthesis of bulk C-DHP in solution in the literature was typically performed through the slow and continuous addition of two separate solutions of C-alcohol in acetone/sodium phosphate buffer and H_2O_2 in water to a third solution of HRP in buffer.[10, 19, 23] Since the C-DHP film was synthesized with only water as the solvent in the previous section, effects of acetone and sodium phosphate buffer on the surface-immobilized HRP-catalyzed dehydrogenative polymerization of C-alcohol were considered.

As shown in Figure 4.3, the use of a 2% aqueous acetone solution as the solvent altered the amount of C-DHP that formed. The adsorption of HRP was unaffected. However, the rate of

polymerization of C-alcohol decreased and the yield of C-DHP was reduced by ~52% compared to that in water. The films had similar surface RMS roughnesses ~4.5 nm (water) to ~4.1 nm (aqueous acetone), as displayed in Figures 4.4b and 4.4d. Apparent decreased HRP activity was attributed to potential enzyme denaturation and enhanced solubility of the C-DHP in the less polar solvent. When the solvent was changed from water to 100 mM pH = 6.5 sodium phosphate buffer, HRP adsorption decreased by ~50% and the yield of C-DHP decreased by ~57%. It seemed that the buffer was not conducive to the adsorption and enzymatic activity of HRP, which might have arisen from effects of pH, ionic strength, and phosphate ions on the stability of the HRP glycoprotein.[24-25] The AFM images in Figures 4.4b and 4.4c further demonstrated the QCM-D data. Compared to that synthesized in water, the C-DHP film synthesized in buffer had fewer and smaller aggregates with a RMS roughness of ~3.7 nm.

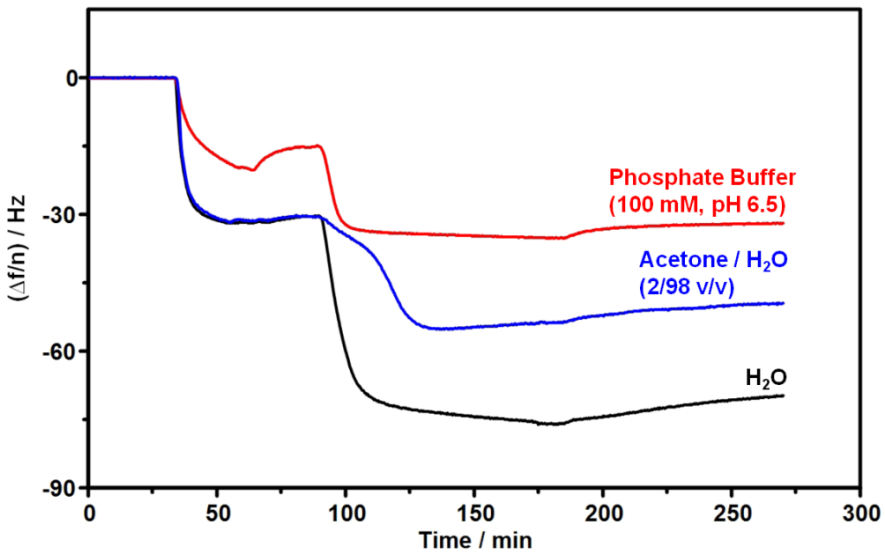

Figure 4.3 Representative $\Delta f/n$ vs. t for the synthesis of C-DHP films through surface-immobilized HRP-catalyzed dehydrogenative polymerization of 0.5 mg/mL C-alcohol in the presence of H_2O_2 in 100 mM phosphate buffer at pH 6.5, acetone/H_2O (2/98 v/v), and H_2O.

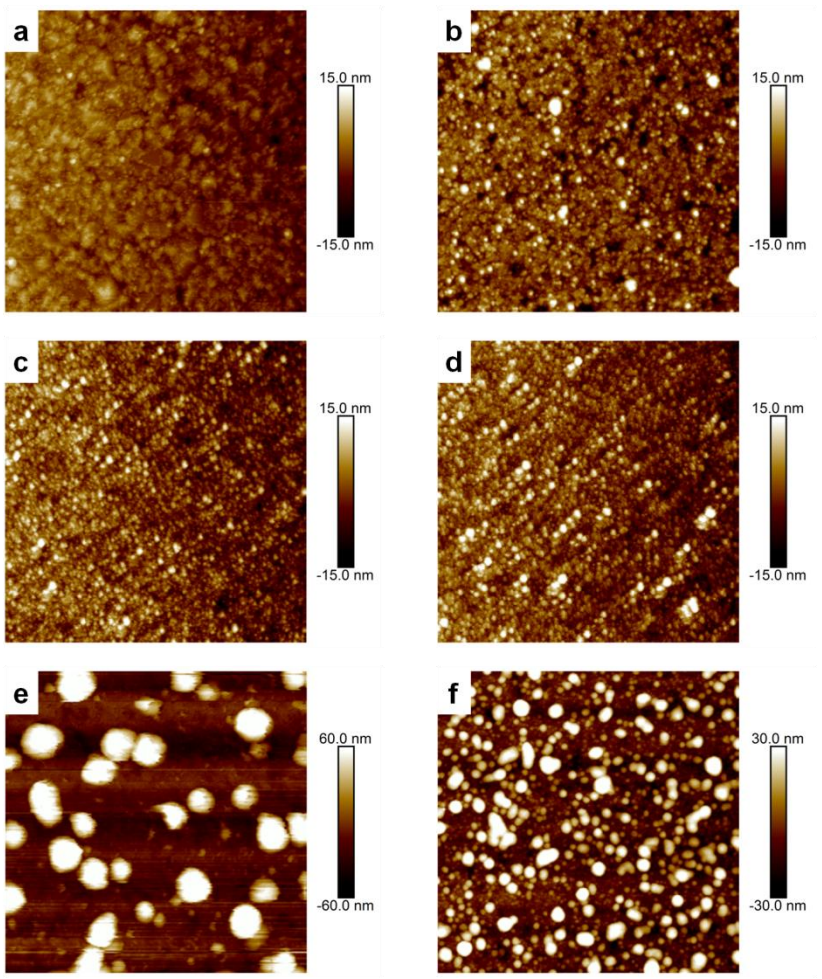

Figure 4.4 Representative AFM height images (2 μm × 2 μm) of (a) bare gold-coated QCM-D sensor surface (~2.3 nm), and DHP films synthesized through surface-initiated dehydrogenative polymerization of 0.5 mg/mL (b) C-alcohol in H_2O (~4.5 nm), (c) C-alcohol in 100 mM pH = 6.5 phosphate buffer (~3.7 nm), (d) C-alcohol in 2% (v/v) aqueous acetone (~4.1 nm), (e) G-alcohol in H_2O (~31 nm), and (f) H-alcohol in H_2O (~14 nm). Numbers in parentheses correspond to RMS roughnesses obtained from the entire image.

4.4.3 Comparison with the Synthesis of G- and H-DHP Films

In order to understand the differences in biosynthesis between the C-lignin and conventional lignin, G-DHP and H-DHP films were synthesized (Figure 4.5). It could be seen that the yields

of G-DHP and H-DHP were much larger than that of C-DHP under the same conditions. The $\Delta f/n$ vs. t curves for the G-DHP and H-DHP reached ~-430 Hz and ~-130 Hz, respectively, after the water wash, while the $\Delta f/n$ vs. t curve for the C-DHP only reached ~-70 Hz. Although the DHP layers on the QCM-D sensors were not strictly evenly distributed and rigidly attached, the Sauerbrey equation could still be used to roughly estimate their surface concentrations. As a result, the synthesized C-DHP, H-DHP, and G-DHP were 6.9 mg/m^2, 18.8 mg/m^2, and 70.3 mg/m^2, respectively, according to equation 4.1. The rates of polymerization were G-DHP > H-DHP > C-DHP. The G-DHP and H-DHP were more readily synthesized than the C-DHP, and a possible reason was that the stable benzodioxane structure acted like a "shield" protecting the C-DHP from oxidation by HRP. After reaching the minimum $\Delta f/n$ value, the C-DHP and H-DHP curves plateaued almost immediately, but the G-DHP curve increased instead. This might be because the fast rate of G-alcohol polymerization led to insufficient reaction that generated some soluble G-DHP oligomers and these G-DHP oligomers flowed away from the G-DHP film.

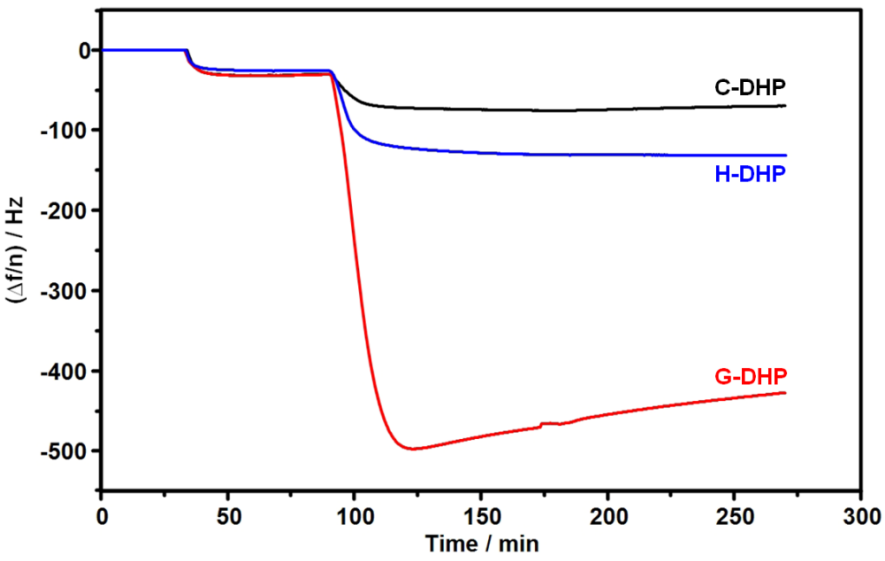

Figure 4.5 Representative $\Delta f/n$ vs. t for the synthesis of C-DHP, H-DHP, and G-DHP films through surface-immobilized HRP-catalyzed dehydrogenative polymerization of 0.5 mg/mL C-alcohol, H-alcohol, and G-alcohol, respectively, in the presence of H_2O_2 in H_2O.

The morphologies of the synthesized DHP layers were investigated by AFM. As exhibited in Figures 4.4b, 4.4e, and 4.4f, the DHPs aggregated into irregular globular particles on the sensor surfaces. The sizes of the aggregates increased in the order C-DHP < H-DHP < G-DHP, and were consistent with an upward trend in surface roughness. The C-DHP layer was the smoothest surface, and the RMS roughnesses were ~4.5 nm (C-DHP), ~14 nm (H-DHP), and ~31 nm (G-DHP).

4.4.4 Enzymatic Degradation of C-DHP Films by Ligninolytic Enzymes

In nature, lignin is usually degraded by microorganisms via oxidation under mild conditions using various ligninolytic enzymes, such as LiP, MnP, versatile peroxidase, dye-decolorizing peroxidase, and laccase.[7, 26] Two common ligninolytic enzymes, LiP and MnP, were employed to degrade the synthesized C-DHP films in this study. H_2O_2 was added to assist in completing the catalytic cycle. In addition, the MnP required Mn^{2+} to be oxidized to Mn^{3+} for the oxidation of

substrates. Therefore, $MnSO_4$ was added to the MnP solution.

As shown in Figure 4.6, sodium tartrate buffer (pH 3.0 for LiP and 4.5 for MnP) was introduced into the QCM-D sensor for the benefit of ligninolytic enzyme activity after the C-DHP film was synthesized and washed with water. The frequency was immediately reduced as soon as the enzyme solution flowed over the sensor, which was attributed to the adsorption of the enzyme onto the C-DHP film. The surface concentrations of LiP and MnP reached 7.7 mg/m^2 and 4.4 mg/m^2, respectively, under the assumption that the Sauerbrey equation was valid. The flow was stopped after 50 min, and the degradation proceeded in the absence of flow. After incubation for 15 h, a frequency increase was observed for the LiP that was slightly larger than the MnP. However, neither LiP nor MnP produced an obvious increase in the frequency. These observations indicated LiP and MnP produced no significant C-DHP film degradation. Although both LiP and MnP have exhibited insignificant degradation on conventional G-DHP or H-DHP in the literature,[27] their performance on the degradation of the C-DHP was even less. Berstis et al.[12] and Kim et al.[28] computed bond dissociation enthalpies for model lignin dimers using density functional theory, and their results showed that higher energy was required to fully break the benzodioxane linkage than the traditional β-*O*-4 linkage. In addition, unlike the conventional G-DHP and H-DHP that had a complex structure containing both phenolic and non-phenolic subunits, there were no phenolic subunits in the structure of the C-DHP. Although LiP with a high redox potential up to 1.4 V was capable of oxidizing both phenolic and non-phenolic substrates, it catalyzed the oxidation of phenolic substrates far more readily and at much faster rates.[29-31] Furthermore, traditional non-phenolic β-*O*-4 lignin subunits were oxidized to cation radicals by the LiP in the catalytic process.[30-31] The electron-donating benzylic hydroxyl group on C_α helped the formation and stabilization of the cation radicals, and thereby facilitated the

reaction.[30-31] Nevertheless, there were no such benzylic hydroxyl groups in the benzodioxane lignin structure. Thus, worse oxidative degradation performance by the LiP on the C-DHP than on the conventional DHPs was observed. Compared to the LiP, the MnP had a relatively low redox potential of ~0.8 V and only oxidized phenolic substrates without the addition of some mediators, such as glutathione in the literature.[26, 30-32] Therefore, MnP hardly degraded the C-DHP film. Finally, fresh buffer was introduced which caused a small increase in the frequency on account of the removal of some reversibly adsorbed degradation products and enzymes, and the injection of water brought about an additional frequency increase due to the alleviated density and viscosity of the water relative to the buffer.

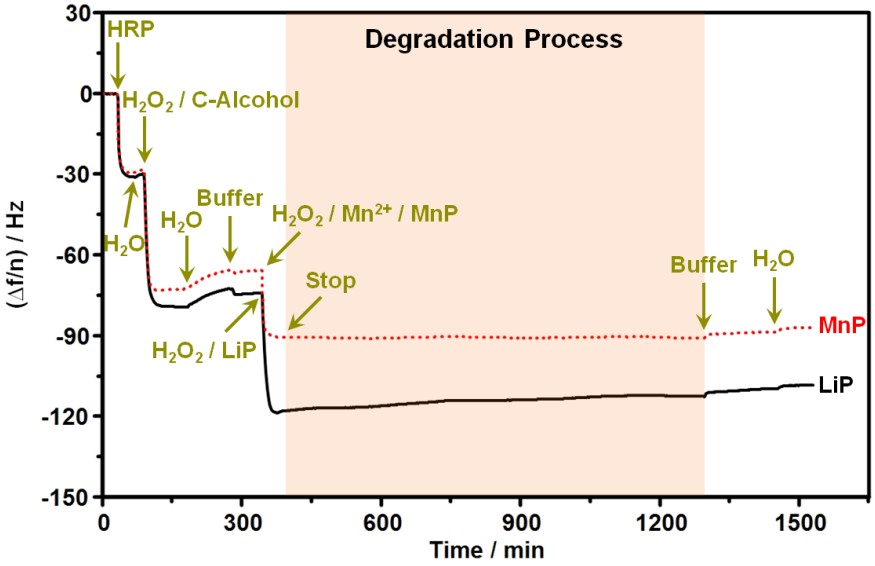

Figure 4.6 Representative $\Delta f/n$ vs. t for the synthesis of C-DHP films through surface-immobilized HRP-catalyzed dehydrogenative polymerization of 0.5 mg/mL C-alcohol in the presence of H_2O_2 in H_2O and the subsequent enzymatic degradation of the synthesized C-DHP films by LiP and MnP, respectively.

The AFM images of the C-DHP films after degradation by LiP and MnP are provided in Figures 4.7a and 4.7b. Their RMS roughnesses increased slightly relative to those before the LiP

or MnP incubation, which might be caused by slight degradation and the presence of irreversibly adsorbed ligninolytic enzymes on the C-DHP film surface.

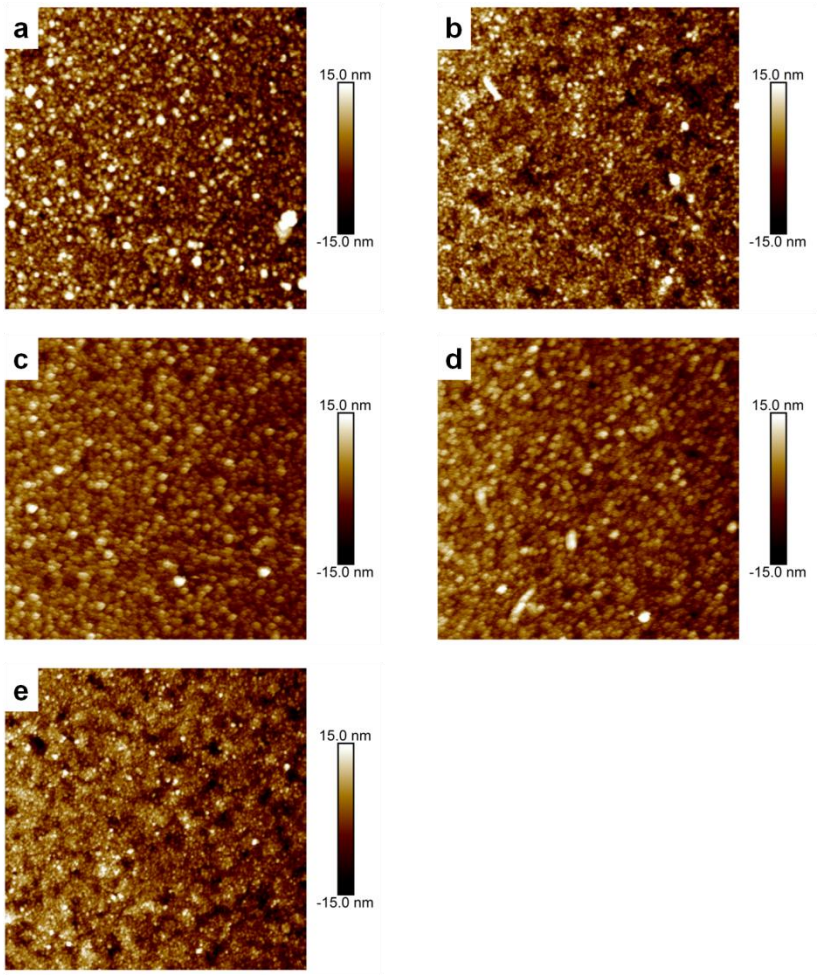

Figure 4.7 Representative AFM height images (2 μm × 2 μm) of C-DHP films synthesized through surface-initiated dehydrogenative polymerization of 0.5 mg/mL C-alcohol in H_2O after degradation by (a) LiP (~5.2 nm), (b) MnP (~4.7 nm), (c) Fe^{2+} + DHBA/H_2O_2 (~3.1 nm), (d) Fe^{3+} + DHBA/H_2O_2 (~3.3 nm), and (e) Fe^{2+} + H_2O_2 (~4.1 nm). Numbers in parentheses correspond to RMS roughnesses obtained from the entire image.

4.4.5 Chemical Degradation of C-DHP Films by Fenton Chemistry

The degradation of C-lignin reported in the literature has been limited to reports on

hydrogenolytic methods which are performed under high-pressure H_2 at no less than 200 ^oC with noble metal catalysts.[13, 19] In this study, the hydroxyl radicals generated by Fenton reactions ($Fe^{2+} + H_2O_2 \rightarrow Fe^{3+} + HO\cdot + OH^-$ and $Fe^{3+} + H_2O_2 \rightarrow Fe^{2+} + HOO\cdot + H^+$) previously applied widely to waste water were applied to C-DHP films at atmospheric pressure and room temperature.

Fenton reagents, Fe^{2+} and H_2O_2, were flowed into the flow modules separately. After the C-DHP films were synthesized, Fe^{2+} ions were introduced, which led to a decrease in frequency as a result of Fe^{2+} ion uptake by the C-DHP film, and then an H_2O_2 solution containing a chelator, DHBA, was flowed over the sensor to initiate the Fenton reactions. The DHBA acted as an organic Fe chelator/reducer that promoted the reduction of Fe^{3+} to Fe^{2+}. As shown in Figure 4.8, the frequency initially decreased because of H_2O_2 and DHBA adsorption, but subsequently, the frequency increased on account of degradation of the C-DHP film. When $\Delta f/n$ vs. t plateaued, the Fenton reactions were stopped through the injection of buffer which brought about an additional increase in frequency. Finally, ultrapure water was introduced which matched the environment after synthesis of the C-DHP film and facilitated a direct comparison of the frequency changes that resulted from polymerization and degradation without effects from different solvents. The frequency after the water wash reached an even higher value than before the polymerization of the C-alcohol, which indicated complete degradation of the C-DHP film and potential degradation of HRP. The synthesized amount of C-DHP was simply related to the difference between the frequency from the beginning of injection of C-alcohol solution at ~85 min to the end of water washing the synthesized C-DHP film at ~275 min, and the degraded amount of C-DHP was related to the difference between the frequency from the end of the water wash at ~275 min to the end of water washing the degraded C-DHP film at ~1830 min. The percentage of the

C-DHP film that was degraded corresponded to the ratio of the degraded amount to the synthesized amount. A degradation percentage as high as 121% was achieved, as presented in Table 4.1.

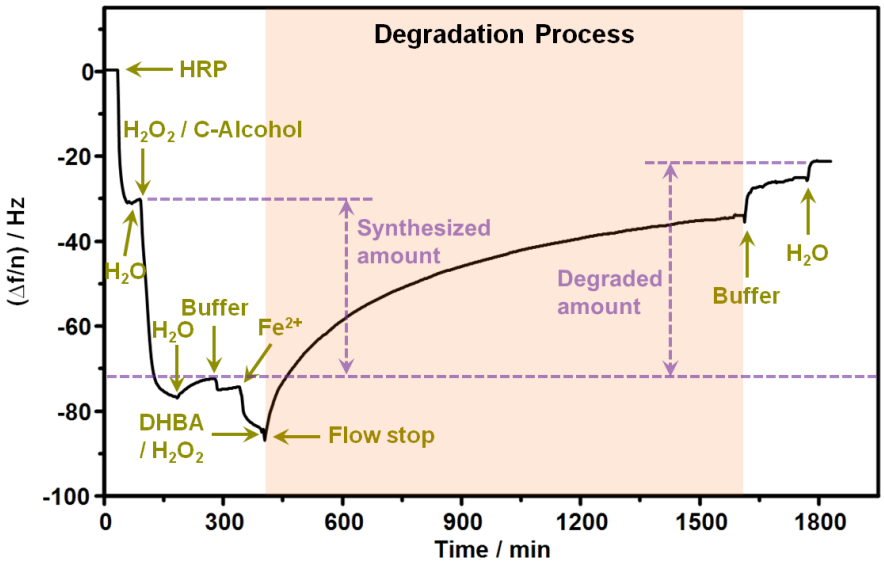

Figure 4.8 Representative $\Delta f/n$ vs. t for the synthesis of C-DHP films through surface-immobilized HRP-catalyzed dehydrogenative polymerization of 0.5 mg/mL C-alcohol in the presence of H_2O_2 in H_2O and the subsequent chemical degradation of the synthesized C-DHP films by Fe^{2+} + DHBA/H_2O_2.

As seen in Table 4.1, 121% of the film was degraded by the Fenton system, Fe^{2+} + DHBA/H_2O_2. Thus, potential Fenton mediated degradation of HRP was explored. In Figure 4.9, representative data for HRP adsorption and Fenton mediated degradation of HRP are provided. As seen in Figure 4.9, HRP without a protective lignin layer underwent nearly complete degradation in the presence of Fe^{2+} + DHBA/H_2O_2 in < 1 h. Thus, degradation percentages in excess of 100% for lignin were reasonable if one considered the degradation of both lignin and HRP in those experiments.

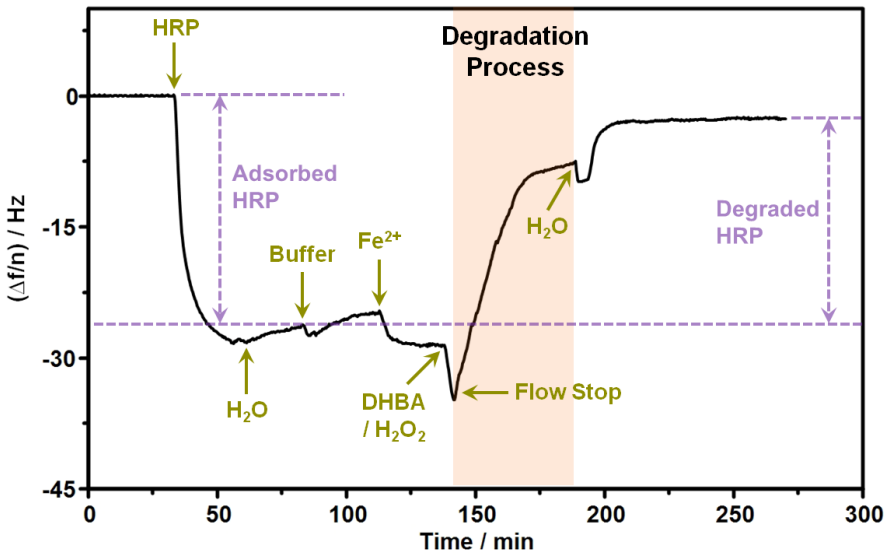

Figure 4.9 Representative $\Delta f/n$ vs. t for the adsorption of HRP onto bare gold-coated QCM-D sensor surface in 1.0 mg/mL aqueous HRP solution and the subsequent chemical degradation of the adsorbed HRP by Fe^{2+} + DHBA/H_2O_2.

4.4.6 Effects of Different Fenton Reagents on the Degradation of C-DHP Films

Based upon the mechanism of the Fenton reactions, they can be carried out without DHBA and with the initial addition of Fe^{3+} ions instead of Fe^{2+} ions. Effects of Fe^{3+} ions and DHBA on lignin degradation by the Fenton system were investigated. As shown in Figure 4.10, the black solid line illustrated representative mass changes for a C-DHP film treated with the Fenton system previously discussed, Fe^{2+} + DHBA/H_2O_2. Figure 4.10 also provided red dotted and blue dashed curves for the degradation of the C-DHP film by Fe^{3+} + DHBA/H_2O_2 and Fe^{2+} + H_2O_2 without a chelator, respectively. Though the reduction-oxidation pair of Fe^{2+} and Fe^{3+} ions were both products and reactants of each other in the catalytic cycle of Fenton reactions, the initial addition of Fe^{2+} ions reduced the consumption of H_2O_2 and directly generated hydroxyl radicals. In contrast, starting with Fe^{3+} meant that some H_2O_2 generated hydroperoxyl radicals instead of hydroxyl radicals. Therefore, both the degradation rate and total degraded amount of the C-DHP

film decreased after replacing Fe^{2+} with Fe^{3+} ions. Nevertheless, the degradation percentage still reached 98% over the same reaction time which indicated almost all of the C-DHP film was degraded, as shown in Table 4.1. A greater difference was observed between the blue dashed and black solid curves in Figure 4.10. The frequency for the blue curve, which corresponded to Fe^{2+} + H_2O_2 without a chelator, increased slightly during the degradation process, but increased almost as much as the other two systems after it was washed with buffer and water. This was probably because the Fe^{2+} ions + H_2O_2 system created larger C-DHP fragments that were unable to leave the sensor surface in the absence of flow which only resumed when buffer and water were introduced at the end of the degradation process. The degradation ability of the Fenton reagents without DHBA was clearly diminished, and the overall degradation percentage was 77%. Fe^{3+} ions needed to be reduced to Fe^{2+} ions in order to continuously generate hydroxyl radicals in Fenton reactions for the oxidative degradation of C-DHP. However, this process was usually slow and inefficient.[33-35] The Fe ion chelator, DHBA, on the other hand, was able to reduce Fe^{3+} to Fe^{2+} ions and thereby enhanced the production of the Fe^{2+} ions, which extended the period of hydroxyl radical formation and alleviated the usage of H_2O_2.

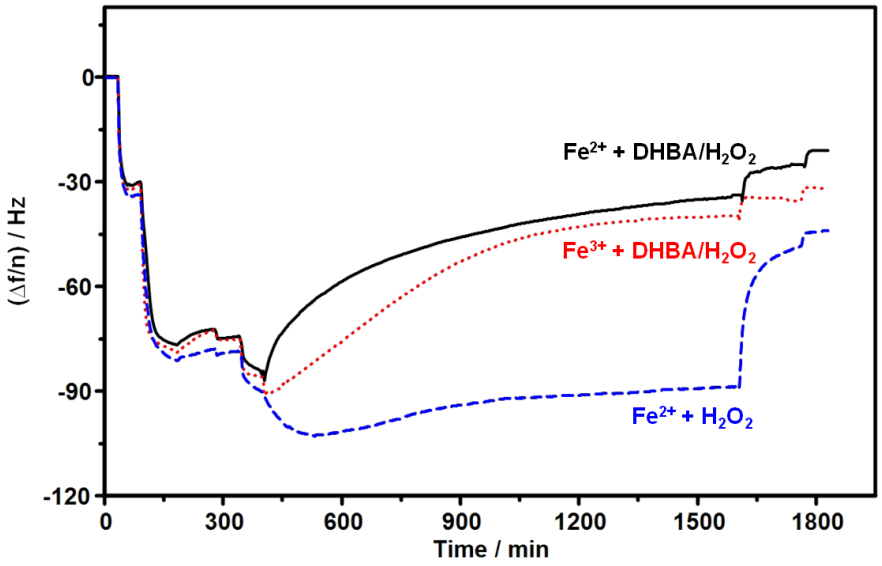

Figure 4.10 Representative $\Delta f/n$ vs. t for the synthesis of C-DHP films through surface-immobilized HRP-catalyzed dehydrogenative polymerization of 0.5 mg/mL C-alcohol in the presence of H_2O_2 in H_2O and the subsequent chemical degradation of the synthesized C-DHP films by Fe^{2+} + DHBA/H_2O_2, Fe^{3+} + DHBA/H_2O_2, and Fe^{2+} + H_2O_2, respectively.

Table 4.1 Effects of Fe ions and DHBA on the Fenton mediated degradation of C-DHP films at 20 ^{o}C according to the data in Figure 4.10.

Fenton System	**$\lvert\Delta f/n\rvert$ (Hz)**		**Percentage Degradation**
	Synthesized Amount	**Degraded Amount**	
Fe^{2+} + DHBA/H_2O_2	42	51	121%
Fe^{3+} + DHBA/H_2O_2	42	41	98%
Fe^{2+} + H_2O_2	44	34	77%

Based upon the above analysis of Figure 4.10, the addition of Fe^{2+} ions and DHBA facilitated the degradation of the C-DHP film, and the degradation ability of the Fenton systems followed the order Fe^{2+} + DHBA/H_2O_2 > Fe^{3+} + DHBA/H_2O_2 > Fe^{2+} + H_2O_2. This trend was consistent

with observations of surface RMS roughnesses by AFM for C-DHP film degradation by Fenton systems. When Fe^{2+} ions with H_2O_2 and DHBA or Fe^{3+} ions with H_2O_2 and DHBA were used as Fenton reagents, the C-DHP films were completely degraded with almost no aggregates observed in Figures 4.7c and 4.7d, which led to smaller surface roughness (~3 nm) than those prior to degradation (~ 5 nm). In contrast, Fe^{2+} ions with H_2O_2 as the Fenton reagents led to partial C-DHP film degradation (Figure 4.7e) with an intermediate surface roughness (~4 nm).

4.4.7 Comparison with the Degradation of G- and H-DHP Films by Fenton Reagents

In order to clarify the effects of lignin structure on degradation, conventional G-DHP and H-DHP films were degraded under the same conditions as those for the C-DHP film using Fe^{2+} + DHBA/H_2O_2 as the Fenton reagents. The concentrations of G-alcohol and H-alcohol solutions during the polymerization process were lowered so the amounts of synthesized G-DHP and H-DHP were similar to C-DHP. For Figure 4.11, the concentrations were 0.05 (G-alcohol) < 0.2 (H-alcohol) < 0.5 (C-alcohol) mg/mL. These concentrations yielded similar initial $\Delta f/n$ ~-75 Hz at the end of the polymerization process in Figure 4.11. For the subsequent degradation process in Figure 4.11, there was an obvious trend. The conventional DHP films were degraded more slowly and to lesser extents than the C-DHP film. Table 4.2 showed that the degradation percentages, calculated from $\Delta f/n$ of the DHP films in water at the end of the polymerization process and $\Delta f/n$ of the final plateau in water at the end of the experiment, for G-DHP and H-DHP were only 47% and 33%, respectively, versus 121% for C-DHP. These results clearly showed that the C-DHP was more readily degraded than conventional DHPs and the enhanced C-lignin degradation was attributed to the linear benzodioxane structure.

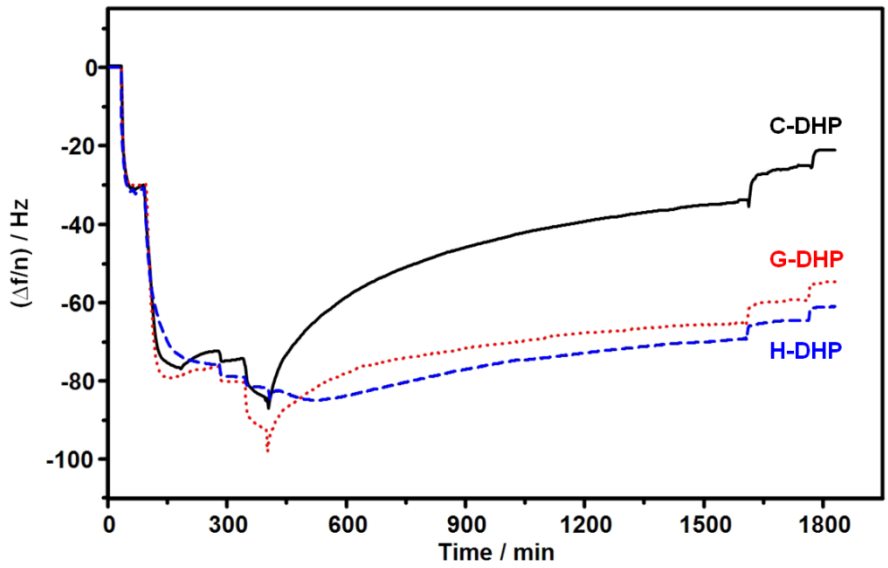

Figure 4.11 Representative $\Delta f/n$ vs. t for the synthesis of C-DHP, G-DHP, and H-DHP films through surface-immobilized HRP-catalyzed dehydrogenative polymerization of 0.5 mg/mL C-alcohol, 0.05 mg/mL G-alcohol, and 0.2 mg/mL H-alcohol, respectively, in the presence of H_2O_2 in H_2O and the subsequent chemical degradation of the synthesized DHP films via the Fenton system of Fe^{2+} + DHBA/H_2O_2.

Table 4.2 Comparison of the degradation of C-DHP to G-DHP and H-DHP films by the Fenton system of Fe^{2+} + DHBA/H_2O_2 at 20 ^oC according to the data in Figure 4.11.

DHP Film	**$\lvert\Delta f/n\rvert$ (Hz)**		**Percentage Degradation**
	Synthesized Amount	**Degraded Amount**	
C-DHP	42	51	121%
G-DHP	47	22	47%
H-DHP	45	15	33%

In contrast to Figure 4.7 where C-DHP films that underwent a Fenton mediated degradation process saw a reduction in surface roughness, G-DHP and H-DHP films showed a different trend.

Figure 4.12 shows representative AFM height images for G-DHP and H-DHP films synthesized and degraded with conditions like those in Figure 4.11. For these images, the RMS roughnesses of the films actually increased after the mediated Fenton reaction. As the degradation progressed, some bonds within the G-DHP and H-DHP films were cleaved, which might have led to an increase in the number of chain ends that promoted film hydration and swelling. Consequently, the surface RMS roughnesses of the G-DHP and H-DHP films increased after degradation. In contrast, most of the C-DHP film was degraded during the degradation process, and therefore, the surface RMS roughness of the C-DHP film decreased after degradation.

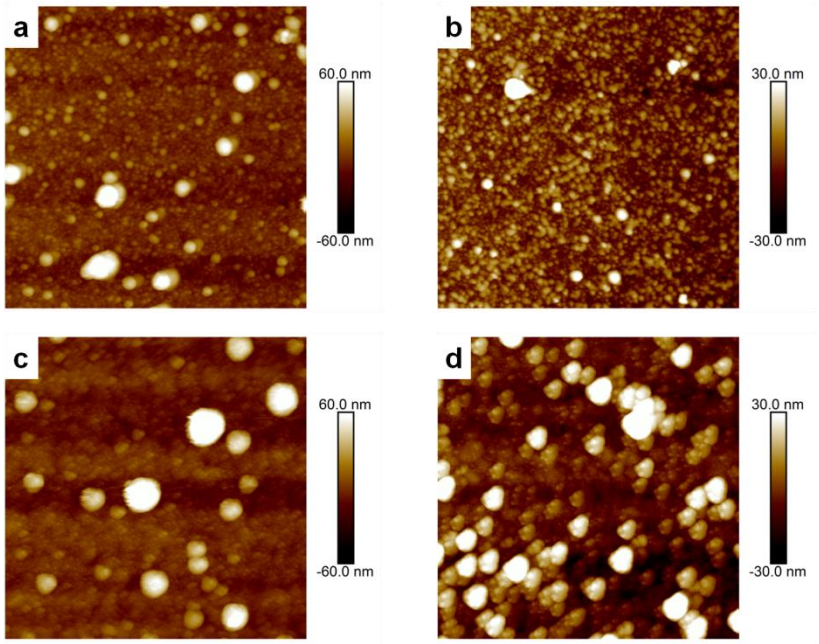

Figure 4.12 Representative AFM height images (2 μm × 2 μm) of DHP films synthesized through surface-initiated dehydrogenative polymerization of (a) 0.05 mg/mL G-alcohol (~13 nm) and (b) 0.2 mg/mL H-alcohol (~7.6 nm) in H_2O, and the same films after subsequent degradation by Fe^{2+} + DHBA/H_2O_2 for (c) G-DHP (~17 nm) and (d) H-DHP (~13 nm). Numbers in parentheses correspond to RMS roughnesses obtained from the entire image.

Film thickness also played a role in the degradation process. Figure 4.13 and Table 4.3

provide representative results for films that are slightly more than double the thickness seen in Figure 4.11 and Table 4.2. When the thickness of the synthesized DHP films doubled, the degradation percentage for the C-DHP film decreased slightly from 121% to 113%. However, it still underwent complete degradation. In contrast, the percentages of the G-DHP and H-DHP films that were degraded decreased to a much greater extent. Calculated values for the degradation percentage obtained from the data in Figure 4.13 and summarized in Table 4.3, showed that only 14% of the G-DHP and just 7% of the H-DHP were degraded to soluble products. One possible explanation for greater recalcitrance for H-DHP is a more closely packed structure arising from the absence of a methoxy group in the benzene ring of H-alcohol. Zhu et al.[36] came to similar conclusions that the G-lignin units in alkaline lignin and milled wood lignin were removed more quickly than the H-lignin units when treated with laccase.

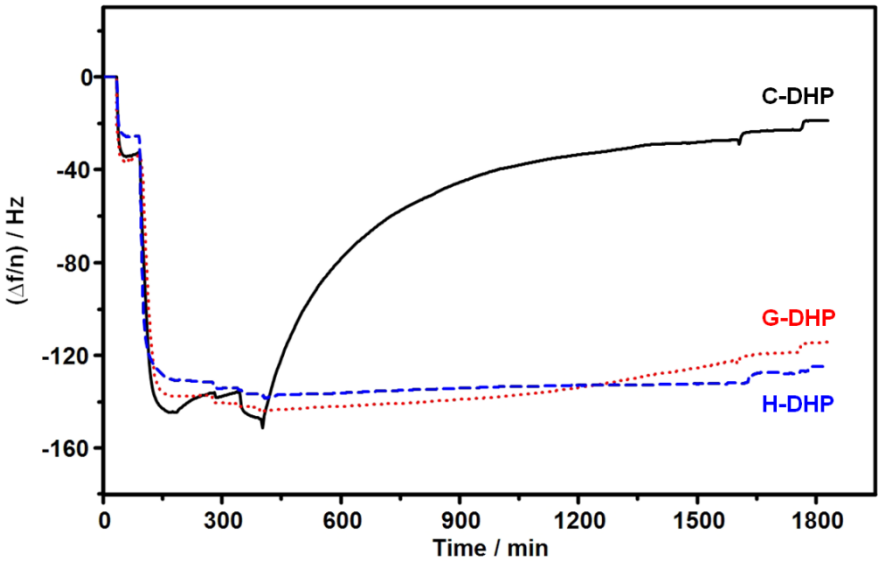

Figure 4.13 Representative Δ*f*/*n* vs. *t* for the synthesis of C-DHP, G-DHP, and H-DHP films through surface-immobilized HRP-catalyzed dehydrogenative polymerization of 1.2 mg/mL C-alcohol, 0.1 mg/mL G-alcohol, and 0.5 mg/mL H-alcohol, respectively, in the presence of H_2O_2 in H_2O and the subsequent chemical degradation of the synthesized DHP films via the Fenton system of Fe^{2+} + DHBA/H_2O_2.

Table 4.3 Comparison of the degradation of C-DHP to G-DHP and H-DHP films by the Fenton system of Fe^{2+} + DHBA/H_2O_2 at 20 ^oC according to the data in Figure 4.13.

DHP Film	**|Δ*f*/*n*| (Hz)**		**Percentage Degradation**
	Synthesized Amount	**Degraded Amount**	
C-DHP	104	117	113%
G-DHP	100	14	14%
H-DHP	106	7	7%

4.5 Conclusions

This work highlights the first reported synthesis of C-DHP films via surface-immobilized

HRP-catalyzed dehydrogenative polymerization of C-alcohol. A soft C-DHP film was generated in an aqueous environment, and both acetone and phosphate buffer were found to be detrimental to the synthesis of C-DHP films. The rate of polymerization for C-DHP was slower and with lower yield than conventional G-DHP and H-DHP under the same conditions. Enzymatic and chemical approaches were explored to degrade the C-DHP films. The degradation performance of LiP and MnP on C-DHP were even worse than on conventional DHPs in the literature, which might result from the non-phenolic benzodioxane structure of the C-DHP which lacked benzylic hydroxyl groups. An effective method was developed to degrade the C-DHP through Fenton chemistry under ambient conditions. The initial addition of Fe^{2+} and Fe chelator/reducer, DHBA, enhanced the effectiveness of the Fenton system, and the C-DHP film was completely degraded. Conversely, conventional G-DHP and H-DHP films of similar thickness were more resistant to degradation. Although the degradation percentage decreased slightly, the C-DHP film could still be fully degraded with a ~2x increase in thickness. Meanwhile, conventional G-DHP and H-DHP films that were ~2x thicker were barely degraded. Despite favorable characteristics for C-lignin relative to conventional lignin, the narrow distribution of C-lignin in nature has severely limited its widespread application. Recently there have been studies about the conversion of β-*O*-4 units to benzodioxanes via chemical treatment and the incorporation of C units into conventional lignin by genetically engineering the plant to address lignin recalcitrance in lignocellulosic biomass.[23, 37-38] This work provides a clear demonstration of C-lignin degradation and a platform for the exploration of C-lignin copolymers in the future.

4.6 References

1. Xiong, W.; Qiu, X.; Zhong, R.; Yang, D., Characterization of the adsorption properties of a phosphorylated kraft lignin-based polymer at the solid/liquid interface by the QCM-D approach.

Holzforschung **2016,** *70*, 937-945.

2. Wang, C.; Qian, C.; Roman, M.; Glasser, W. G.; Esker, A. R., Surface-initiated dehydrogenative polymerization of monolignols: a quartz crystal microbalance with dissipation monitoring and atomic force microscopy study. *Biomacromolecules* **2013,** *14*, 3964-3972.

3. Aadil, K. R.; Barapatre, A.; Meena, A. S.; Jha, H., Hydrogen peroxide sensing and cytotoxicity activity of *Acacia* lignin stabilized silver nanoparticles. *Int J Biol Macromol* **2016,** *82*, 39-47.

4. Tolbert, A.; Akinosho, H.; Khunsupat, R.; Naskar, A. K.; Ragauskas, A. J., Characterization and analysis of the molecular weight of lignin for biorefining studies. *Biofuels, Bioprod Biorefin* **2014,** *8*, 836-856.

5. Notley, S. M.; Norgren, M., Adsorption of a strong polyelectrolyte to model lignin surfaces. *Biomacromolecules* **2009,** *9*, 2081-2086.

6. Saarinen, T.; Orelma, H.; Gronqvist, S.; Andberg, M.; Holappa, S.; Laine, J., Adsorption of different laccases on cellulose and lignin surfaces. *BioResources* **2009,** *4*, 94-110.

7. Xu, Z.; Lei, P.; Zhai, R.; Wen, Z.; Jin, M., Recent advances in lignin valorization with bacterial cultures: microorganisms, metabolic pathways, and bio-products. *Biotechnol Biofuels* **2019,** *12*, 32.

8. Nar, M.; Rizvi, H. R.; Dixon, R. A.; Chen, F.; Kovalcik, A.; D'Souza, N., Superior plant based carbon fibers from electrospun poly-(caffeyl alcohol) lignin. *Carbon* **2016,** *103*, 372-383.

9. Rawal, T. B.; Zahran, M.; Dhital, B.; Akbilgic, O.; Petridis, L., The relation between lignin sequence and its 3D structure. *Biochim Biophys Acta Gen Subj* **2020,** *1864*, 129547.

10. Chen, F.; Tobimatsu, Y.; Havkin-Frenkel, D.; Dixon, R. A.; Ralph, J., A polymer of caffeyl

alcohol in plant seeds. *Proc Natl Acad Sci USA* **2012,** *109*, 1772-1777.

11. Tobimatsu, Y.; Chen, F.; Nakashima, J.; Escamilla-Trevino, L. L.; Jackson, L.; Dixon, R. A.; Ralph, J., Coexistence but independent biosynthesis of catechyl and guaiacyl/syringyl lignin polymers in seed coats. *Plant Cell* **2013,** *25*, 2587-2600.

12. Berstis, L.; Elder, T.; Crowley, M.; Beckham, G. T., Radical nature of C-lignin. *ACS Sustainable Chem Eng* **2016,** *4*, 5327-5335.

13. Stone, M. L.; Anderson, E. M.; Meek, K. M.; Reed, M.; Katahira, R.; Chen, F.; Dixon, R. A.; Beckham, G. T.; Roman-Leshkov, Y., Reductive catalytic fractionation of C-lignin. *ACS Sustainable Chem Eng* **2018,** *6*, 11211-11218.

14. Chen, F.; Tobimatsu, Y.; Jackson, L.; Nakashima, J.; Ralph, J.; Dixon, R. A., Novel seed coat lignins in the Cactaceae: structure, distribution and implications for the evolution of lignin diversity. *Plant J* **2013,** *73*, 201-211.

15. Barta, K.; Warner, G. R.; Beach, E. S.; Anastas, P. T., Depolymerization of organosolv lignin to aromatic compounds over Cu-doped porous metal oxides. *Green Chem* **2014,** *16*, 191-196.

16. Ouyang, X.-P.; Tan, Y.-D.; Qiu, X.-Q., Oxidative degradation of lignin for producing monophenolic compounds. *J Fuel Chem Technol* **2014,** *42*, 677-682.

17. Lan, W.; Amiri, M. T.; Hunston, C. M.; Luterbacher, J. S., Protection group effects during α,γ-diol lignin stabilization promote high-selectivity monomer production. *Angew Chem Int Ed Engl* **2018,** *57*, 1356-1360.

18. Dai, J.; Patti, A. F.; Saito, K., Recent developments in chemical degradation of lignin: catalytic oxidation and ionic liquids. *Tetrahedron Lett* **2016,** *57*, 4945-4951.

19. Li, Y.; Shuai, L.; Kim, H.; Motagamwala, A. H.; Mobley, J. K.; Yue, F.; Tobimatsu, Y.;

Havkin-Frenkel, D.; Chen, F.; Dixon, R. A.; Luterbacher, J. S.; Dumesic, J. A.; Ralph, J., An "ideal lignin" facilitates full biomass utilization. *Sci Adv* **2018,** *4*, eaau2968.

20. Dixon, M. C., Quartz crystal microbalance with dissipation monitoring: enabling real-time characterization of biological materials and their interactions. *J Biomol Tech* **2008,** *19*, 151-158.

21. Zhang, X. Adsorption of biomacromolecules onto polysaccharide surfaces. Ph.D. Dissertation, Virginia Tech, Blacksburg, VA, 2014.

22. Chen, Q.; Xu, S.; Liu, Q.; Masliyah, J.; Xu, Z., QCM-D study of nanoparticle interactions. *Adv Colloid Interface Sci* **2016,** *233*, 94-114.

23. Wagner, A.; Tobimatsu, Y.; Phillips, L.; Flint, H.; Torr, K.; Donaldson, L.; Pears, L.; Ralph, J., CCoAOMT suppression modifies lignin composition in *Pinus radiata*. *Plant J* **2011,** *67*, 119-129.

24. Lenhoff, H. M.; Ngo, T. T.; Bovaird, J. H., Optimizing the *o*-phenylenediamine assay for horseradish peroxidase: effects of phosphate and pH, substrate and enzyme concentrations, and stopping reagents. *Clin Chem* **1982,** *28*, 2423-2426.

25. Ferapontova, E.; Dominguez, E., Adsorption of differently charged forms of horseradish peroxidase on metal electrodes of different nature: effect of surface charges. *Bioelectrochemistry* **2002,** *55*, 127-130.

26. Wang, X.; Yao, B.; Su, X., Linking enzymatic oxidative degradation of lignin to organics detoxification. *Int J Mol Sci* **2018,** *19*, 3373.

27. Wang, C. Renewable natural polymer thin films and their interactions with biomacromolecules. Ph.D. Dissertation, Virginia Tech, Blacksburg, VA, 2014.

28. Kim, S.; Chmely, S. C.; Nimlos, M. R.; Bomble, Y. J.; Foust, T. D.; Paton, R. S.; Beckham,

G. T., Computational study of bond dissociation enthalpies for a large range of native and modified lignins. *J Phys Chem Lett* **2011,** *2*, 2846-2852.

29. Chen, Y. R.; Sarkanen, S.; Wang, Y. Y., Lignin-degrading enzyme activities. *Methods Mol Biol* **2012,** *908*, 251-268.

30. Kumar, A.; Chandra, R., Ligninolytic enzymes and its mechanisms for degradation of lignocellulosic waste in environment. *Heliyon* **2020,** *6*, e03170.

31. Wong, D. W., Structure and action mechanism of ligninolytic enzymes. *Appl Biochem Biotechnol* **2009,** *157*, 174-209.

32. Hofrichter, M., Review: lignin conversion by manganese peroxidase (MnP). *Enzyme Microb Technol* **2002,** *30*, 454-466.

33. Kent, M. S.; Zeng, J.; Rader, N.; Avina, I. C.; Simoes, C. T.; Brenden, C. K.; Busse, M. L.; Watt, J.; Giron, N. H.; Alam, T. M.; Allendorf, M. D.; Simmons, B. A.; Bell, N. S.; Sale, K. L., Efficient conversion of lignin into a water-soluble polymer by a chelator-mediated Fenton reaction: optimization of H_2O_2 use and performance as a dispersant. *Green Chem* **2018,** *20*, 3024-3037.

34. Brillas, E.; Garcia-Segura, S., Benchmarking recent advances and innovative technology approaches of Fenton, photo-Fenton, electro-Fenton, and related processes: a review on the relevance of phenol as model molecule. *Sep Purif Technol* **2020,** *237*, 116337.

35. Aguiar, A.; Ferraz, A., Fe^{3+}- and Cu^{2+}-reduction by phenol derivatives associated with Azure B degradation in Fenton-like reactions. *Chemosphere* **2007,** *66*, 947-954.

36. Zhu, D.; Liang, N.; Zhang, R.; Ahmad, F.; Zhang, W.; Yang, B.; Wu, J.; Geng, A.; Gabriel, M.; Sun, J., Insight into depolymerization mechanism of bacterial laccase for lignin. *ACS*

Sustainable Chem Eng **2020,** *8*, 12920-12933.

37. Li, N.; Li, Y.; Yoo, C. G.; Yang, X.; Lin, X.; Ralph, J.; Pan, X., An uncondensed lignin depolymerized in the solid state and isolated from lignocellulosic biomass: a mechanistic study. *Green Chem* **2018,** *20*, 4224-4235.

38. Zhuo, C.; Rao, X.; Azad, R.; Pandey, R.; Xiao, X.; Harkelroad, A.; Wang, X.; Chen, F.; Dixon, R. A., Enzymatic basis for C-lignin monomer biosynthesis in the seed coat of *Cleome hassleriana*. *Plant J* **2019,** *99*, 506-520.

Chapter 5: Effects of C Units on the Synthesis and Degradation of Conventional Lignin Films

5.1 Abstract

Conventional lignin is widely distributed in nature, but has low valorization because of heterogeneously complex structures and recalcitrance to degradation. As a result, most lignin generated in the biorefinery is discarded or burned. In this study, a quartz crystal microbalance with dissipation monitoring (QCM-D) was used to study the formation and degradation of dehydrogenative polymers (DHPs) for lignin copolymers. A relatively new monolignol, caffeyl alcohol (C-alcohol), was copolymerized with conventional monolignols, coniferyl alcohol (G-alcohol) and *p*-coumaryl alcohol (H-alcohol), by a horseradish peroxidase (HRP) immobilized on the surface of a gold-coated QCM-D sensor. As the amount of C-alcohol present in the copolymerization increased, the amount of DHP lignin formed decreased. However, the DHP lignin that formed was degraded faster and to a greater extent than the corresponding copolymers formed in the absence of C-alcohol by a chelator-mediated Fenton system. Nearly complete degradation of copolymers of C-alcohol and G-alcohol or C-alcohol, G-alcohol, and H-alcohol where the feed ratio of G-alcohol to H-alcohol was fixed at 1 : 1 occurred when the feed amount of C-alcohol exceeded 75% and 60%, respectively. Enhanced degradation was attributed to a more linear and less crosslinked structure as C-alcohol incorporation increased.

5.2 Introduction

Lignin is one of the most abundant natural polymers along with cellulose and chitin and can be found in all vascular plants.[1-3] Conventional lignin is an amorphous and crosslinked aromatic heteropolymer carrying many functional groups, such as phenolic hydroxyl, aliphatic hydroxyl, and methoxy groups.[3-5] It is generally composed of guaiacyl (G), *p*-hydroxyphenyl (H), and

syringyl (S) units that are derived from the dehydrogenative polymerization of coniferyl alcohol (G-alcohol), *p*-coumaryl alcohol (H-alcohol), and sinapyl alcohol (S-alcohol), respectively.[6-8] These units are joined via various linkages, such as β-aryl ether (β-*O*-4, usually > 50% of the total linkages), resinol (β-β), phenylcoumaran (β-5), dibenzodioxocin (5-5/β-*O*-4), and biphenyl ether (5-*O*-4).[9-12] Lignin can be primarily divided into three categories based upon their sources: softwood, hardwood, and grass lignins, and their abundance follows the order of softwoods > hardwoods > grasses.[13] Softwood lignin mostly contains G units, G and S units are the main components of hardwood lignin, and grass lignin is a mixture of G, H, and S units.[7, 14]

The biorefining processes of lignocellulosic biomass, such as the production of bio-ethanol and pulp/paper, usually generates large amounts of lignin. It is estimated that tens or even hundreds of millions of tons of lignin are produced every year in the United States.[15-19] However, most lignins are discarded or burned for energy. One predominant strategy for enhanced lignin utilization is to valorize it through degradation into feedstocks for chemicals and fuels. Nevertheless, the heterogeneously complex structure of lignin leads to strong recalcitrance to degradation and wide distribution of degradation products, which largely impedes the economical efficiency of lignin degradation and greatly increases the costs to separate and purify the degradation products.[17-19] Therefore, new lignin valorization technology is desired.

A new naturally occurring lignin, catechyl lignin (C-lignin), was discovered recently in the seed coat tissues of vanilla orchids and several cactus species.[20-21] It is a linear homopolymer of catechyl (C) units derived solely from caffeyl alcohol (C-alcohol), and the C units are almost exclusively connected through benzodioxane linkages, as shown in Figure 5.1.[21-23] Due to these structural characteristics, the C-lignin has exhibited some distinct properties from conventional lignin. Li et al.[24] found that the depolymerization of C-lignin could bring about a narrower

distribution of products. Chapter 4 showed that the C-lignin film underwent complete Fenton mediated degradation in contrast to conventional lignin films. These features of C-lignin afford opportunities to circumvent the challenges faced in conventional lignin valorization.

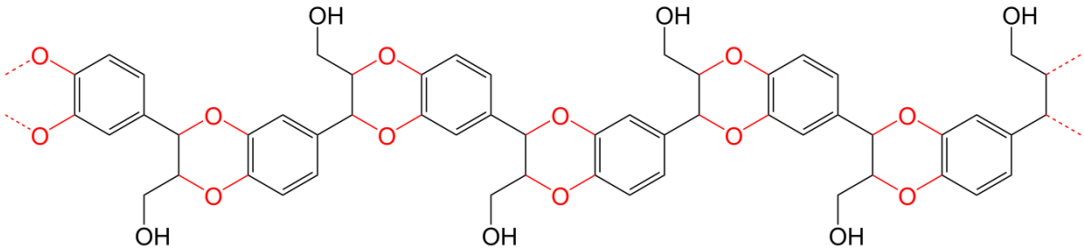

Figure 5.1 Molecular structure of C-lignin.

It is generally believed that the biosynthesis of C-lignin and conventional lignin follows the same combinatorial oxidative radical coupling mechanism that occurs under simple chemical control.[20-21, 25-27] The C-alcohol and the growing C-lignin polymer are first oxidized to radicals by enzymes, such as peroxidases and laccases. An end-wise β-*O*-4-type radical coupling reaction subsequently occurs between the caffeyl alcohol radical at its β-position and the end catechol unit of the growing polymer at its 4-*O*-position. The generated quinone methide (QM) intermediate is then rearomatized to form a benzodioxane linkage via an internal trapping by the 3-OH group on the end unit of the growing polymer which acts as a nucleophile. The only difference in the synthesis of conventional lignin is the generated QM intermediate is attacked by an external nucleophilic water molecule which contributes a hydroxyl group to the Cα of the conventional monolignol in the last step.

Due to the similarities in biosynthesis between the C-lignin and conventional lignin, it is highly possible to copolymerize their monolignols into a lignin copolymer containing both C units and conventional units. In addition, the fact that C-lignin is easily degraded with a high selectivity towards degradation products creates the question of whether incorporation of some C

units into the conventional lignin can enhance its degradation. In this work, for the first time, the copolymerization of C-alcohol with conventional G-alcohol and a mixture of G-alcohol and H-alcohol is used to generate CG-DHP and CGH-DHP copolymer films and degradation studies of the synthesized DHP copolymer films by a Fenton system were performed. This study is expected to contribute to the development of effective methods to improve the valorization of lignins.

5.3 Experimental Section

5.3.1 Materials

Caffeyl alcohol (C-alcohol, ≥ 95%) was synthesized by Syntame Ltd. in Ningbo, China. Coniferyl alcohol (G-alcohol) and *p*-coumaryl alcohol (H-alcohol) were synthesized in our lab following published procedures.[6, 28] Horseradish peroxidase (HRP, type I, essentially salt-free, lyophilized powder), hydrogen peroxide (H_2O_2, 30 wt% in H_2O), and iron (II) sulfate heptahydrate ($FeSO_4 \cdot 7H_2O$) were purchased from Sigma-Aldrich. Ammonium hydroxide (30% NH_3 in H_2O), acetone (≥ 99.9%), and methanol (≥ 99.9%) were supplied by Fisher Scientific. 2,3-Dihydroxybenzoic acid (DHBA) was obtained from TCI America. Sodium acetate and acetic acid were purchased from Sigma-Aldrich and used for the preparation of 100 mM acetate buffer at pH 4.0. Nitrogen (N_2, ultrahigh purity) was supplied by Airgas, and ultrapure water (Millipore Milli-Q, 18.2 MΩ·cm) was used in all experiments.

5.3.2 Quartz Crystal Microbalance with Dissipation Monitoring (QCM-D) Sensor Cleaning

Prior to use, gold-coated QCM-D sensors (QSX 301 from Biolin Scientific) were cleaned by treatment with UV/ozone for 20 min and immersion in H_2O_2/ammonium hydroxide/ultrapure water (1/1/5 v/v) at 80 ^oC for 1 h, rinsed using ultrapure water, and dried under N_2 gas.

5.3.3 Synthesis of DHP Films and Their Degradation by Chelator-Mediated Fenton Chemistry

The cleaned sensors were placed into the flow modules of a QCM-D (QSense E4 Analyzer, Biolin Scientific) and equilibrated in ultrapure water at a flow rate of 0.1 mL/min until the baseline was stable. Next, aqueous HRP solution at a concentration of 1.0 mg/mL was introduced into the flow modules at the same flow rate for 25 min. After that, ultrapure water was injected for 20 min for the purpose of reversibly adsorbed HRP removal. Then, the polymerization reaction was initiated as the solution was switched to aqueous monolignol solution containing 20 mM H_2O_2 at the flow rate of 0.1 mL/min. After 90 min, ultrapure water was flowed over the sensors for the removal of reversibly adsorbed monolignols and low molecular weight DHPs.

After the synthesis of the DHP films, 100 mM acetate buffer at pH 4.0 was flowed over the sensors at a flow rate of 0.1 mL/min for 60 min which changed the aqueous environment in the flow modules. Next, $FeSO_4$ in acetate buffer solution at a concentration of 10 mM was injected at the same flow rate for 50 min. Then, 0.4 M H_2O_2 buffered solution which contained 5 mM DHBA was introduced into the flow modules. After 8 min when the frequency started to increase, the flow was stopped and the degradation proceeded in the absence of flow for 20 h. After that, acetate buffer was flowed over the sensors for the removal of reversibly adsorbed chemicals, such as degradation products. Finally, ultrapure water was injected and returned the aqueous environment in the flow modules to the state after the synthesis of the DHP films.

5.3.4 Mass Spectrometry (MS) Measurements

The solution that flowed out of the QCM-D after the polymerization reaction started but before the $\Delta f/n$ vs. t curve plateaued was collected and dried at 60 ^{o}C under vacuum. The

obtained solids were dissolved in methanol at a concentration of 1.0 mg/mL for the preparation of the MS samples. An Agilent 6220 Accurate Mass TOF LC/MS with an Agilent 1311 HPLC pump and a 1367B autosampler was employed for MS measurements. The HPLC was operated in isocratic mode using methanol/H_2O (65/35 v/v) that contained 0.1% formic acid as the mobile phase at a flow rate of 0.5 mL/min. All data were obtained using both positive and negative modes.

5.3.5 QCM-D Analysis

All the QCM-D experiments were conducted at 20 ^{o}C. Changes in frequency (Δf) and energy dissipation (ΔD) at the fundamental frequency and 6 odd overtones (n = 3, 5, 7, …, 13) were recorded simultaneously. Data from the fifth overtone (n = 5) were presented in this work.

If a thin and rigid film is firmly attached to the sensor surface, mass changes in the film follow the Sauerbrey equation:[29-31]

$$\Delta \mathrm{m} = -C\left(\frac{\Delta f}{n}\right) \tag{5.1}$$

where C = 0.177 mg m^{-2} Hz^{-1}.

Nevertheless, the Sauerbrey relation will underestimate the mass if the film is soft. The viscoelasticity of the film is related to energy dissipation (D) of the sensor, and D is defined as a ratio of the energy dissipated ($E_{\mathrm{dissipated}}$) to the energy stored (E_{stored}) during a single oscillation.[29-31]

$$D = \frac{E_{\mathrm{dissipated}}}{2\pi E_{\mathrm{stored}}} \tag{5.2}$$

Qualitatively, as the frequency increased, the mass of the film decreased, and an increase in dissipation meant the film became softer.

5.4 Results and Discussion

5.4.1 Synthesis and Degradation of CG-DHP Films

The CG-DHP films were synthesized using QCM-D via surface-immobilized HRP-catalyzed dehydrogenative copolymerization of C-alcohol and G-alcohol in the presence of H_2O_2. The operational procedures and data presentation in this chapter will be similar to the synthesis of and degradation of C-DHP and G-DHP films in Chapter 4. As seen in Figure 5.2, there was a decrease in frequency from ~30 min caused by the adsorption of HRP onto the bare gold-coated sensor surface. After the sensor was washed with water, the introduction of mixtures of C-alcohol and G-alcohol caused a dramatic drop in frequency that was attributed to the formation of CG-DHP films. It could be seen that the amount of the synthesized DHP decreased with an increase in the concentration of C-alcohol in the feed solution at a fixed G-alcohol concentration. This feature implied the copolymerization of C-alcohol and G-alcohol occurred. Since the yield of the G-DHP film was much larger than that of the C-DHP film under the same conditions, yields for the copolymerization of C-alcohol and G-alcohol were expected between those of pure C-DHP and G-DHP films. It was also observed that as the concentration of the C-alcohol increased, the yield of the CG-DHP film was non-linear with respect to C-alcohol concentration. After polymerization, water was injected at 180 min for the removal of reversibly adsorbed C-alcohol and soluble CG-DHP oligomers, and this led to a small increase in frequency.

After the CG-DHP films were synthesized, they were subjected to degradation through a chelator-mediated Fenton system using DHBA as the Fe chelator. Fenton reagents, Fe^{2+} and DHBA/H_2O_2 buffered solutions, were flowed over the sensors sequentially. The frequency initially declined on account of Fe^{2+} ion, DHBA, and H_2O_2 uptake by the CG-DHP film, but then rose as degradation of the CG-DHP film via Fenton reactions began. The increase of the $\Delta f/n$ vs.

t curve indicated the degradation rate increased as the amount of the C-alcohol in the feed solution for polymerization increased. After that, buffer and then water were introduced for removal of reversibly adsorbed DHBA and degradation products. The switch to water facilitated direct comparisons between the end of the synthesis and degradation processes without effects from different solvents.

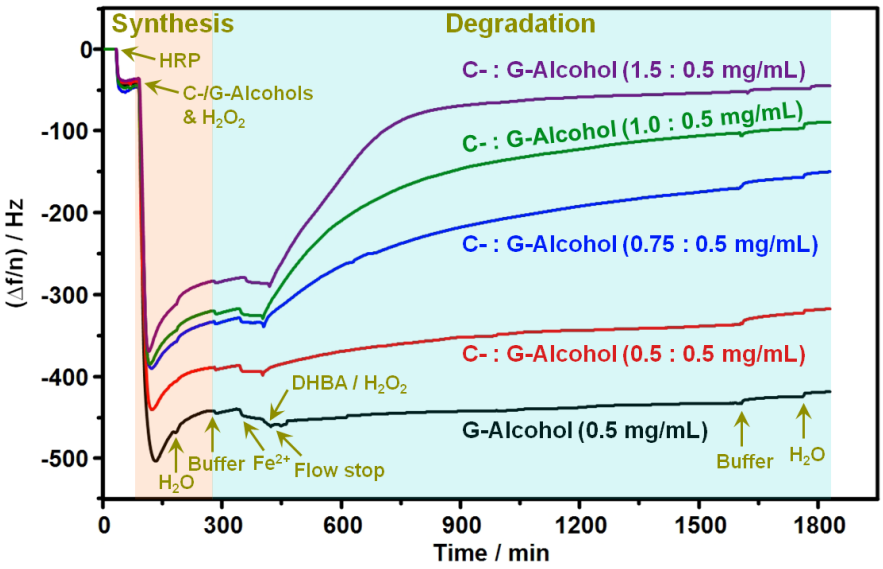

Figure 5.2 Representatie Δ*f*/*n* vs. *t* for the synthesis of CG-DHP films through surface-immobilized HRP-catalyzed dehydrogenative copolymerization of G-alcohol with various concentrations of C-alcohol in the presence of H_2O_2 and the subsequent degradation of the synthesized CG-DHP films via a chelator-mediated Fenton system of Fe^{2+} + DHBA/H_2O_2. The frequency changes on the orange (~85 min to ~275 min) and cyan (~275 min to ~1830 min) backgrounds represented the synthesis and degradation of CG-DHP films, respectively.

The effects of C-alcohol on the synthesis and degradation of G-DHP films are summarized in Table 5.1. Values of Δ*f*/*n* at the end of the experiment were compared with Δ*f*/*n* values at the end of synthesis process after correction for enzyme adsorption. This analysis assumed the Sauerbrey equation held and $\Delta f/n \propto \Delta m$. The degradation percentage for the G-DHP film clearly increased

with the addition of C-alcohol to the feed solution for the polymerization. Only a slight change in frequency was observed during the degradation of pure G-DHP film, and accordingly, only a small amount, ~6%, was degraded. When the amounts of C-alcohol and G-alcohol in the feed solution was equal, the degradation percentage increased by ~3x. The amount of degraded CG-DHP film increased further as the amount of C-alcohol increased in the feed solution during the polymerization, and was nearly 100% when the concentration of C-alcohol was 1.5 mg/mL. For the last three entries in Table 5.1, the amounts of CG-DHP synthesized were relatively similar, but the amount of C-alcohol incorporated into the CG-DHP must have increased as the percentage degradation rose further with an increase of C-alcohol in the polymerization feed. In Chapter 4, it was shown that lignin degradation by the Fenton system was dependent upon thickness, hence the reason for the focus on the last three entries in Table 5.1 where film thicknesses were comparable.

Table 5.1 Effects of C-alcohol on the synthesis and degradation of G-DHP films by a chelator-mediated Fenton system of Fe^{2+} + DHBA/H_2O_2 at 20 ^oC according to the data in Figure 5.2.

C-Alcohol : G-Alcohol (mg/mL : mg/mL)	**$\|\Delta f/n\|$ (Hz)**		**Percentage Degradation ***
	Synthesis	**Degradation**	
0 : 0.5	407	23	6%
0.5 : 0.5	349	69	20%
0.75 : 0.5	282	177	63%
1.0 : 0.5	273	227	83%
1.5 : 0.5	243	234	96%

* Percentage degradation equals the ratio of $|\Delta f/n|$ for degradation to $|\Delta f/n|$ for synthesis $\times 100\%$.

The solution that flowed out of the QCM-D as the frequency dropped during the

copolymerization process was collected and analyzed by MS. Peaks corresponding to C-homodimer, G-homodimer, CG-dimer with β-*O*-4 bonds, and GC-dimer with benzodioxane linkages were present (Figure 5.3). These data demonstrated homo-coupling and co-coupling of the C-alcohol and G-alcohol occurred, in line with the combinatorial radical coupling mechanism. Since the MS samples only included soluble DHP oligomers, copolymer formation between C-alcohol and G-alcohol for the insoluble materials with larger molecular weights on the QCM-D sensors was a reasonable assumption.

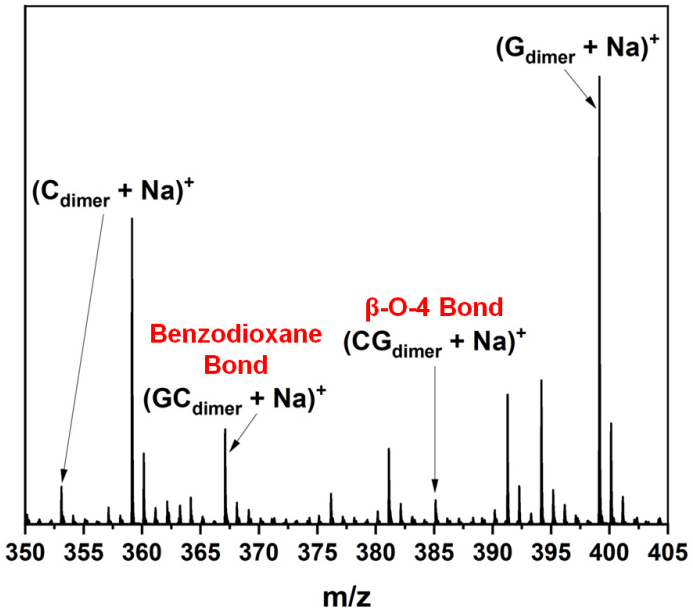

Figure 5.3 A representative mass spectrum for solids recovered from the solution that flowed out of the QCM-D for copolymerization with 0.5 mg/mL C-alcohol and 0.5 mg/mL G-alcohol at 20 ^{o}C.

5.4.2 Synthesis and Degradation of CGH-DHP Films

Figure 5.4 shows representative plots of $\Delta f/n$ vs. t for the synthesis and degradation of CGH-DHP films. These results were qualitatively similar to those for the CG-DHP films in Figure 5.2. The synthesized amounts of CGH-DHP films were relatively similar for 0.5 mg/mL G-alcohol,

0.5 mg/mL H-alcohol, and ≥ 0.5 mg/mL C-alcohol. Much like Figure 5.2, the GH-DHP formed in much greater amounts than the CGH-DHP when 0.5 mg/mL G-alcohol and 0.5 mg/mL H-alcohol were used. Thus, a 0.15 mg/mL G-alcohol and 0.15 mg/mL H-alcohol polymerization feed was found adequate for the production of GH-DHP films with comparable amounts (thicknesses) to the CGH-DHP films.

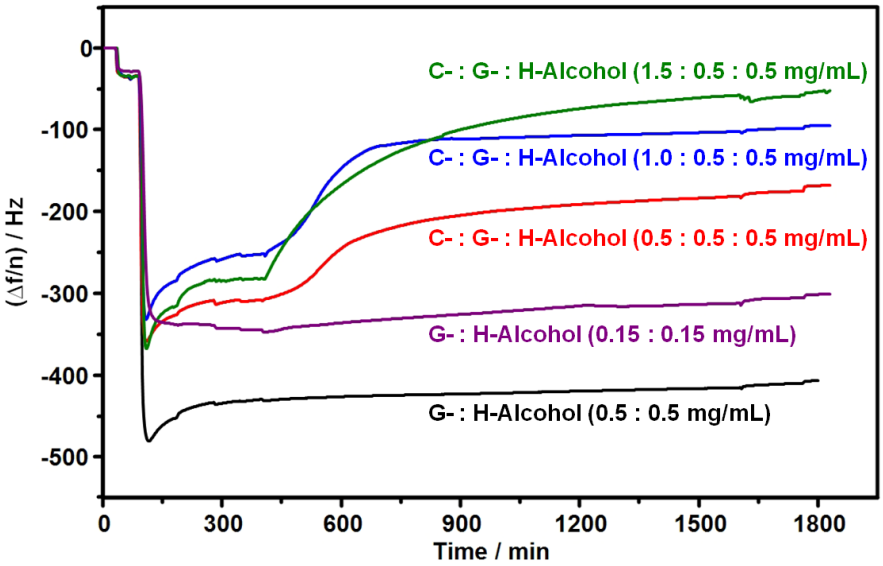

Figure 5.4 Representatie $\Delta f/n$ vs. t for the synthesis of CGH-DHP films through surface-immobilized HRP-catalyzed dehydrogenative copolymerization of C-alcohol, G-alcohol, and H-alcohol at different concentrations in the presence of H_2O_2 and the subsequent degradation of the synthesized CGH-DHP films via a chelator-mediated Fenton system of Fe^{2+} + DHBA/H_2O_2.

With respect to degradation by the Fe^{2+} + DHBA/H_2O_2, the percentage degradation increased only slightly as the thickness of GH-DHP films decreased: 7% for 0.5 mg/mL G-alcohol and 0.5 mg/mL H-alcohol for the polymerization feed versus 12% for 0.15 mg/mL G-alcohol and 0.15 mg/mL H-alcohol for the polymerization feed (Table 5.2). In contrast, all three polymerization feeds that contained C-alcohol showed enhanced degradation (> 50%) with a systematic increase in degradation as the concentration of C-alcohol in the polymerization feed increased. The CGH-

DHP films approached complete degradation for the polymerization feed of 1.5 mg/mL C-alcohol, 0.5 mg/mL G-alcohol, and 0.5 mg/mL H-alcohol (versus 12% degradation for GH-DHP films with a comparable thickness).

Table 5.2 Effects of C-alcohol on the synthesis and degradation of GH-DHP films by a chelator-mediated Fenton system of Fe^{2+} + DHBA/H_2O_2 at 20 ^oC according to the data in Figure 5.4.

C-Alcohol : G-Alcohol : H-Alcohol (mg/mL : mg/mL : mg/mL)	|Δ*f*/*n*| (Hz)		Percentage Degradation *
	Synthesis	Degradation	
0 : 0.5 : 0.5	393	26	7%
0 : 0.15 : 0.15	304	37	12%
0.5 : 0.5 : 0.5	282	144	51%
1.0 : 0.5 : 0.5	231	168	73%
1.5 : 0.5 : 0.5	256	237	93%

* Percentage degradation equals the ratio of |Δ*f*/*n*| for degradation to |Δ*f*/*n*| for synthesis × 100%.

5.4.3 Possible Reasons for the Improved Degradability Caused by C Units

Based upon the above data and analysis, the incorporation of C-alcohol into G-alcohol or mixtures of G-alcohol and H-alcohol for polymerization enhanced lignin degradation by a chelator-mediated Fenton system of Fe^{2+} + DHBA/H_2O_2. The computational work of Berstis et al.[26] and Kim et al.[32] showed that the bond dissociation enthalpy for benzodioxane β-*O*-4 linkages in C-lignin was higher than β-*O*-4 bonds in conventional lignins but the energies required to break them were still much lower relative to C-C bonds in lignin. The studies in Chapter 4 and work from Li et al.[24] found that the C-lignin was highly acid-resistant and could barely be degraded via oxidation by lignin peroxidase or alkaline nitrobenzene. Therefore, it was

unlikely that the enhanced degradability of the CG-DHP and CGH-DHP films was the result of easier benzodioxane linkage cleavage. Since the C-lignin has a linear structure, it was more likely that the introduction of C units reduced the degree of crosslinking in the generated CG-DHP and CGH-DHP films. As the degree of crosslinking decreased, the molecular structure became simpler, which allowed water soluble products with fewer bond cleavage events. Consequently, the degradation of the CG-DHP and CGH-DHP films was enhanced.

5.5 Conclusions

This work highlights the first report on surface-initiated copolymerization of C-alcohol with conventional G-alcohol and H-alcohol and the effects of C units on the degradation of conventional G-DHP and GH-DHP films by a chelator-mediated Fenton system of Fe^{2+} + DHBA/H_2O_2. The CG-DHP and CGH-DHP films were successfully prepared through surface-immobilized HRP-catalyzed dehydrogenative copolymerization of their monolignols. With the addition of C-alcohol to a fixed concentration of G-alcohol or a mixture of G-alcohol and H-alcohol for the polymerization feed, the synthesized amounts of the DHP copolymer films decreased as the amount of C-alcohol in the feed increased. The degradation kinetics were monitored in real time via QCM-D. As the feed ratio of the C-alcohol to G-alcohol or mixtures of G-alcohol and H-alcohol increased, the degradation of the resultant DHP copolymer films greatly increased. Both the rate of degradation and total percentage of the film degraded increased. For the CG-DHP and CGH-DHP films, near complete degradation of the films occurred when C-alcohol represented $\geq$ 75% and $\geq$ 60%, respectively, of the polymerization feed. Enhanced degradation was attributed to the incorporation of C units into the DHP films along with a simpler molecular structure and lower degrees of crosslinking. This work developed a new approach and studied the factors that influence lignin formation and degradation that are

relevant to efforts toward the incorporation of C units into conventional lignin through genetically engineered plants.[24, 33-34]

5.6 References

1. Whetten, R.; Sederoff, R., Lignin biosynthesis. *Plant Cell* **1995,** *7*, 1001-1013.

2. Barcelo, A. R., Lignification in plant cell walls. *Int Rev Cytol* **1997,** *176*, 87-132.

3. Xiong, W.; Qiu, X.; Zhong, R.; Yang, D., Characterization of the adsorption properties of a phosphorylated kraft lignin-based polymer at the solid/liquid interface by the QCM-D approach. *Holzforschung* **2016,** *70*, 937-945.

4. Notley, S. M.; Norgren, M., Adsorption of a strong polyelectrolyte to model lignin surfaces. *Biomacromolecules* **2009,** *9*, 2081-2086.

5. Saarinen, T.; Orelma, H.; Gronqvist, S.; Andberg, M.; Holappa, S.; Laine, J., Adsorption of different laccases on cellulose and lignin surfaces. *BioResources* **2009,** *4*, 94-110.

6. Wang, C. Renewable natural polymer thin films and their interactions with biomacromolecules. Ph.D. Dissertation, Virginia Tech, Blacksburg, VA, 2014.

7. Tolbert, A.; Akinosho, H.; Khunsupat, R.; Naskar, A. K.; Ragauskas, A. J., Characterization and analysis of the molecular weight of lignin for biorefining studies. *Biofuels, Bioprod Biorefin* **2014,** *8*, 836-856.

8. Dai, J.; Patti, A. F.; Saito, K., Recent developments in chemical degradation of lignin: catalytic oxidation and ionic liquids. *Tetrahedron Lett* **2016,** *57*, 4945-4951.

9. Nar, M.; Rizvi, H. R.; Dixon, R. A.; Chen, F.; Kovalcik, A.; D'Souza, N., Superior plant based carbon fibers from electrospun poly-(caffeyl alcohol) lignin. *Carbon* **2016,** *103*, 372-383.

10. Li, N.; Li, Y.; Yoo, C. G.; Yang, X.; Lin, X.; Ralph, J.; Pan, X., An uncondensed lignin depolymerized in the solid state and isolated from lignocellulosic biomass: a mechanistic study. *Green Chem* **2018,** *20*, 4224-4235.

11. Lancefield, C. S.; Ojo, O. S.; Tran, F.; Westwood, N. J., Isolation of functionalized phenolic monomers through selective oxidation and C-O bond cleavage of the β-O-4 linkages in lignin. *Angew Chem Int Ed Engl* **2015,** *54*, 258-262.

12. Zhu, D.; Liang, N.; Zhang, R.; Ahmad, F.; Zhang, W.; Yang, B.; Wu, J.; Geng, A.; Gabriel, M.; Sun, J., Insight into depolymerization mechanism of bacterial laccase for lignin. *ACS Sustainable Chem Eng* **2020,** *8*, 12920-12933.

13. Zakzeski, J.; Bruijnincx, P. C. A.; Jongerius, A. L.; Weckhuysen, B. M., The catalytic valorization of lignin for the production of renewable chemicals. *Chem Rev* **2010,** *110*, 3552-3599.

14. Liu, Q.; Luo, L.; Zheng, L., Lignins: biosynthesis and biological functions in plants. *Int J Mol Sci* **2018,** *19*, 335.

15. Ragauskas, A. J.; Beckham, G. T.; Biddy, M. J.; Chandra, R.; Chen, F.; Davis, M. F.; Davison, B. H.; Dixon, R. A.; Gilna, P.; Keller, M.; Langan, P.; Naskar, A. K.; Saddler, J. N.; Tschaplinski, T. J.; Tuskan, G. A.; Wyman, C. E., Lignin valorization: improving lignin processing in the biorefinery. *Science* **2014,** *344*, 1246843.

16. Gillet, S.; Aguedo, M.; Petitjean, L.; Morais, A. R. C.; da Costa Lopes, A. M.; Łukasik, R. M.; Anastas, P. T., Lignin transformations for high value applications: towards targeted modifications using green chemistry. *Green Chem* **2017,** *19*, 4200-4233.

17. Xu, Z.; Lei, P.; Zhai, R.; Wen, Z.; Jin, M., Recent advances in lignin valorization with

bacterial cultures: microorganisms, metabolic pathways, and bio-products. *Biotechnol Biofuels* **2019,** *12*, 32.

18. Bruijnincx, P. C. A.; Rinaldi, R.; Weckhuysen, B. M., Unlocking the potential of a sleeping giant: lignins as sustainable raw materials for renewable fuels, chemicals and materials. *Green Chem* **2015,** *17*, 4860-4861.

19. Wang, H.; Pu, Y.; Ragauskas, A.; Yang, B., From lignin to valuable products-strategies, challenges, and prospects. *Bioresour Technol* **2019,** *271*, 449-461.

20. Chen, F.; Tobimatsu, Y.; Jackson, L.; Nakashima, J.; Ralph, J.; Dixon, R. A., Novel seed coat lignins in the Cactaceae: structure, distribution and implications for the evolution of lignin diversity. *Plant J* **2013,** *73*, 201-211.

21. Chen, F.; Tobimatsu, Y.; Havkin-Frenkel, D.; Dixon, R. A.; Ralph, J., A polymer of caffeyl alcohol in plant seeds. *Proc Natl Acad Sci USA* **2012,** *109*, 1772-1777.

22. Rawal, T. B.; Zahran, M.; Dhital, B.; Akbilgic, O.; Petridis, L., The relation between lignin sequence and its 3D structure. *Biochim Biophys Acta Gen Subj* **2020,** *1864*, 129547.

23. Liu, C.; Wang, S.; Wang, B.; Song, G., Catalytic hydrogenolysis of castor seeds C-lignin in deep eutectic solvents. *Ind Crop Prod* **2021,** *169*, 113666.

24. Li, Y.; Shuai, L.; Kim, H.; Motagamwala, A. H.; Mobley, J. K.; Yue, F.; Tobimatsu, Y.; Havkin-Frenkel, D.; Chen, F.; Dixon, R. A.; Luterbacher, J. S.; Dumesic, J. A.; Ralph, J., An "ideal lignin" facilitates full biomass utilization. *Sci Adv* **2018,** *4*, eaau2968.

25. Tobimatsu, Y.; Chen, F.; Nakashima, J.; Escamilla-Trevino, L. L.; Jackson, L.; Dixon, R. A.; Ralph, J., Coexistence but independent biosynthesis of catechyl and guaiacyl/syringyl lignin polymers in seed coats. *Plant Cell* **2013,** *25*, 2587-2600.

26. Berstis, L.; Elder, T.; Crowley, M.; Beckham, G. T., Radical nature of C-lignin. *ACS Sustainable Chem Eng* **2016,** *4*, 5327-5335.

27. Stone, M. L.; Anderson, E. M.; Meek, K. M.; Reed, M.; Katahira, R.; Chen, F.; Dixon, R. A.; Beckham, G. T.; Roman-Leshkov, Y., Reductive catalytic fractionation of C-lignin. *ACS Sustainable Chem Eng* **2018,** *6*, 11211-11218.

28. Wang, C.; Qian, C.; Roman, M.; Glasser, W. G.; Esker, A. R., Surface-initiated dehydrogenative polymerization of monolignols: a quartz crystal microbalance with dissipation monitoring and atomic force microscopy study. *Biomacromolecules* **2013,** *14*, 3964-3972.

29. Dixon, M. C., Quartz crystal microbalance with dissipation monitoring: enabling real-time characterization of biological materials and their interactions. *J Biomol Tech* **2008,** *19*, 151-158.

30. Zhang, X. Adsorption of biomacromolecules onto polysaccharide surfaces. Ph.D. Dissertation, Virginia Tech, Blacksburg, VA, 2014.

31. Chen, Q.; Xu, S.; Liu, Q.; Masliyah, J.; Xu, Z., QCM-D study of nanoparticle interactions. *Adv Colloid Interface Sci* **2016,** *233*, 94-114.

32. Kim, S.; Chmely, S. C.; Nimlos, M. R.; Bomble, Y. J.; Foust, T. D.; Paton, R. S.; Beckham, G. T., Computational study of bond dissociation enthalpies for a large range of native and modified lignins. *J Phys Chem Lett* **2011,** *2*, 2846-2852.

33. Wagner, A.; Tobimatsu, Y.; Phillips, L.; Flint, H.; Torr, K.; Donaldson, L.; Pears, L.; Ralph, J., CCoAOMT suppression modifies lignin composition in *Pinus radiata*. *Plant J* **2011,** *67*, 119-129.

34. Zhuo, C.; Rao, X.; Azad, R.; Pandey, R.; Xiao, X.; Harkelroad, A.; Wang, X.; Chen, F.; Dixon, R. A., Enzymatic basis for C-lignin monomer biosynthesis in the seed coat of *Cleome*

hassleriana. *Plant J* **2019,** *99*, 506-520.

Chapter 6: Conclusions and Suggested Future Work

6.1 Overall Conclusions

This study focused on the fabrication of chitin and lignin thin films and their interactions with other molecules. Surface characterization techniques included a quartz crystal microbalance with dissipation monitoring (QCM-D) and atomic force microscopy (AFM) and were used for the investigation of surface-initiated dehydrogenative polymerization of monolignols and the degradation of chitin and lignin thin films.

Smooth and uniform amorphous regenerated chitin (RChitin) thin films were prepared via spin-coating and regeneration from trimethylsilyl chitin as done previously in the literature.[1-2] The activity of family 18 chitinases from *Trichoderma viride* on the prepared RChitin films was studied. Compared to literature reports on the degradation of colloidal chitin and dissolved chitin derivatives and analogues, the degradation of RChitin films was deeply affected by the adsorption of the family 18 chitinases. Thus, the optimal temperature for the activity of the family 18 chitinases decreased. The viscoelasticity of the RChitin film initially increased and then decreased after treatment with the family 18 chitinases, in line with morphology changes. Effects of pH on the activity of the family 18 chitinases were consistent with bulk solution studies in the literature[3-6] and an acidic environment yielded greater enzymatic activity. Additionally, the endochitinases were more stable than the exochitinases in terms of activity as pH increased. The family 18 chitinases exhibited a low activity on RChitin films but a high activity on dissolved chitin oligosaccharides. In contrast, the family 19 chitinases from *Streptomyces griseus* exhibited greater activity on RChitin films and less activity on chitin oligosaccharides. These differences were attributed to chitin-binding domains which were absent in the family 18 chitinases but present in the family 19 chitinases.

A soft C-DHP lignin film was synthesized on gold-coated QCM-D sensor surface in an "end-wise" approach via surface-immobilized horseradish peroxidase (HRP)-catalyzed dehydrogenative polymerization of C-alcohol in an aqueous environment. Effects of different solvents on the polymerization kinetics were investigated, and both acetone and phosphate buffer had a negative effect relative to polymerization in ultrapure water. Compared to dehydrogenative polymers (DHPs) prepared from coniferyl alcohol (G-alcohol) and *p*-coumaryl alcohol (H-alcohol), C-DHP was characterized by a slower synthetic rate and lower yield under the same experimental conditions. Enzymatic and chemical degradation of the C-DHP film was explored. Lignin peroxidase (LiP) and manganese peroxidase (MnP) degraded less of the C-DHP films than G-DHP or H-DHP films. This observation was attributed to the non-phenolic benzodioxane structure of the C-DHP and the absence of benzylic hydroxyl groups. Nevertheless, the C-DHP films underwent complete Fenton mediated degradation in contrast to the G-DHP and H-DHP films regardless of their thicknesses. Greater degradation of C-DHP films was attributed to the linear chain structure. The addition of Fe^{2+} ions (instead of Fe^{3+} ions) and the iron chelator/reducer, 2,3-dihydroxybenzoic acid (DHBA), enhanced the degradation by the Fenton reactions.

Catechyl (C) units were incorporated into conventional G-DHP or GH-DHP copolymer lignin films through surface-initiated dehydrogenative copolymerization of C-alcohol with G-alcohol or mixtures of G-alcohol and H-alcohol. As the amount of C-alcohol in the polymerization feed increased, the synthesized amount of CG-DHP or CGH-DHP film decreased. Next, the synthesized CG-DHP and CGH-DHP films were degraded by a chelator-mediated Fenton system. With an increase in the ratio of C-alcohol to G-alcohol or a mixture of G-alcohol and H-alcohol in the polymerization feed, the percentage degradation of the resulting CG-DHP

or CGH-DHP film increased. Essentially total degradation of the film occurred for ≥ 75% and ≥ 60% C-alcohol in the polymerization feed for the CG-DHP and CGH-DHP films, respectively. It was believed that the enhanced degradation of the CG-DHP and CGH-DHP films relative to G-DHP and GH-DHP films was caused by the incorporation of C units that brought about a more linear structure with a lower degree of crosslinking.

6.2 Suggested Future Work

6.2.1 Effects of Glucan on the Degradation of Chitin Thin Films by Chitinases

The fungal cell wall has a multilayered structure, as shown in Figure 6.1.[7-11] The chitin layer is sandwiched between the plasma membrane and a layer of β-glucan. When endosymbiont bacteria penetrate into fungal cells or hosts suffer from fungal infections, chitinases are secreted by bacteria or hosts for an attack on the chitin layer of the fungal cell wall. These chitinases need to traverse the β-glucan layer in the fungal cell wall prior to an attack upon the chitin layer.[12-14] It would be interesting to explore the effects of the β-glucan layer structure on chitinase access to the chitin layer. Addressing this question is expected to promote overall understanding of the process of bacterial invasion of fungi and host defense against fungal infections.

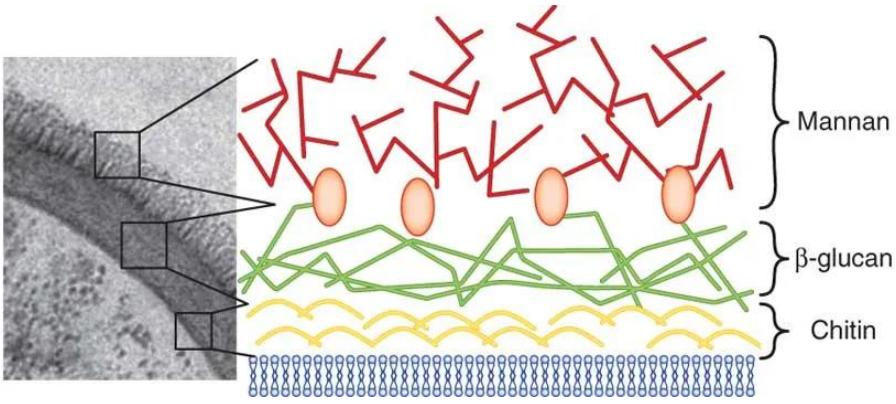

Figure 6.1 Structure of the fungal cell wall (*Candida albicans*). Adapted from Hardison et al. (Copyright 2012 Springer Nature).[7]

A possible research plan is to fabricate a glucan thin film on top of the RChitin thin film via spin-coating or adsorption, as exhibited in Figure 6.2. Next, the glucan/chitin film would be incubated with chitinases and monitored with a QCM-D and AFM for changes in mass, viscoelasticity, and morphology. Results would be compared with those obtained from RChitin films. It is hoped that the effects of the β-glucan film on chitinase access to and degradation of RChitin films would be revealed in this manner. Additionally, since the β-glucan layer is covered with a layer of mannan in the fungal cell wall, a thin film of mannan could also be deposited onto the glucan film for an investigation of the effects on the degradation of the RChitin film by chitinases.

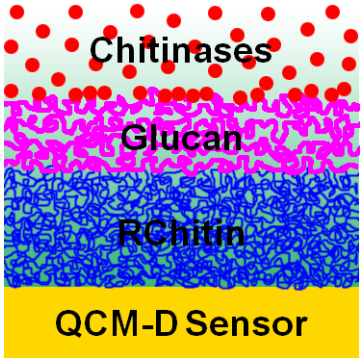

Figure 6.2 A schematic depiction of degradation for a RChitin film covered with a glucan layer by chitinases.

6.2.2 Activity of Endochitinase and Exochitinase on RChitin Thin Films

QCM-D was used for the study of chitinase activity on RChitin thin films in Chapter 3 for family 18 chitinases from *Trichoderma viride*. The chitinases were a mixture of endochitinases and exochitinases. The endochitinases were mainly responsible for the dissipation changes in the QCM-D data, and the exochitinases were primarily responsible for the frequency changes. However, their action was symbiotic. The endochitinases increased the roughnesses and surface

areas of the RChitin films that facilitated adsorption of exochitinases. Accordingly, the degradation rates and total amount of degraded film increased. Meanwhile, the dissipation was reduced as the exochitinases consumed the RChitin film. Hence, it was difficult to simply assign the frequency and dissipation changes to exochitinase or endochitinase activity. In addition, the effects of temperature and pH on the activities of endochitinases and exochitinases were different. Thus, the acquisition of individual endochitinases and exochitinases would be ideal for a greater understanding of chitin film degradation by chitinases. Several protein purification methods, such as affinity chromatography, ion exchange chromatography, size exclusion chromatography, and hydrophobic interaction chromatography, could potentially be used for the separation of endochitinases and exochitinases.

6.2.3 Molecular Structure of CG-DHP and CGH-DHP Films

In Chapter 5, it was demonstrated that the incorporation of C units into conventional G-DHP homopolymer and GH-DHP copolymer lignin films greatly enhanced their degradation by the Fenton system, Fe^{2+} + H_2O_2 mediated by DHBA. The enhanced degradation was believed to be caused by a reduction in the degree of crosslinking as C units favored more linear structures. However, the exact molecular structure of the synthesized CG-DHP and CGH-DHP films remained unknown. QCM-D experiments were sensitive to mass and viscoelasticity changes in thin films in real time, but the challenge of the molecular structure of thin films on the QCM-D sensor surfaces is still a major challenge. A more feasible approach would be to synthesize the CG-DHP and CGH-DHP in bulk solution. Next, various techniques, such as two-dimensional nuclear magnetic resonance (2D NMR) spectroscopy, solid-state NMR (ssNMR) spectroscopy, and size exclusion chromatography (SEC), could be applied to characterize their molecular structures. Once their molecular structure is determined, it is anticipated that a better

understanding of the cause of the enhanced degradation of the CG-DHP and CGH-DHP films would be obtained.

6.2.4 Others

It is generally believed that the synthesis of C-lignin follows a combinatorial oxidative radical coupling mechanism.[15-19] However, little mechanistic proof exists for this hypothesis. Therefore, it would be an interesting study if the radicals generated during the synthetic process could be detected and even identified using electron paramagnetic resonance (EPR) spectroscopy. Clarification of the synthetic mechanism is expected to inform the design and production of lignocellulosic biomass for greater utilization.

Besides C-lignin, 5-hydroxyguaiacyl lignin (5H-lignin) is another unconventional lignin. Reports of 5H-lignin in the literature are even rarer than the C-lignin. Similar to the C-lignin, the 5H-lignin has a linear structure with benzodioxane linkages, but it consists of 5-hydroxyguaiacyl units that are derived from 5-hydroxyconiferyl alcohol (5H-alcohol). It would be interesting to investigate the synthesis and degradation of the 5H-lignin, which offers an excellent platform to study differences from the C-lignin and explore how the 5H-alcohol affects the structure and properties of lignin.

Since chitin occurs as ordered crystalline microfibrils in the fungal cell wall and it has two polymorphs, α-chitin and β-chitin, in nature,[9, 20-22] crystalline chitin thin films are expected to provide a better model than amorphous chitin thin films for the study of the interactions of native chitin with family 18 chitinases. Unlike the amorphous chitin films, the crystalline chitin films are thought to be quite porous and allow the chitinase molecules to enter their interior at the beginning of the degradation process. Furthermore, the differences between the α-chitin and β-chitin thin films in their degradation by the family 18 chitinases could be explored.

Chen et al.[15] found that synthesized C-DHP in vitro had a small number-average degree of polymerization relative to isolated natural C-lignin. Therefore, Fenton mediated degradation of the natural C-lignin films may be different from the C-DHP film degradation, and a study of these differences would be interesting.

It was found in Chapter 4 that C-DHP films were barely degraded by LiP and MnP, but it does not mean enzymatic degradation is not feasible. In fact, lignin is commonly degraded by microorganisms through a series of ligninolytic enzymes in nature. Hence, it will be worthwhile to conduct further study on enzymatic degradation of C-lignin using enzymes, such as versatile peroxidase or a mixture of ligninolytic enzymes. In addition, given the difference in molecular weight between the synthesized C-DHP in vitro and the isolated natural C-lignin,[15] it would be interesting to investigate the effects of temperature, HRP concentration, H_2O_2 concentration, C-alcohol concentration, and flow rate on the synthesis of C-DHP films using QCM-D.

6.3 References

1. Kurita, K.; Sugita, K.; Kodaira, N.; Hirakawa, M.; Yang, J., Preparation and evaluation of trimethylsilylated chitin as a versatile precursor for facile chemical modifications. *Biomacromolecules* **2005,** *6,* 1414-1418.

2. Kittle, J. D.; Wang, C.; Qian, C.; Zhang, Y.; Zhang, M.; Roman, M.; Morris, J. R.; Moore, R. B.; Esker, A. R., Ultrathin chitin films for nanocomposites and biosensors. *Biomacromolecules* **2012,** *13,* 714-718.

3. Berini, F.; Caccia, S.; Franzetti, E.; Congiu, T.; Marinelli, F.; Casartelli, M.; Tettamanti, G., Effects of *Trichoderma viride* chitinases on the peritrophic matrix of Lepidoptera. *Pest Manag Sci* **2016,** *72,* 980-989.

4. Omumasaba, C. A.; Yoshida, N.; Ogawa, K., Purification and characterization of a chitinase from *Trichoderma viride*. *J Gen Appl Microbiol* **2001,** *47*, 53-61.

5. Jenifer, S.; Jeyasree, J.; Laveena, D. K.; Manikandan, K., Purification and characterization of chitinase from *Trichoderma viride* N9 and its antifungal activity against phytopathogenic fungi. *World J Pharm Pharm Sci* **2014,** *3*, 1604-1611.

6. da Silva, L. C.; Honorato, T. L.; Cavalcante, R. S.; Franco, T. T.; Rodrigues, S., Effect of pH and temperature on enzyme activity of chitosanase produced under solid stated fermentation by *Trichoderma* spp. *Indian J Microbiol* **2012,** *52*, 60-65.

7. Hardison, S. E.; Brown, G. D., C-type lectin receptors orchestrate antifungal immunity. *Nat Immunol* **2012,** *13*, 817-822.

8. Kang, X.; Kirui, A.; Muszynski, A.; Widanage, M. C. D.; Chen, A.; Azadi, P.; Wang, P.; Mentink-Vigier, F.; Wang, T., Molecular architecture of fungal cell walls revealed by solid-state NMR. *Nat Commun* **2018,** *9*, 2747.

9. Bowman, S. M.; Free, S. J., The structure and synthesis of the fungal cell wall. *Bioessays* **2006,** *28*, 799-808.

10. Gow, N. A. R.; Latge, J. P.; Munro, C. A., The fungal cell wall: structure, biosynthesis, and function. *Microbiol Spectr* **2017,** *5*, FUNK-0035-2016.

11. Free, S. J., Fungal cell wall organization and biosynthesis. *Adv Genet* **2013,** *81*, 33-82.

12. Moebius, N.; Uzum, Z.; Dijksterhuis, J.; Lackner, G.; Hertweck, C., Active invasion of bacteria into living fungal cells. *Elife* **2014,** *3*, e03007.

13. Wiesner, D. L.; Specht, C. A.; Lee, C. K.; Smith, K. D.; Mukaremera, L.; Lee, S. T.; Lee, C. G.; Elias, J. A.; Nielsen, J. N.; Boulware, D. R.; Bohjanen, P. R.; Jenkins, M. K.; Levitz, S. M.;

Nielsen, K., Chitin recognition via chitotriosidase promotes pathologic type-2 helper T cell responses to cryptococcal infection. *PLoS Pathog* **2015,** *11*, e1004701.

14. Vega, K.; Kalkum, M., Chitin, chitinase responses, and invasive fungal infections. *Int J Microbiol* **2012,** *2012*, 920459.

15. Chen, F.; Tobimatsu, Y.; Havkin-Frenkel, D.; Dixon, R. A.; Ralph, J., A polymer of caffeyl alcohol in plant seeds. *Proc Natl Acad Sci USA* **2012,** *109*, 1772-1777.

16. Tobimatsu, Y.; Chen, F.; Nakashima, J.; Escamilla-Trevino, L. L.; Jackson, L.; Dixon, R. A.; Ralph, J., Coexistence but independent biosynthesis of catechyl and guaiacyl/syringyl lignin polymers in seed coats. *Plant Cell* **2013,** *25*, 2587-2600.

17. Berstis, L.; Elder, T.; Crowley, M.; Beckham, G. T., Radical nature of C-lignin. *ACS Sustainable Chem Eng* **2016,** *4*, 5327-5335.

18. Stone, M. L.; Anderson, E. M.; Meek, K. M.; Reed, M.; Katahira, R.; Chen, F.; Dixon, R. A.; Beckham, G. T.; Roman-Leshkov, Y., Reductive catalytic fractionation of C-lignin. *ACS Sustainable Chem Eng* **2018,** *6*, 11211-11218.

19. Chen, F.; Tobimatsu, Y.; Jackson, L.; Nakashima, J.; Ralph, J.; Dixon, R. A., Novel seed coat lignins in the Cactaceae: structure, distribution and implications for the evolution of lignin diversity. *Plant J* **2013,** *73*, 201-211.

20. Rinaudo, M., Chitin and chitosan: properties and applications. *Prog Polym Sci* **2006,** *31*, 603-632.

21. Saito, Y.; Okano, T.; Gaill, F.; Chanzy, H.; Putaux, J.-L., Structural data on the intra-crystalline swelling of β-chitin. *Int J Biol Macromol* **2000,** *28*, 81-88.

22. Saito, Y.; Putaux, J.-L.; Okano, T.; Gaill, F.; Chanzy, H., Structural aspects of the swelling of

β chitin in HCl and its conversion into α chitin. *Macromolecules* **1997,** *30,* 3867-3873.